

**The Migrating Diurnal Tide in the Tropical Troposphere: Theory
and Observations Compared**

by
Timothy D. Stoker and Duane E. Stevens

Department of Atmospheric Science
Colorado State University
Fort Collins, Colorado

**Colorado
State**
University

**Department of
Atmospheric Science**

Paper No. 359

THE MIGRATING DIURNAL TIDE IN THE TROPICAL TROPOSPHERE:
THEORY AND OBSERVATIONS COMPARED

by

Timothy D. Stoker
and
Duane E. Stevens

Research supported by the
National Science Foundation
under grants
ATM-7826764 and ATM-8107136

Department of Atmospheric Science
Colorado State University
Fort Collins, Colorado

November, 1982

Atmospheric Science Paper No. 359

Volume 100
Part 1

U.S. GOVERNMENT PRINTING OFFICE
WASHINGTON, D. C. 20540

Copyright © 1961 by the National Bureau of Standards
All rights reserved.

1961

For sale by the Superintendent of Documents

ABSTRACT

A new theoretical study of the migrating diurnal thermal tide was carried out using classical tidal theory and placing particular emphasis upon the response in the tropical troposphere. Recent observational analyses indicate that preceding theoretical treatments have been inadequate to provide even a first-order understanding of the measurable tropospheric diurnal variations. Rather than resorting to a more sophisticated theoretical treatment, it was hypothesized that a more careful application of classical tidal theory should be sufficient to provide at least approximate agreement between the theory and the observations. Three methodological improvements were incorporated into the calculation: (1) a more representative tropospheric heating function, (2) the use of a greater number of basis functions to represent the structure of the heating, and (3) greater horizontal resolution in the results. Also, results were obtained for cases with realistic atmospheric static stability profiles. Heating due to the absorption of shortwave radiation by water vapor and ozone was considered to be the primary forcing mechanism.

The present results were found to differ significantly from the most detailed preceding theoretical treatment (Lindzen, 1967). An interesting tidal circulation pattern was discovered which opposes the Hadley circulation at the time of maximum heating. No physical explanation was found for this phenomenon. The addition of a very approximate

The first step in the analysis of the data is to determine the distribution of the variables. In this case, the variables are the number of children and the number of children who are under the age of 10. The distribution of the number of children is shown in Figure 1. The distribution of the number of children who are under the age of 10 is shown in Figure 2. The results of the analysis are shown in Table 1. The results show that the number of children is normally distributed with a mean of 2.5 and a standard deviation of 1.5. The number of children who are under the age of 10 is also normally distributed with a mean of 1.5 and a standard deviation of 1.0. The results also show that the number of children who are under the age of 10 is significantly correlated with the total number of children.

The second step in the analysis is to determine the relationship between the variables. In this case, the variables are the number of children and the number of children who are under the age of 10. The relationship between the variables is shown in Figure 3. The results of the analysis are shown in Table 2. The results show that the number of children who are under the age of 10 is significantly correlated with the total number of children. The correlation coefficient is 0.75, which is statistically significant at the 0.05 level.

ACKNOWLEDGEMENTS

We would like to give special thanks to Dr. William Gray for his enthusiastic interest in this research and his many helpful discussions concerning the results. Dr. Steve Cox is thanked for his instruction on the use and interpretation of the results from his radiative transfer routine, as are also Drs. Wayne Schubert and David Zachmann for their careful reviews of this research. Mr. Francis Crum is thanked for the time and thoughts he shared in our many profitable discussions. Finally, but certainly not least, we acknowledge our special appreciation to Machel Sandfort for her tireless and uncomplaining patience in skillfully typing this manuscript.

This work was sponsored by the National Science Foundation, under grants ATM-7826764 and ATM-8107136.

This paper is from a thesis submitted to the Academic Faculty of Colorado State University in partial fulfillment of the requirements for the degree of Master of Science.

cumulus heating parameterization produced only a 10 to 20% amplitude increase and a one to two hour phase shift in the diurnal variations. Comparisons to local and regional observational results were improved, but still remained disappointing -- presumably because other effects are operating on these scales. However, comparisons to three distinct observational analyses showed a consistent four hour phase difference between the theoretical and observed temperature (and geopotential) variations. The best comparison was to the global scale diurnal temperature variation analysis of Foltz and Gray. It was concluded that progress has been made in providing a theoretical understanding of the observed global diurnal variations.

TABLE OF CONTENTS

	<u>Page</u>
ABSTRACT.....	ii
ACKNOWLEDGEMENTS.....	iv
TABLE OF CONTENTS.....	v
LIST OF SYMBOLS.....	vi
1. MOTIVATION FOR A NEW THEORETICAL STUDY OF THE DIURNAL TIDE...	1
2. THE CLASSICAL TIDAL THEORY.....	11
3. METHODOLOGICAL IMPROVEMENTS.....	27
3.1 Improved Forcing.....	27
3.2 Improved Hough Mode Representation.....	40
3.3 Improved Presentation of Results.....	44
4. RESULTS AND COMPARISONS.....	48
4.1 Results.....	48
4.1.a Sensitivity study.....	49
4.1.b Component contributions.....	59
4.1.c Principal results of this research.....	68
4.2 Comparison with Earlier Theoretical Results.....	93
4.3 Comparison with Observations.....	111
4.3.a General remarks about observed diurnal variations.....	111
4.3.b Observational comparisons.....	114
5. SUMMARY OF CONCLUSIONS.....	144
LIST OF REFERENCES.....	150
APPENDIX 1: THE FAILURE OF THE FINITE DIFFERENCE APPROACH.....	153
APPENDIX 2: NOTES ON THE COMPUTER MODEL.....	159
APPENDIX 3: STUDY OF ANALYTIC AND QUASI-ANALYTIC SOLUTIONS.....	173
APPENDIX 4: REQUIREMENTS FOR A SOLSTICE CALCULATION.....	185

LIST OF SYMBOLS

A	amplitude of the heating (Appendix 2 and 3)
C_p	specific heat of dry air at constant pressure
E_n	the <u>n</u> th horizontal structure function of the diurnal westerly wind component
F	the θ -operator in Laplace's tidal equation. Also, the forcing (Appendix 3)
J	heating
$\bar{J}, J', J^{\sigma, s}$	mean, perturbation, and diurnal component of the perturbation heating
J_n	the component of the heating which projects onto the <u>n</u> th Hough mode
N_n	the <u>n</u> th horizontal structure function of the diurnal southerly wind component
R	gas constant for dry air
T	temperature
$\bar{T}, T', T^{\sigma, s}$	mean, perturbation, and diurnal component of the perturbation temperature
T_0	Environmental temperature at $z^*=0$
a	radius of the earth
a_1, a_2	constants in the boundary condition equations for the generalized vertical structure equation (Appendix 2)
b	exponential coefficient for the cumulus heating function
b_1, b_2	constants in the boundary condition equations for the generalized vertical structure equation (Appendix 2).
c	coriolis parameter ($\equiv 2\Omega \sin\theta$)

$c(x)$	functional coefficient in the generalized vertical structure equation (Appendix 2)
d_1, d_2	constants in the boundary condition equation for the generalized vertical structure equation (Appendix 2)
$d(x)$	functional coefficient in the generalized vertical structure equation (Appendix 2)
f	non-dimensional angular frequency ($\equiv \sigma/2\Omega$); also, an unspecified function of x (Appendix 2)
$f(z^*)$	vertical structure function (Appendix 2)
g	gravitational constant
$g(\theta)$	horizontal structure function (Appendix 2)
h_n	the equivalent depth corresponding to the n th Hough function
$h(x)$	functional coefficient in the generalized vertical structure equation (Appendix 2)
j	latitudinal grid-point index in numerical model
k	vertical grid-point index in numerical model
n	Hough mode index
p	pressure
\bar{p}, p'	mean and perturbation pressure fields
p_n	projection coefficient of the normalized horizontal structure of the heating
p_0	environmental pressure at $z^*=0$ ($\equiv 100$ kPa)
$r(x)$	functional coefficient in the generalized vertical structure equation
s	zonal wavenumber of the tidal component under consideration
t	time
u	westerly wind
$\bar{u}, u', u^{\sigma, s}$	mean, perturbation, and diurnal component of the perturbation westerly wind
v	southerly wind

$\bar{v}, v', v^{\sigma, s}$	mean, perturbation, and diurnal component of the perturbation southerly wind
w	vertical velocity (geometric vertical coordinate)
$\bar{w}, w', w^{\sigma, s}$	mean, perturbation, and diurnal component of the perturbation southerly wind
$\hat{w}^{\sigma, s}$	canonical form of the diurnal component of the perturbation vertical (z^*) velocity
\hat{w}_n	the projection of the canonical vertical velocity onto the <u>n</u> th Hough mode
w^*	vertical velocity (log-pressure vertical coordinate)
$\bar{w}^*, w^{*'}, w^{*\sigma, s}$	mean, perturbation, and diurnal component of the perturbation vertical velocity
x	arbitrary vertical coordinate (Appendix 2)
x_{top}	upper boundary (Appendix 2)
z	geometric vertical coordinate
z_B, z_T	lower and upper boundaries (of heating layer)
z^*	log-pressure vertical coordinate ($\equiv -\ln(p/p_0)$)
z_B^*, z_T^*	lower and upper boundaries (of heating layer)
Γ	static stability
Γ_T	static stability at the upper boundary of the model
θ_n	the <u>n</u> th Hough function
ϕ	geopotential
$\bar{\phi}, \phi', \phi^{\sigma, s}$	mean, perturbation, and the diurnal component of the perturbation geopotential
Ω	Angular velocity of the earth's rotation
δ	$1-\mu^2$, where $\mu=\sin\theta$
η	$f^2-\mu^2$, where $\mu=\sin\theta$
θ	latitudinal coordinate
κ	R/C_p
λ_n	vertical wavelength or decay scale of the <u>n</u> th Hough mode

μ	latitudinal coordinate ($\equiv \sin\theta$)
ρ	phase
$\bar{\rho}$	mean environmental density
σ	angular frequency of the tidal component under consideration
ϕ	longitudinal coordinate
χ	horizontal divergence
$\bar{\chi}, \chi', \chi^{\sigma, s}$	mean, perturbation, and diurnal component of the perturbation horizontal divergence
w	vertical velocity (pressure vertical coordinate)
$\bar{w}, w', w^{\sigma, s}$	mean, perturbation, and diurnal component of the perturbation vertical velocity

1. MOTIVATION FOR A NEW THEORETICAL STUDY OF THE DIURNAL TIDE

To begin with, it is essential to identify and distinguish the particular aspect of the atmospheric tide which has been investigated. The results of a study of the migrating diurnal thermal tide are presented in this report.

It is, first of all, the thermally forced component of the atmospheric tide which is to be discussed. Although, just as in the oceans, the gravitational forces of the sun and moon produce a tidal response in the atmosphere, this mechanism accounts for only a minor fraction of the observed atmospheric tide (Chapman and Lindzen, 1970). Instead, the atmospheric tidal response is primarily a response to thermal forcing. Very simply, what happens is that, when the atmosphere is diabatically heated, it warms and expands, and the wind components begin to adjust so as to be consistent with the new temperature and geopotential fields. In the opposite part of the heating cycle, there is a net cooling of the atmosphere, and it contracts again. Computing the dynamic response to this diabatic heating on a rotating sphere with a realistic atmospheric structure becomes a fairly complicated problem. This is the thermal tide which is discussed in this report. In particular, three components of the diabatic heating will be considered: heating due to the absorption of shortwave radiation by (1) water vapor molecules and (2) ozone molecules, and heating due to (3) latent heat release and precipitation of, particularly, tropical cumulus convection.

Second, it is only the diurnal component of the thermal tide which is considered. For any particular fixed point in the earth's atmosphere, the curves representing the daily cycles of shortwave heating and latent heat release can be subjected to Fourier analysis. The tidal response forced by the first non-constant Fourier component of the heating (which has a period of 24 hours) is the only component of the thermal tide considered in this report.

Finally, it is only the "migrating" component of the diurnal thermal tide which is considered. Due to inhomogeneities around any particular latitude circle (such as land/sea contrasts, varying ozone or water vapor distributions, topography, variations in the diurnal cycle of latent heat release, etc.), the amplitude of the diurnal component of the thermal tide will vary around a latitude circle. The curve representing this amplitude variation can also be subjected to Fourier analysis. Again, it is only the first non-constant component (with a zonal wavenumber of one) which will be considered in this report. This component is called the "migrating" component because it propagates around the earth in 24 hours -- following the sun. None of the higher order components (which also migrate, but with slower velocities) have been studied in this treatment.

It is important to remember exactly what part of the atmospheric tide it is that is being discussed. Many of the standard criticisms levied against the type of tidal calculation used in this research can be obviated by retaining a clear understanding of what is being considered here. Likewise, much confusion about the meaning of the results of the tidal calculation and of the comparison between the theoretical

results and the observed results can be avoided by remembering that only a very specific component of the diurnal thermal tide is being considered here.

It must also be mentioned at the outset here that this study focused exclusively on the tropospheric tidal response. Historically, most of the attention regarding atmospheric migrating tides has focused on two distinct aspects of the meteorological response: (1) the wind and temperature changes in the upper atmosphere (in and above the stratosphere), and (2) the surface pressure oscillation.

The upper atmospheric tidal response has been investigated because of the relatively large amplitude of the tidal variations in that region. Two factors are responsible for these large amplitudes. First, in the stratosphere, the substantial local heating due to the absorption of shortwave radiation by ozone is in part responsible for the larger stratospheric amplitudes. However, throughout the upper atmosphere (above the troposphere), these large amplitudes also result, theoretically, from the conservation of energy for vertically propagating waves. This causes the amplitudes to increase above the forcing regions as the mean air density decreases; so that to a good approximation, amplitudes are inversely proportional to the square root of the mean density. Because of these large tidal variations, rocket-borne observing systems have been able to quantitatively measure the daily variability and verify the classical tidal calculations.

The daily surface pressure variation is miniscule and subtle compared to the pressure changes associated with synoptic-scale systems in mid-latitudes; but in the tropics, the semi-diurnal component of the surface pressure variation is an obvious and dominating feature. By

differentiating between vertical propagation characteristics of tidal oscillations with various periods, the tidal theory has proven sufficient as an explanation for the dominance of the semi-diurnal surface pressure oscillation (as opposed to the dominance of the diurnal component in the upper atmosphere) and the dependence of its amplitude on latitude. Because surface pressure can be measured very accurately, and because very long data records of surface pressure measurements exist, it is a very useful indicator of tidal activity.

By way of contrast, the structure of the migrating tide within the troposphere itself has been given very little attention. This situation seems paradoxical given that:

- (1) over 80% of the atmosphere's mass is in the troposphere;
- (2) "weather", as commonly understood, is confined primarily to the troposphere, and the attention of most meteorologists is largely restricted to the troposphere;
- (3) the troposphere is the most readily accessible region of the atmosphere, and vast amounts of data have been collected in the troposphere; and
- (4) a significant portion of the excitation of the solar migrating tide occurs in the troposphere, where the bulk of the water vapor is located.

The relative neglect of the tropospheric tide probably stems in part from the very low amplitude of the signal. Preceding calculations (Lindzen, 1967) have suggested typical tropospheric amplitudes of 10 cm/sec for the westerly wind component, 0.1 K for temperature, and 0.1 cm/sec for vertical velocity. Such small amplitudes would be very difficult to measure accurately by using observations from the standard

rawinsonde network; but even with very accurate measurements, the troposphere is a region characterized by ubiquitous large amplitude variations caused by many different factors, so that it would still be difficult to isolate that small fraction of the variation for which the diurnal tide accounts.

Perhaps another reason why the tropospheric tide has not been given much theoretical attention is that geographically localized complicating factors appear to have such a significant impact. Particularly over continents, surface topography and sensible heat flux from the surface affect the tidal variations, as do also the local sea-breeze circulations caused by contrasts in the thermal capacity of the earth's surface at the land/ocean boundary. Geographical variations in tropospheric water vapor mixing ratio affect the local diabatic heating due to absorption of shortwave radiation. Likewise, the predominant local time of thunderstorm activity, heavy precipitation, and, hence, of latent heat release varies from place to place. From a study of inland data, Wallace and Tadd (1974) concluded that such factors as these strongly influence the diurnal fluctuations throughout the troposphere over the North American continent. One might further conclude that if indeed these factors are everywhere overwhelmingly dominant, there might be little usefulness in studying such an insignificant component of the diurnal tide as the one treated in this report.

However, it was maintained as a premise of this research that the migrating diurnal thermal tide is not insignificant in the troposphere. Furthermore, it was maintained (Chapman and Lindzen, 1970) that, from a global perspective, the responses due to these irregularly distributed local and regional factors should tend to destructively interfere

because their phases are so incoherent. If this is truly the case, it would be concluded that the migrating diurnal thermal tidal component should comprise a major fraction of the observed diurnal variations -- globally, and even regionally.

Certain recent observational analyses appear to lend credence to this line of reasoning. In particular, attention should be drawn to the results shown by Foltz and Gray (1979). They analyzed the temperature and wind measurements from vast quantities of rawinsonde data collected all over the northern hemisphere. Their results showed a predominantly diurnal variation of the mean temperature through a deep layer (85 to 30 kPa) of the troposphere with a maximum peak-to-peak amplitude of about 0.5 to 0.7 K in the tropics and a phase such that the maximum temperature was reached between 1200 and 1600 LT. According to Foltz and Gray, this trend was definitely evident throughout the hemisphere, though they noted that the amplitude of the variation decreases with increasing latitude and decreased in summer relative to winter. The seasonal change at lower latitudes was found to be minimal. Considering the variation of insolation with latitude, these results seem plausible. More importantly, however, the authors also noted that there was no evidence of any systematic longitudinal bias. These consistent longitude-independent temperature fluctuations point toward the existence of a migrating diurnal tide of measureable amplitude in the deep troposphere.

A similar analysis (Foltz and Gray, 1979) of sounding data from five tropical marine experiments spread out around the globe and in which soundings were taken four to eight times per day provided further

evidence for the existence of a migrating diurnal tide. Again, temperature variations through a deep layer of the troposphere showed an average amplitude of 0.58 K, with the temperature reaching a maximum at 1400 LT.

Foltz and Gray investigated the possibility of instrumental error due to heating of the thermistor during daytime ascents. They determined that this effect could introduce errors no larger than about 0.2 K. This is a significant amount, but it cannot explain the major part of the observed temperature variation.

Foltz and Gray concluded that a dynamic mechanism for producing warming or cooling is required in order to explain the observation of a temperature maximum several hours before local sunset and a temperature minimum several hours before local sunrise. Without any dynamics, diabatic heating by shortwave solar radiation and cooling by atmospheric longwave radiation would yield a temperature maximum at local sunset and a temperature minimum at local sunrise. They suggested that the "required warming" that is needed to give an early morning temperature rise results from the adiabatic heating of morning subsidence in a deep layer of the troposphere. Similarly, afternoon and evening ascent produce adiabatic cooling.

Foltz and Gray found corroborating evidence for their hypothesized mechanism for achieving this "required warming" in the results shown by McBride and Gray (1978). McBride and Gray showed that over both the western Pacific and the western Atlantic, clear area composites of many years of summer months of data indicate relative subsidence (adiabatic warming) in the morning hours and relative upward motion (adiabatic cooling) in the evening.

The observed vertical motion field also provided strong, independent support for the physical reality of the temperature observation (as opposed to attributing all of the temperature variation to measurement uncertainty). The observed wind fields do not depend on the thermodynamic data, but the first law of thermodynamics constrains the thermal changes to be consistent with the motion field and the diabatic forcing. The fact that the observed wind and temperature fields are at least qualitatively consistent strengthens the credibility of each set of observations.

These observations have not been adequately explained in any preceding theoretical treatment of the diurnal tide. The objective of this study was to remedy the inconsistency between such recent observations and the predictions of preceding theoretical treatments. A second fundamental premise of this research was that classical tidal theory should be sufficient to obtain a first-order understanding of the migrating diurnal thermal tide if all the important forcing mechanisms are taken into consideration in such a treatment.

Since this is by no means the first attempt to apply classical tidal theory, it is necessary to justify the repetition of such a study. The most recent thorough presentation of classical tidal theory was given by Chapman and Lindzen (1970). The basic methodology used in this study does not differ significantly from theirs. That is, the diabatic heating is prescribed as a function of local time, subjected to Fourier analysis in the longitudinal direction, and then used to force a linear response in the atmospheric fields. The most detailed preceding treatment of the diurnal tide (which applied classical tidal theory) was executed by Lindzen (1967, 1968). For the troposphere, the results

which he shows are inadequate to account for recent observations. In particular, except right at the equator (where the agreement is somewhat better), the amplitudes which his results predicted for the temperature variations appear to be too small by a factor of five to ten. (It should be mentioned that Lindzen's primary focus was on the diurnal tide in the upper atmosphere, and that the results which he shows for the troposphere are somewhat incidental.)

Given this situation, there are two possible courses of action. The first would be to abandon the classical tidal theory and to conclude that it is inadequate for obtaining even a first-order understanding of the diurnal tide. Proponents of this course would suggest that unless the tidal theory were modified (and greatly complicated) to include such factors as topography, horizontal temperature gradients, and longitudinal inhomogeneities, it will never provide satisfactory results comparable to the observational results.

In this study, it was believed that this extreme would not be necessary. If it is true that the migrating diurnal thermal tide is the dominant component of the diurnal tide, and if it is true that this component is primarily forced by shortwave heating and latent heat release, then classical tidal theory should be capable of providing the approximate theoretical understanding of the diurnal tide which is still lacking.

In examining previous applications of classical tidal theory, several ideas evolved for improving upon the detailed methodology of earlier studies. These improvements include the following: (1) a more realistic tropospheric heating function, (2) the utilization of more

basis functions for representing the horizontal structure of the heating, (3) a greater horizontal resolution in the output of the results, and (4) a realistic tropospheric static stability profile.

It is crucial to remember that this treatment of the diurnal tide cannot be expected to completely or exactly account for the observations. A complete treatment would have to take into account the complicating factors mentioned above and to consider other components of the diurnal tide. The objective of this study was to carry out a more accurate classical treatment of the diurnal tide, thereby providing a theoretical explanation for a much larger fraction of the observed diurnal variations while simultaneously retaining the simplicity and ease of interpretation afforded by classical tidal theory. As will be shown, this objective was only partially attained.

The next chapter provides a discussion of classical tidal theory and the assumptions and approximations which it entails. Chapter 3 covers the methodological improvements incorporated into this study. Chapter 4 contains the results of this present study and comparisons to preceding theoretical and observational results. Included in this chapter are studies of the sensitivity of the computer model which was used and of the individual contributions to the total response provided by the three components of the heating. The conclusions drawn from this research will be summarized in the last chapter.

2. THE CLASSICAL TIDAL THEORY

The theory underlying the computer model used to produce the results shown in this report does not differ in any significant way from that used by Lindzen 15 years ago (Lindzen, 1967). Slight variations have been made in the notation to make it more consistent with the usual meteorological conventions, but the assumptions and simplifications incorporated in the theoretical formulation have not been changed. The most organized and thorough treatment of this "classical" tidal theory was presented by Chapman and Lindzen (1970). The purpose in reviewing the theory here is twofold. First, to provide a framework for understanding the three methodological improvements used to obtain the results presented in this report. Second, to enumerate the various assumptions and simplifications utilized here which must be considered when assessing the significance of the results and their departures from results derived from observations.

In order to simplify the tidal calculation and to obtain results which are more readily subject to interpretation, a number of assumptions and simplifications are made. Only the essential physics and what are believed to be the principle forcing mechanisms are retained. First of all, as mentioned by Chapman and Lindzen (1970), there is a set of almost universally accepted approximations which do not pose any real limitation on tidal theory. These include the following:

- (1) The atmosphere is in local thermodynamic equilibrium. This assumption breaks down in the thermosphere.
- (2) The atmosphere behaves as an ideal gas ($p = \rho RT$) and is of uniform composition (R is a constant). The latter assumption breaks down above the turbopause.
- (3) The earth is regarded as a sphere (radius, a , is a constant).
- (4) The atmosphere is regarded as a geometrically thin fluid, so that $r = a + z$, where r is the distance from the center of the earth and z is the distance above the surface. Thus $\partial/\partial r$ is equivalent to $\partial/\partial z$. Also, the acceleration due to gravity, g , can be regarded as a constant. This assumption is in error by less than 3% below 100 km.
- (5) The atmosphere is assumed to be in hydrostatic equilibrium.

A number of potentially significant factors are ignored. The neglect of these factors is justified in various ways.

- (1) Neglect radiative cooling of the atmosphere. It is assumed that the atmosphere cools at a uniform rate, without significant diurnal variation.
- (2) Neglect sensible heat transfer from the surface. It can be argued that over a predominantly ocean covered sphere, the diurnal variation of sensible heat transfer to the atmosphere should be relatively small.
- (3) Neglect gravitational tidal effects. Generally, the tidal response due to the gravitational forces of the sun and the moon is very small. It is assumed that thermal forcing is by far the predominant factor in forcing the observed atmospheric tidal response.

- (4) Neglect dissipative processes. Molecular viscosity, turbulent viscosity, conductivity, and ion drag are all assumed negligible. This assumption breaks down in the thermosphere. Simple dissipations, such as Newtonian cooling and Rayleigh friction, could have been included, but were not.
- (5) Neglect thermal forcing due to absorption of shortwave radiation by dust and clouds in the atmosphere. Aside from being very difficult to quantify and highly variable, the diurnal variation of these effects is assumed to be of secondary importance.
- (6) Neglect surface topography. The influences of mountain ranges and land/sea distributions are assumed to provide no significant coherent contribution to the forcing of the migrating diurnal thermal tide. Whether or not this is a valid assumption is debatable. The analysis of Foltz and Gray suggests a lack of longitudinal dependence for the diurnal tide in the tropics (Foltz and Gray, 1979). Chapman and Lindzen also argue that effects caused by these factors should be of secondary concern (Chapman and Lindzen, 1970).
- (7) Neglect variations of water vapor concentration and ozone concentration around a latitude circle. Conceivably, the influence of these variations could be greater than any of the preceding effects. However, it is assumed that over the vast expanses of tropical oceans these parameters will be relatively constant with longitude, and that any variations will not produce any coherent contribution to the migrating diurnal tide.

This is not to say that these effects are of no importance in the atmosphere. It is just to say that these effects either do not have significant diurnal variations or are not of any significant consequence in the region of the atmosphere which is included in the model calculation. As noted, several of the assumptions upon which the model is based break down in the thermosphere. For this reason, the mesopause was used as the upper boundary for the tidal calculation. Some of the quasi-analytical results have shown that the specific mesospheric structure (and presumably the thermospheric structure as well) can still have a surprising effect on the tidal response in the troposphere (see Appendix 3). However, it seemed very likely that including a simple thermospheric structure without accounting for the breakdown of these several assumptions would introduce just as much error as ignoring the thermosphere all together.

A system of five linearized primitive equations in five unknowns is solved to obtain the tidal variations of the five variables. The system consists of two horizontal momentum equations, a hydrostatic equation, a mass continuity equation, and a thermodynamic energy equation (TEE). When written in spherical coordinates, the equations appear in their full non-linear form as follows:

$$\frac{du}{dt} - cv = \frac{-1}{a \cos \theta} \frac{\partial \phi}{\partial \phi} \quad (1)$$

$$\frac{dv}{dt} + cu = \frac{-1}{a} \frac{\partial \phi}{\partial \theta} \quad (2)$$

$$RT = \frac{\partial \phi}{\partial z^*} \quad (3)$$

$$\frac{1}{a \cos \theta} \left(\frac{\partial u}{\partial \phi} + \frac{\partial}{\partial \theta} (v \cdot \cos \theta) \right) + \left(\frac{\partial w^*}{\partial z^*} - w^* = 0 \right) \quad (4)$$

$$\frac{dT}{dt} + \kappa w^* T = \frac{J}{C_p} \quad (5)$$

The vertical coordinate z^* is defined by the relation $z^* = -\ln(p/p_0)$, where p is the pressure, and p_0 is a reference pressure taken to be 100 kPa. The horizontal coordinates, for longitude ϕ , and latitude θ , increase in the eastward and northward directions respectively, with $\theta = 0$ at the equator. The velocity components u , v , and w^* are, respectively, the eastward, northward, and upward velocities, where $w^* = dz^*/dt = -w/p$ and w is the vertical velocity in pressure coordinates. The parameters a , c , T , and ϕ are, respectively, the radius of the earth, the Coriolis parameter, the temperature, and the geopotential. The quantity κ equals R/C_p , where R is the universal gas constant and C_p is the specific heat of air at constant pressure. The heating which provides the thermal tidal forcing in the TEE is represented by J .

This set of equations incorporates many of the complexities and non-linear effects of the real atmosphere, and therefore contains far more than is of interest in this study. The first step in producing a set of equations useful for studying the diurnal tide is to linearize the equations and subtract out the basic state equations. Several assumptions are made in doing this.

- (1) The tidal fields are assumed to be linearizable perturbations about the basic state fields. That is, the perturbations neither alter the basic state, nor interact with other perturbation quantities. The way to apply this assumption is to assume that the products of perturbation quantities are very

small -- an assumption that would seem somewhat questionable for the large tidal variations in the upper atmosphere above the region of primary interest. This assumption permits the quantities u , v , w^* , T , ϕ , and J to be written as the sums of mean and perturbation parts (e.g., $u = \bar{u} + u'$).

- (2) The basic state parameters are assumed to be steady in time (varying, at most, with time scales much longer than tidal periods) and to be constant around latitude circles. They are assumed to satisfy the basic governing equations when the perturbations are set equal to zero.
- (3) To simplify the problem considerably, it is assumed that the basic state is at rest; i.e., $\bar{u} = \bar{v} = \bar{w}^* = 0$. This in turn implies that \bar{T} , \bar{p} , $\bar{\rho}$, and the static stability, Γ , are all constrained to be functions of only z^* . This assumption is justified by noting that the appropriate velocity scale is the velocity of the migrating tide, which in the tropics is on the order of 400 m/sec -- much greater than any mean wind.

After substituting the variables in the form $u = \bar{u} + u'$ into the primitive equations and subtracting out the equations which characterize the basic state, the following set of linearized equations is obtained:

$$\frac{\partial u'}{\partial t} - cv' = \frac{-1}{a \cos \theta} \frac{\partial \phi'}{\partial \phi} \quad (6)$$

$$\frac{\partial v'}{\partial t} + cu' = \frac{-1}{a} \frac{\partial \phi'}{\partial \theta} \quad (7)$$

$$RT' = \frac{\partial \phi'}{\partial z^*} \quad (8)$$

$$\frac{1}{a \cos \theta} \frac{\partial u'}{\partial \phi} + \left(\frac{\partial}{\partial \theta} (v' \cdot \cos \theta) \right) + e^{z^*} \frac{\partial}{\partial z^*} (e^{-z^*} w^{*'}) = 0 \quad (9)$$

$$\frac{\partial T'}{\partial t} + \Gamma w^{*'} = \frac{J'}{C_p} \quad (10)$$

Here, Γ is the static stability and equals $(\partial \bar{T} / \partial z^*) + \kappa \bar{T}$. It is important to remember that Γ is only a function of z^* .

Although more will be said later, it is appropriate here to say a few words about the heating, J' , in the TEE which provides the forcing for the diurnal tide. Three kinds of thermal forcing are considered: (1) shortwave (primarily infrared) absorption by water vapor, (2) shortwave (ultraviolet and visible light) absorption by ozone, and (3) latent heat release or so-called cumulus heating. The first and third kinds provide tropospheric forcing, while absorption by ozone occurs primarily in the stratosphere and lower mesosphere. In a linear treatment such as this, the response produced by each kind of forcing can be computed independently, and the total response is just the sum of the three component responses. This makes it very easy to determine the relative importance of the various kinds of forcing in producing a tropospheric response and in causing the various features and characteristics of that response. The first of the three methodological improvements incorporated into this research was to use a more representative structure for the tropospheric forcing than the approximate functional form used in the past by Lindzen and others (Lindzen, 1966).

Going back to the set of linearized primitive equations, the components of the general solution to this system of equations which will be considered here are those which are wave-like in ϕ and t , such that

u' , v' , w'^* , ϕ' , T' , and J' can all be expressed in this form:

$$u' = u^{\sigma,s}(\theta, z^*)e^{i(\sigma t + s\phi)},$$

where the unprimed variables now have a different meaning than in equations (1-5). At this point, the diurnal tide is isolated by choosing particular (consistent) values for σ and s : $\sigma = (2\pi/\text{day})$ and $s = 1$. All other tidal components will be ignored. The σ, s superscript uniquely identifies which component of the tide is being examined. Substituting these wave-like solutions into equations (6-10) and cancelling the exponential factors yields this final set of equations:

$$i\sigma u^{\sigma,s} - cv^{\sigma,s} = -\frac{is\phi^{\sigma,s}}{a\cos\theta} \quad (11)$$

$$i\sigma v^{\sigma,s} + cu^{\sigma,s} = -\frac{1}{a} \frac{\partial \phi^{\sigma,s}}{\partial \theta} \quad (12)$$

$$RT^{\sigma,s} = \frac{\partial \phi^{\sigma,s}}{\partial z^*} \quad (13)$$

$$\frac{1}{a\cos\theta} \left(isu^{\sigma,s} + \frac{\partial}{\partial \theta} (\cos\theta \cdot v^{\sigma,s}) \right) + e^{z^*} \frac{\partial}{\partial z^*} (e^{-z^*} w^{*\sigma,s}) = 0 \quad (14)$$

$$i\sigma T^{\sigma,s} + \Gamma w^{*\sigma,s} = \frac{J^{\sigma,s}}{C_p} \quad (15)$$

With a little calculus and a fair amount of algebra, these equations can be reduced to one equation in one unknown. The simplest such equation is the one for $w^{*\sigma,s}$. It has this form:

$$\left[\frac{\partial^2}{\partial z^{*2}} - \frac{\partial}{\partial z^*} - \frac{R\Gamma}{4a^2\Omega^2} F \right] w^{*\sigma,s} = \frac{-K}{4a^2\Omega^2} F(J^{\sigma,s}), \quad (16)$$

where F is a complicated θ operator which (with a change of variables to $\mu = \sin\theta$) looks like the following:

$$F: \frac{\partial}{\partial \mu} \left(\frac{1-\mu^2}{f^2-\mu^2} \frac{\partial}{\partial \mu} \right) - \frac{1}{f^2-\mu^2} \left(\frac{s}{f} \cdot \frac{f^2+\mu^2}{f^2-\mu^2} + \frac{s^2}{1-\mu^2} \right).$$

Here, now, $f = \sigma/2\Omega \cong 0.5$ for the diurnal tide, and Ω is the angular velocity of the earth's rotation.

Next, for convenience, a new variable, $\hat{w}^{\sigma,s}$, is defined such that

$$\hat{w}^{\sigma,s} = e^{-z^*/2} w^{\sigma,s}.$$

Because of the exponential decrease of density with height, a vertically propagating wave will produce velocity perturbations which grow exponentially with height. It is nicer to work with a variable like $\hat{w}^{\sigma,s}$ which is more nearly constant with height. When applying the method of separation of variables to solve equation (16), this variable causes the vertical structure equation to be in canonical form. Upon substitution, equation (16) becomes:

$$\left[\frac{\partial^2}{\partial z^{*2}} - \frac{1}{4} - \frac{R\Gamma}{4a^2\Omega^2} F \right] \hat{w}^{\sigma,s} = \frac{-ke^{-z^*/2}}{4a^2\Omega^2} F(J^{\sigma,s}). \quad (17)$$

This is the tidal equation which must be solved. The usual method for solving this problem is to apply the Galerkin (spectral) method in the latitudinal direction and a finite difference method in the vertical. The failure of the attempt to solve the entire problem using finite difference techniques is documented in Appendix 1.

The first step in solving this equation is to express $\hat{w}^{\sigma,s}$ and $J^{\sigma,s}$ as summations of an as yet unspecified set of functions of θ with coefficients dependent on z^* :

$$\hat{w}^{\sigma,s} = \sum_n \hat{w}_n(z^*) \theta_n(\theta) \quad (18)$$

$$J^{\sigma, s} = \sum_n J_n(z^*) \theta_n(\theta) \quad (19)$$

At this point, the second methodological improvement is suggested. Ideally, the sums should be infinite. In practice, they must be truncated at some point. Lindzen and others have assumed that five mode representations of the tidal parameters are sufficient. As will be shown later, this assumption appears to be inadequate. The sixteen mode representations used in this research are much better.

Substituting these series expansions into equation (17), bringing the summation signs to the front of each side, and taking the appropriate derivatives, the following equation results:

$$\sum_n \left[\theta_n \left(\frac{d^2 \hat{w}_n}{dz^{*2}} - \frac{1}{4} \hat{w}_n \right) - \frac{R \Gamma \hat{w}_n}{4a^2 \Omega^2} F(\theta_n) \right] = \sum_n \left[\frac{-k e^{-z^*/2}}{4a^2 \Omega^2} J_n F(\theta_n) \right] \quad (20)$$

If it is assumed that the basis functions are all mutually orthogonal, the summation signs may be dropped and the equality holds for each n . Then, the equation can be easily separated into two second order ordinary differential equations, one in θ and one in z^* :

$$\left[\frac{d^2 \hat{w}_n}{dz^{*2}} - \frac{\hat{w}_n}{4} \right] \left[R \Gamma \hat{w}_n - k e^{-z^*/2} J_n \right]^{-1} = \frac{1}{4a^2 \Omega^2} \frac{F(\theta_n)}{\theta_n} = \frac{-1}{gh_n} \quad (21)$$

Because the left and middle parts of equation (21) are functions of independent variables and yet are still equal to each other, they must be at most equal to the same constant, written here in the form $-1/gh_n$, where g is the (constant) acceleration due to gravity. The middle and right parts of equation (21) constitute Laplace's tidal equation. It takes the form of an eigenvalue problem, and it is the set of functions that satisfy this equation which has been chosen (by the assumption

after equation (20)) to be the set of horizontal basis functions, θ_n . These functions are called Hough functions, and the corresponding eigenvalues, h_n , are called equivalent depths. It has been proven that the set of Hough functions is complete and that they are all mutually orthogonal (Flattery, 1967). Approximations to the Hough functions and equivalent depths can be found by expressing the Hough functions as series of associated Legendre functions, substituting the series expressions into Laplace's tidal equation, truncating the series, and solving the matrix eigenvalue problem for the coefficients of the associated Legendre functions (which are known functions).

Two types of Hough functions result: those which are symmetric about the equator, and those which are anti-symmetric. All calculations in this report were done for equinox, and it was assumed that all parameters were symmetric about the equator for this condition (which is not strictly true for the real world). Thus, the set of anti-symmetric Hough functions does not enter into the calculation and can be discarded.

Applying the Galerkin method now to equation (20), a vertical structure equation can eventually be derived:

$$\left[\frac{d^2}{dz^2} - \frac{1}{4} + \frac{R\Gamma}{gh_n} \right] \hat{w}_n = \frac{\kappa e^{-z^*/2}}{gh_n} J_n, \quad (22)$$

where

$$J_n = \int_{\mu=-1}^{+1} J^{\sigma,s} \theta_n d\mu,$$

and

$$J_n = J_n(z^*).$$

The quantity J_n now is the projection of the heating onto the n th Hough function and is in general a function of z^* .

Given suitable boundary conditions, equation (22) can be solved using finite difference techniques in z^* . There are n such equations which must be solved for the $\hat{w}_n(z^*)$ functions required in equation (18). Knowing the \hat{w}_n 's at each level and the θ_n 's at each latitude increment, it is a simple matter to compute $w^{\sigma,s}$ at each grid point in the model. Working backward through the steps required to obtain the single equation in w^* , the tidal variations of the other four variables in the set of primitive equations (11-15) can be computed. The finite difference forms used to compute these variables are recorded in Appendix 2. In the computer model, the horizontal increment used in the θ direction was $\Delta\theta = 1^\circ$ of latitude, and the vertical resolution was $\Delta z^* = 0.02$, which is on the order of 100 meters.

Something must be said about boundary conditions as well. The lower boundary condition applied was $w' = 0$ at $z^* = 0$. That is, the geometric height velocity goes to 0 at the 100 kPa level. This is an approximation for which Holton argues the validity (Holton, 1975). By expanding the total derivative dz/dt , linearizing the resulting equation, applying the assumptions listed before, and applying the Galerkin method, the lower boundary condition can be expressed in this form:

$$\left(\frac{R\bar{T}_0}{gh_n} - \frac{1}{2} \right) \hat{w}_n + \frac{d\hat{w}_n}{dz^*} = 0, \quad (23)$$

where \bar{T}_0 is the basic state temperature at 100 kPa.

It turns out that the upper boundary requires two conditions. If the static stability, Γ_T , becomes constant near the upper boundary (the mesopause) and the heating goes to zero, equation (22) reduces to this:

$$\frac{d^2 \hat{w}_n}{dz^*{}^2} + \left(\frac{R\Gamma_T}{gh_n} - \frac{1}{4} \right) \hat{w}_n = 0 \quad (24)$$

The set of symmetric Hough functions has two subsets: those with positive equivalent depths and those with negative equivalent depths. Positive (and sufficiently small) equivalent depths imply solutions to equation (24) which propagate vertically. These solutions exhibit gravity wave type behavior and, like their associated Hough functions, are primarily confined to tropical latitudes -- i.e., they have very small amplitudes outside of the tropics (see Fig. 2.1). The boundary condition for these modes is that energy cannot be allowed to propagate in from the top of the model. Energy is only permitted to leak out the top from below. As Wilkes has shown, this implies the elimination of the solution $Be^{-i\lambda_n z^*}$, where $\lambda_n^2 = (R\Gamma_T/gh_n - \frac{1}{4})$ (Wilkes, 1949). This is called the radiation condition.

Negative equivalent depths imply solutions to equation (24) which are evanescent -- i.e. which are non-propagating and decay exponentially away from the source of forcing. These solutions behave like Rossby waves and, like their associated Hough functions, are confined to latitudes more than 30° from the equator. For negative equivalent depth modes, the boundary condition is that the kinetic energy density of a particular mode cannot be allowed to increase exponentially with height, unbounded as z^* goes to infinity. Again, as Wilkes shows, this elimi-

The first part of the paper is devoted to the study of the stability of the equilibrium state of a system of particles in a magnetic field. It is shown that the equilibrium is stable if the magnetic field is sufficiently strong and the particles are sufficiently close to the equilibrium state.

$$(2.1) \quad \frac{d}{dt} \left(\frac{\partial L}{\partial \dot{q}_i} \right) - \frac{\partial L}{\partial q_i} = 0$$

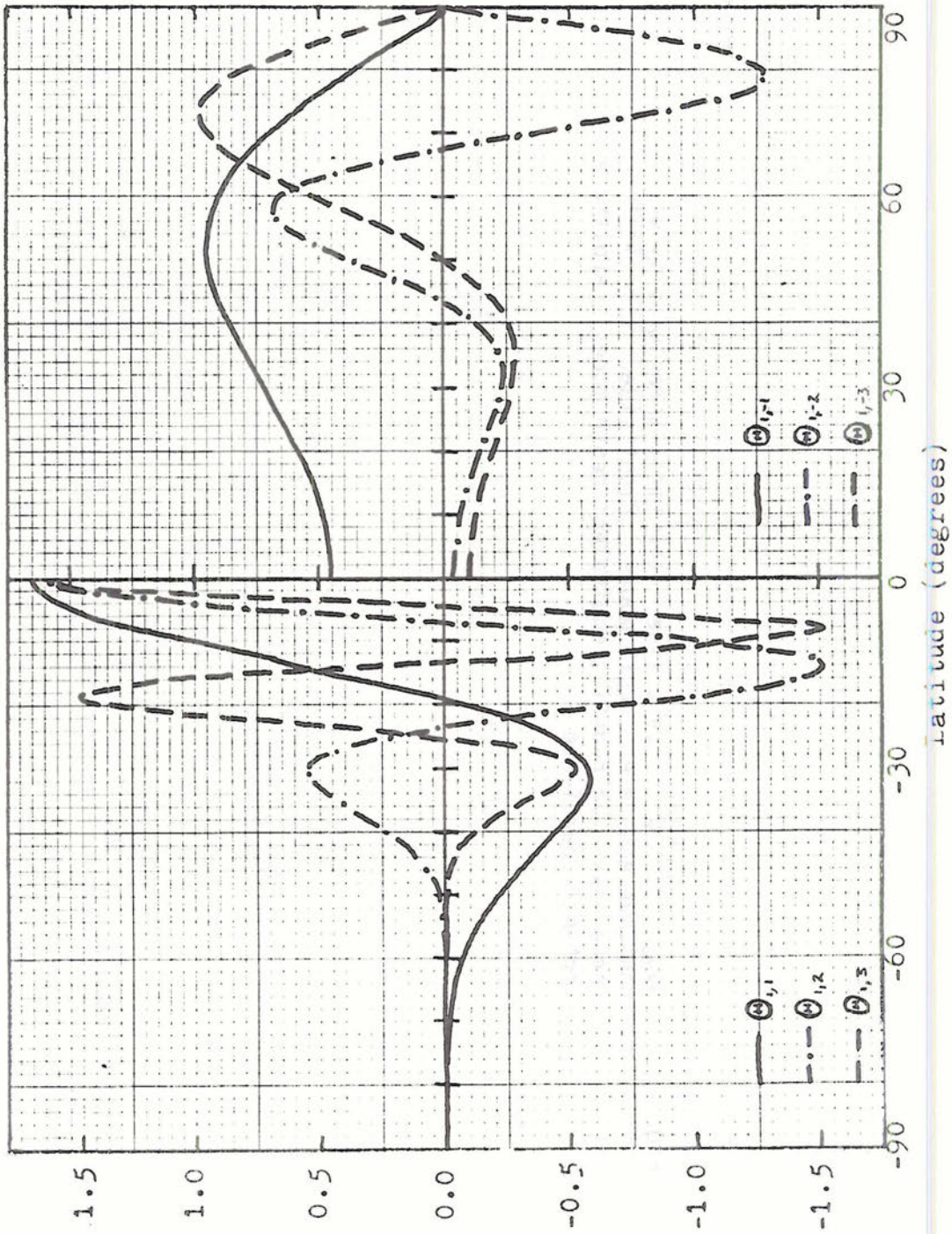
The second part of the paper is devoted to the study of the stability of the equilibrium state of a system of particles in a magnetic field. It is shown that the equilibrium is stable if the magnetic field is sufficiently strong and the particles are sufficiently close to the equilibrium state. The third part of the paper is devoted to the study of the stability of the equilibrium state of a system of particles in a magnetic field. It is shown that the equilibrium is stable if the magnetic field is sufficiently strong and the particles are sufficiently close to the equilibrium state.

$$(2.2) \quad \frac{d}{dt} \left(\frac{\partial L}{\partial \dot{q}_i} \right) - \frac{\partial L}{\partial q_i} = 0$$

The fourth part of the paper is devoted to the study of the stability of the equilibrium state of a system of particles in a magnetic field. It is shown that the equilibrium is stable if the magnetic field is sufficiently strong and the particles are sufficiently close to the equilibrium state. The fifth part of the paper is devoted to the study of the stability of the equilibrium state of a system of particles in a magnetic field. It is shown that the equilibrium is stable if the magnetic field is sufficiently strong and the particles are sufficiently close to the equilibrium state.

Fig. 2.1 Hough functions. Left side: the first three gravity or positive equivalent depth modes. Right side: the first three Rossby or negative equivalent depth modes. Arbitrary vertical coordinate.





nates the solution $Be^{-i\lambda_n z^*}$, where λ_n is now a pure positive imaginary quantity. This is the boundedness condition.

Both upper boundary conditions can be accounted for by using a single equation at the upper boundary, which is obtained after going through the same process as for the lower boundary condition:

$$\frac{d\hat{w}_n}{dz^*} - i\lambda_n \hat{w}_n = 0 \quad (25)$$

For Laplace's tidal equation, a boundedness condition is applied at the poles, which (for $s = 1$) actually causes all the symmetric modes to go to zero at the poles.

At this point, the general discussion of the classical tidal theory is concluded. The assumptions and simplifications which are made in order to make the problem tractable have been outlined. The initial set of equations has been shown, and the method for obtaining solutions has been discussed. It may be debated whether or not the problem has been oversimplified. However, if it is able to give an unambiguous first order understanding of and explanation for the migrating diurnal thermal tide, then the purpose of this research has been achieved.

3. METHODOLOGICAL IMPROVEMENTS

In this research, three methodological improvements have been incorporated into the classical tidal calculation in an effort to obtain theoretical values for the tropospheric tidal variations which are in better agreement with values derived from observational data. The three improvements are these: (1) A radiative transfer routine was used to obtain a more accurate tropospheric forcing function to put into the thermodynamic energy equation (TEE). (2) A greater number of Hough functions were used to represent the forcing and the responses of the various tidal parameters. (3) The results were produced with a greater resolution in the latitudinal direction.

3.1 Improved Forcing

As mentioned in the preceding chapter, three types of heating were used in this research to force the diurnal tidal response: heating due to absorption of shortwave (SW) radiation by water vapor (hereafter called H₂O heating), cumulus heating, and heating due to absorption of SW radiation by ozone (ozone heating). The first two sources lie mostly or totally within the troposphere. Ozone heating occurs primarily in the stratosphere and lower mesosphere.

The chief objective of this research is to obtain a better theoretical understanding of the structure and amplitude of the diurnal tide in the troposphere. In order to attain this goal, it is essential to have a representation of the tropospheric forcing which is as accurate

as possible. A theoretical argument can be given to support this claim (Butler and Small, 1963). The only forcing which occurs above the troposphere is (presumably) that due to ozone heating. Though this forcing is very strong, it is almost totally ineffective in producing any significant tropospheric response. The layer of ozone heating has a depth of about 60 km. Most of the forcing in the ozone layer of the tropics projects onto the Hough functions with positive equivalent depths - the modes which permit vertical propagation of energy. However, the vertical wavelengths associated with these modes are much smaller than the thickness of the ozone layer, with the longest wavelength being 27.9 km, the second longest being 11.1 km, and all the rest being shorter. It happens that, for a thick band of forcing in which waves with short wavelengths are initiated along a vertical continuum, destructive interference among waves initiated at different points along the continuum will effectively destroy any response above or below the region of forcing. Thus, the ozone forcing produces little response in the troposphere, and therefore almost all of the tropospheric response must be the result of tropospheric forcing. It follows that the structure of the diurnal tide in the troposphere will depend very much on the structure of the tropospheric forcing.

A radiative transfer routine was used only for computing the H_2O heating in the troposphere and lower stratosphere. (The reason why the ozone heating could not be treated in the same way is discussed on the following page.) Temperature and water vapor mixing ratio profiles were entered into a simple broadband shortwave radiative transfer routine developed under Stephen Cox (Cox, et al., 1976). Temperature profiles (Fig. 3.1) for spring equinox were obtained by averaging the January and

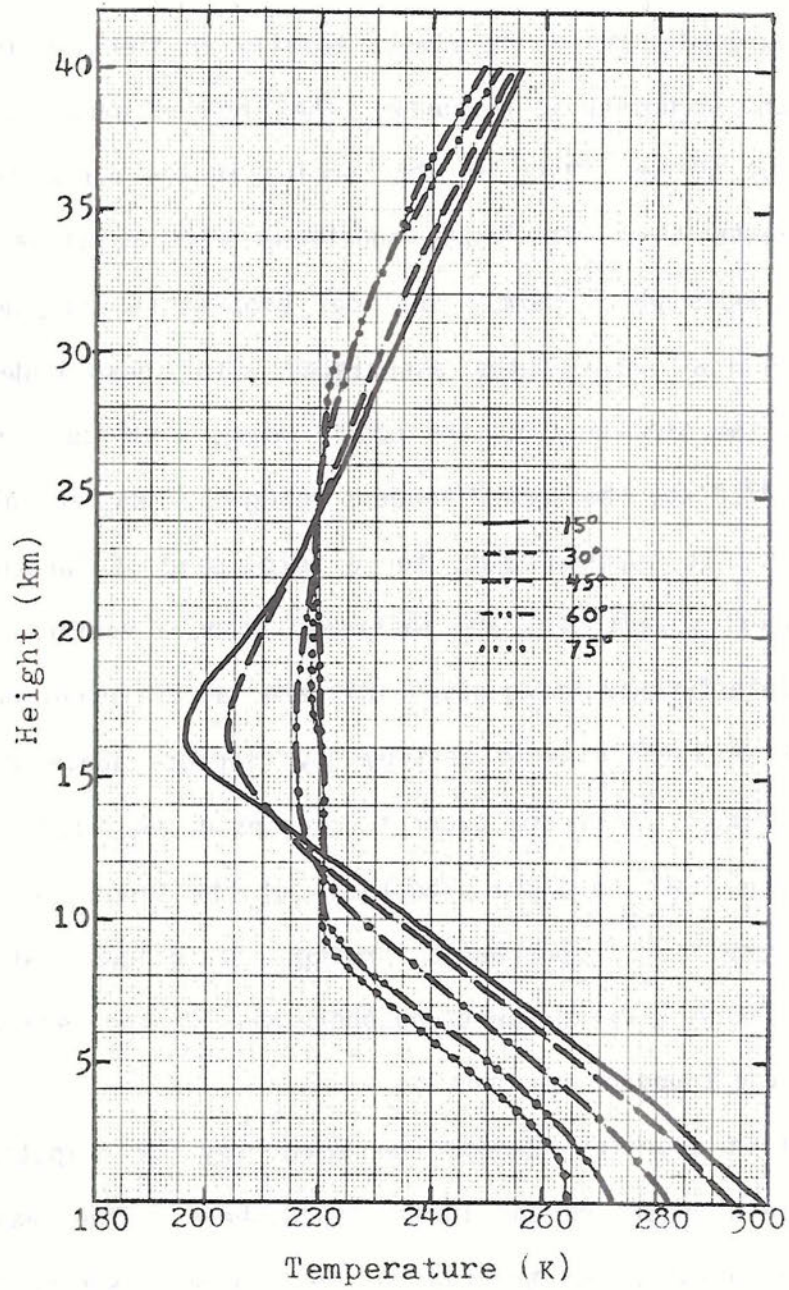


Fig. 3.1 Temperature profiles used in the radiative transfer routine.

July profiles in the U.S. Standard Atmosphere Supplements, 1966. Water vapor profiles up to 10 km (Fig. 3.2) were obtained from the same source, while values at higher levels were obtained from Manabe and Strickler (1964) and from Mastenbrook (1968). The radiative transfer routine computed the H_2O heating rate as a function of date, latitude, time of day, and height. The examples shown for equinox at the equator (Fig. 3.3) and for several heights (Fig. 3.4) show the variations of structure which occur. The SW heating is, of course, taken to be zero at night. At each height and latitude, the daily heating curve was subjected to Fourier analysis in order to obtain the diurnal component (Fig. 3.5). In terms of the notation of the preceding chapter, where

$$J^i = J_{H_2O}^{\sigma, s}(\theta, z^*) e^{i(\sigma t + s\phi)},$$

$J^{\sigma, s}$ has now been determined at discrete values of θ and z^* for $\sigma = 2\pi/\text{day}$ and $s = 1$. The fact that $J^{\sigma, s}$ is not separable into independent functions of θ and z^* adds some difficulty to the problem, in that $J^{\sigma, s}$ must eventually be projected onto the Hough functions at each level where radiative heating values are obtained.

Lindzen, in his work on the diurnal tide, and others who have followed him, used a simple functional form (separable in θ and z^*) to describe the H_2O heating (Lindzen, 1966). This function, based upon some simple physical considerations and a few numbers in the literature on radiative transfer, was extended at least into the mesosphere, whereas the H_2O heating in this research only extended to about 40 km. A comparison between the vertical structure of the two H_2O heating functions at the equator is shown in Fig. 3.6. The specific vertical structure of the new function is quite different, but the general shape and magnitude are not far different from Lindzen's.

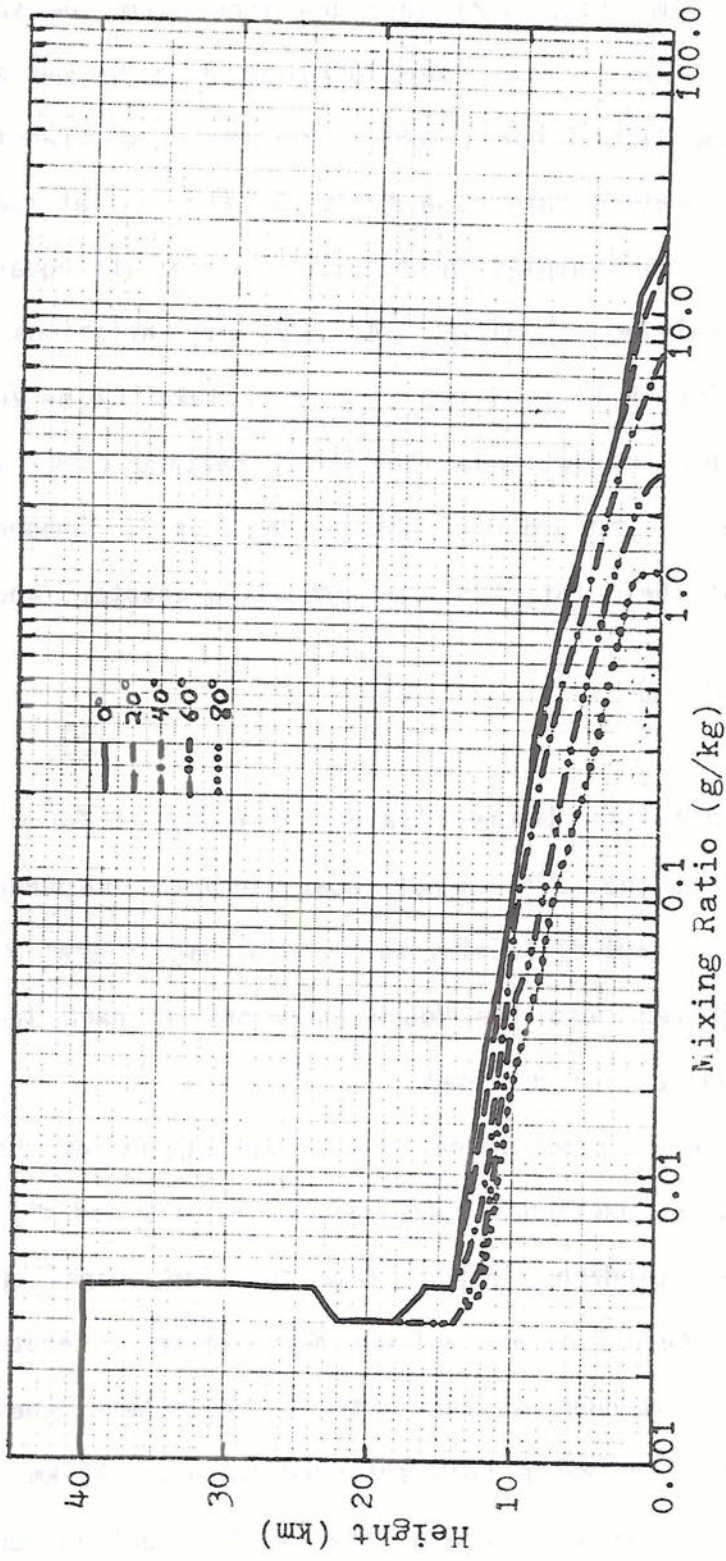


Fig. 3.2 Water vapor mixing ratio profiles used in the radiative transfer routine.

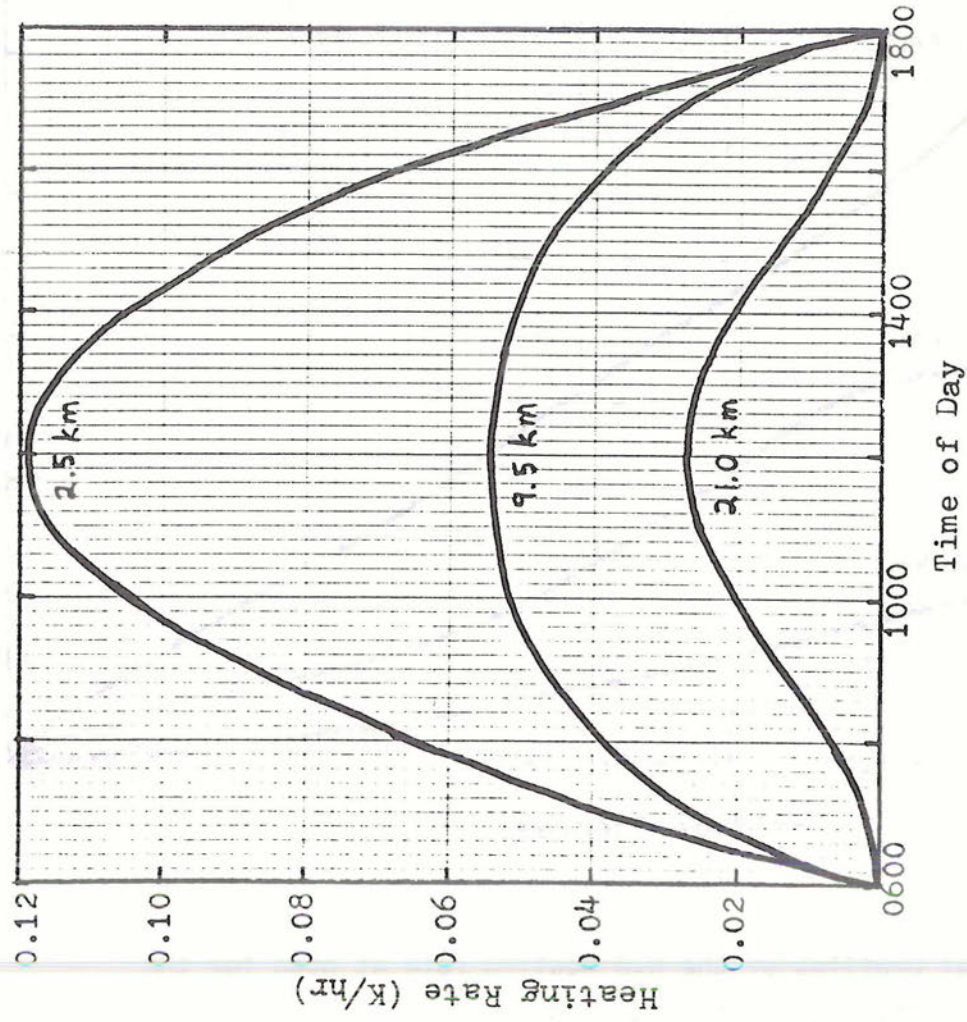


Fig. 3.3 H₂O heating rate at equinox as a function of the time of day for three different altitudes. (The heating rate is zero at night.)

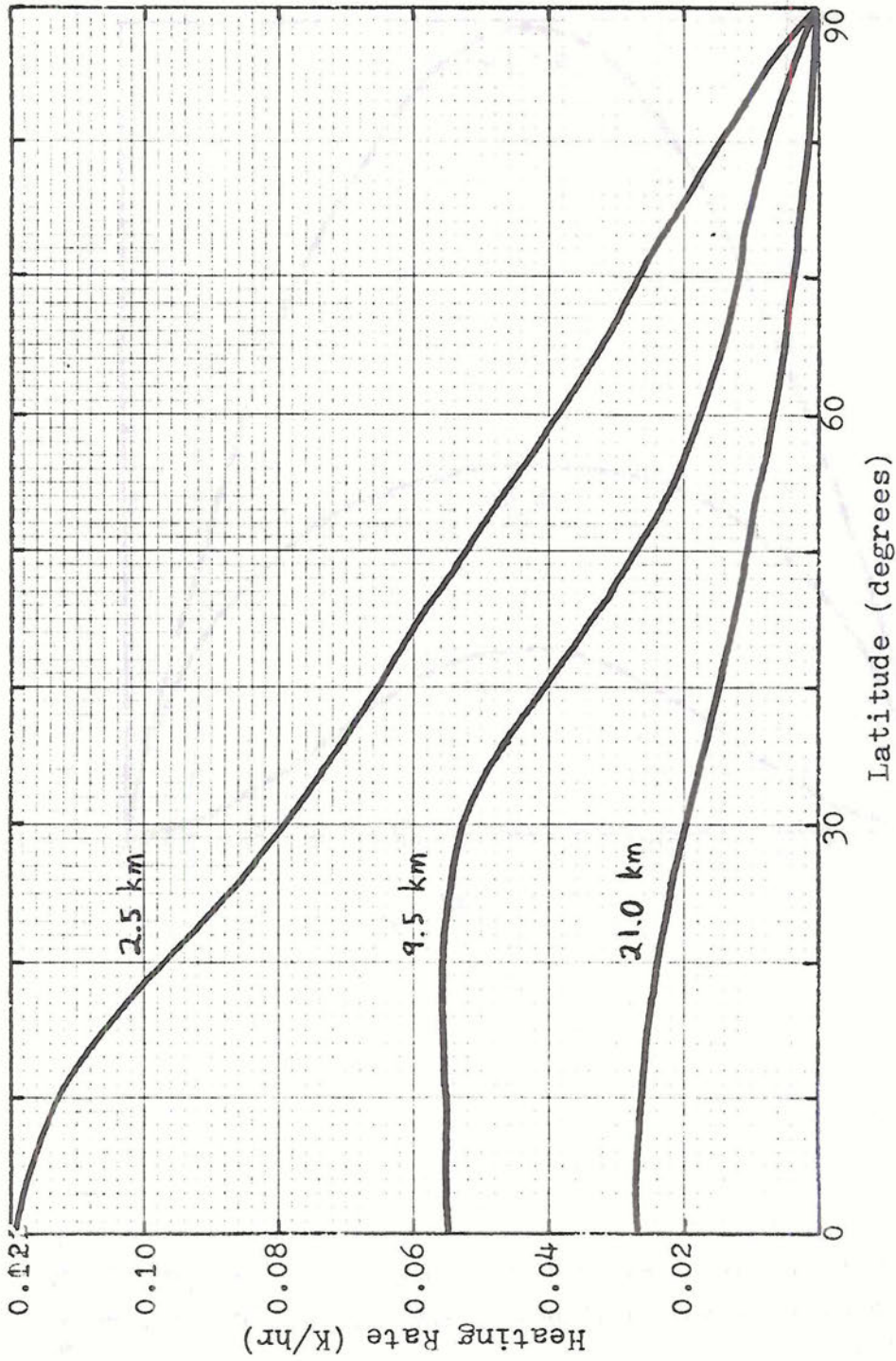


Fig. 3.4 Latitudinal profiles of the H_2O heating rate at noon for the same three altitudes as in Fig. 3.3.

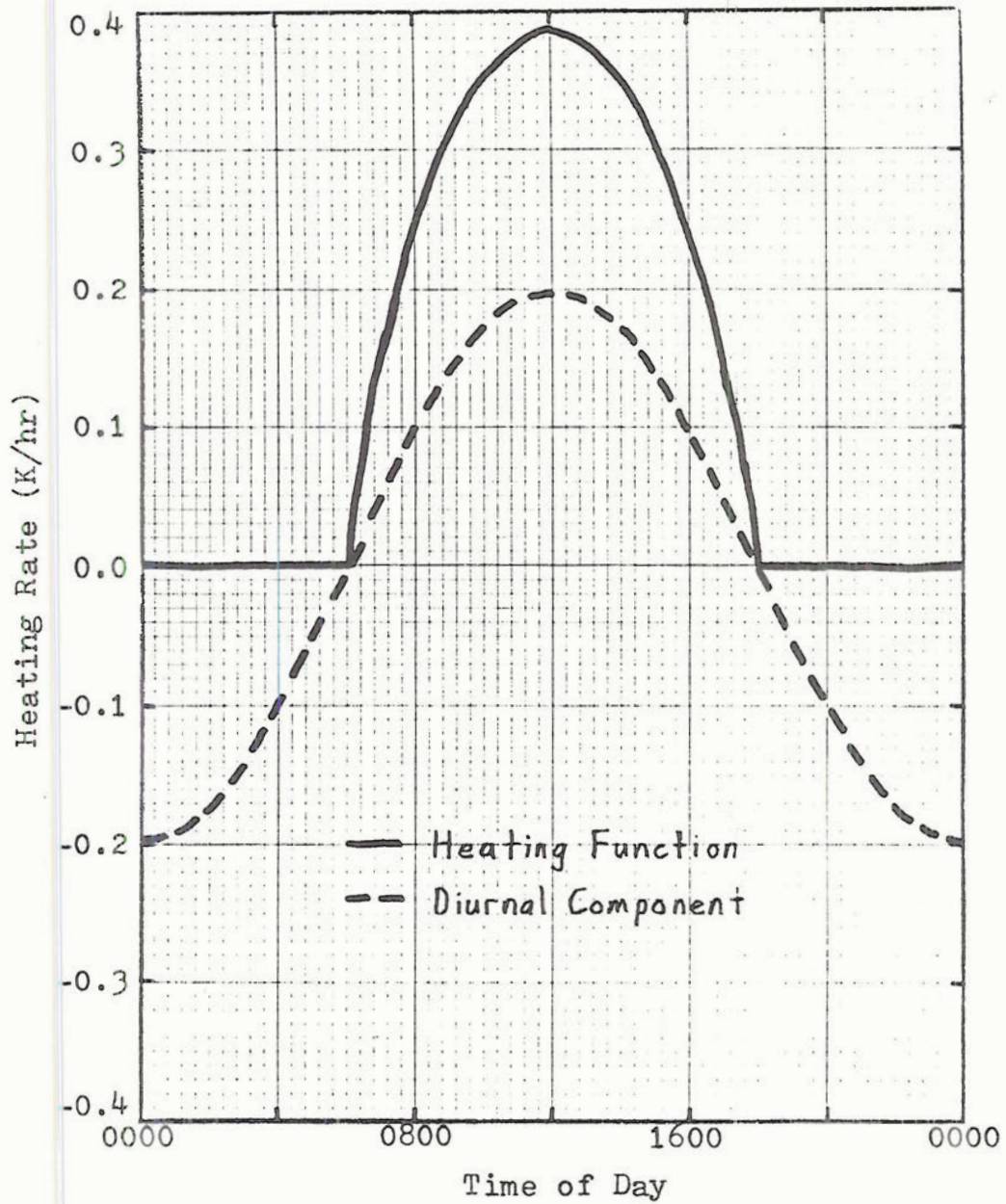
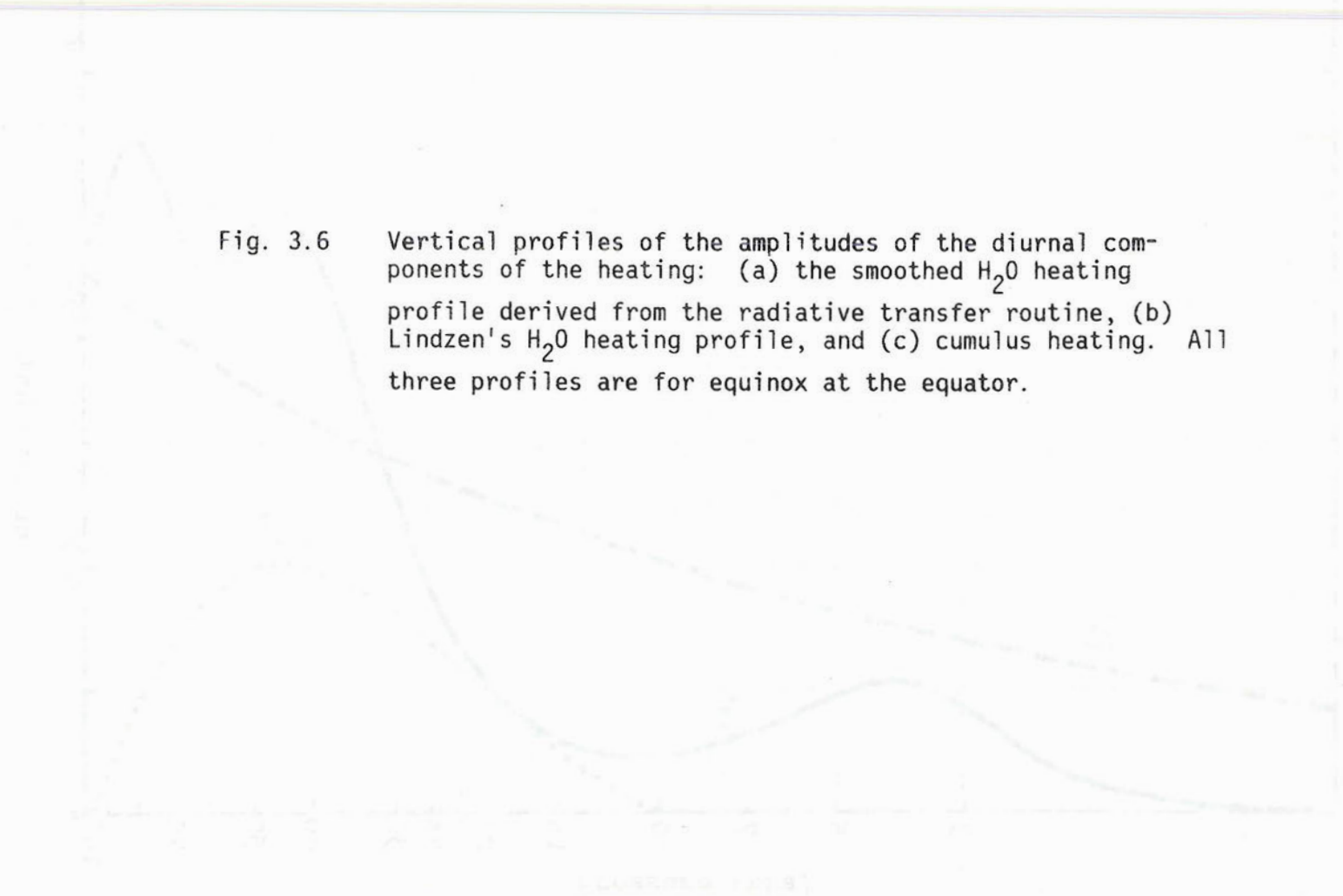


Fig. 3.5 An example showing the diurnal component of the heating function.

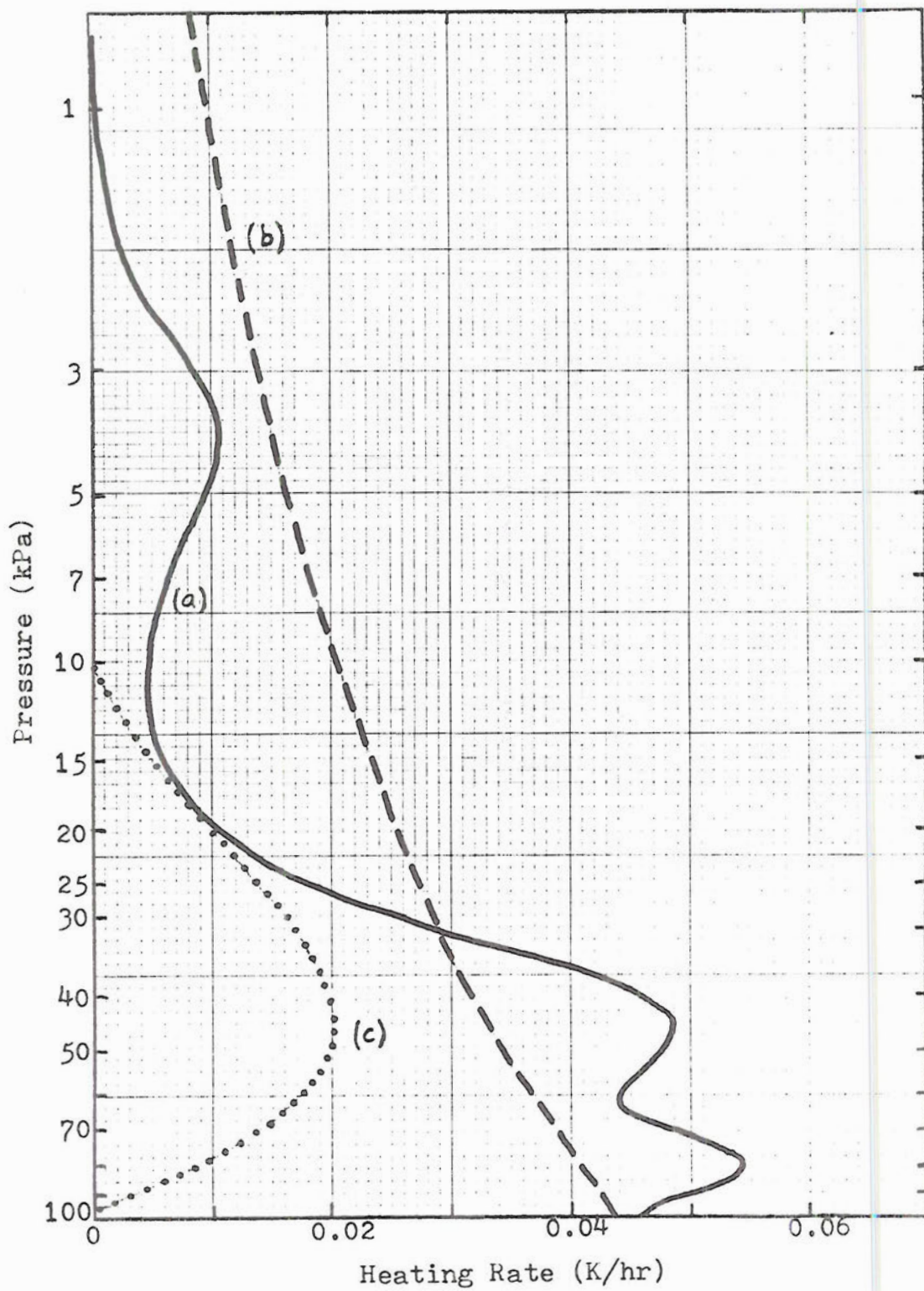


Figure 1: A graph showing two bell-shaped curves, one taller and narrower than the other, both centered on the horizontal axis.



The figure shows three vertical profiles of heating amplitudes. The vertical axis represents pressure in mb, with major ticks at 1000, 500, and 200. The horizontal axis represents altitude in km, with major ticks at 0, 5, 10, 15, and 20. Profile (a), the smoothed H₂O heating, is a solid line that starts at approximately 1000 mb (0 km) with a value of about 0.5, decreases to a minimum of about 0.1 at 1000 mb (5 km), and then rises to a secondary peak of about 0.3 at 500 mb (10 km) before decreasing again. Profile (b), Lindzen's H₂O heating, is a dashed line that starts at about 0.5 at 1000 mb and decreases steadily to about 0.1 at 200 mb. Profile (c), cumulus heating, is a dotted line that starts at about 0.5 at 1000 mb, peaks at about 0.8 at 800 mb (7 km), and then decreases to about 0.1 at 200 mb.

Fig. 3.6 Vertical profiles of the amplitudes of the diurnal components of the heating: (a) the smoothed H₂O heating profile derived from the radiative transfer routine, (b) Lindzen's H₂O heating profile, and (c) cumulus heating. All three profiles are for equinox at the equator.



It was originally intended that ozone heating and carbon dioxide heating would also be computed by using the same radiative transfer routine. However, after tinkering with the initial results for quite some time, the undocumented fact was discovered that the routine cannot give valid results above 0.4 kPa. Both the ozone and carbon dioxide heating extend to much greater heights than this. Lacking a more sophisticated radiative transfer model and being unable to locate the desired data in the literature, it was decided to utilize Lindzen's ozone heating as a reasonable approximation to the real heating (Lindzen, 1966). When the results of this research later showed the tropospheric response to be quite insensitive to the exact structure and magnitude of the ozone forcing, it was determined that this was a satisfactory choice. The ozone heating function used in this research looked like this:

$$J_{03}^{\sigma, s} = \sigma C_p e^{0.0116(z-z_B)} \sin \left(\pi \frac{(z-z_B)}{(z_T-z_B)} \right) \cdot f(\theta),$$

where z is now the mean geopotential height and $f(\theta)$ is very nearly a cosine function. The ozone heating is confined between $z_B = 18$ km and $z_T = 78$ km. The vertical structure of this heating function at the equator is shown in comparison to the H_2O forcing in Fig. 3.7.

The CO_2 forcing is negligible in the region where Cox's model is valid, but it may not be negligible everywhere in the atmosphere. Other minor constituents might also contribute to the SW heating of the upper atmosphere at various levels. However, it had to be assumed that their contribution to the tropospheric diurnal tidal response would be negligible.

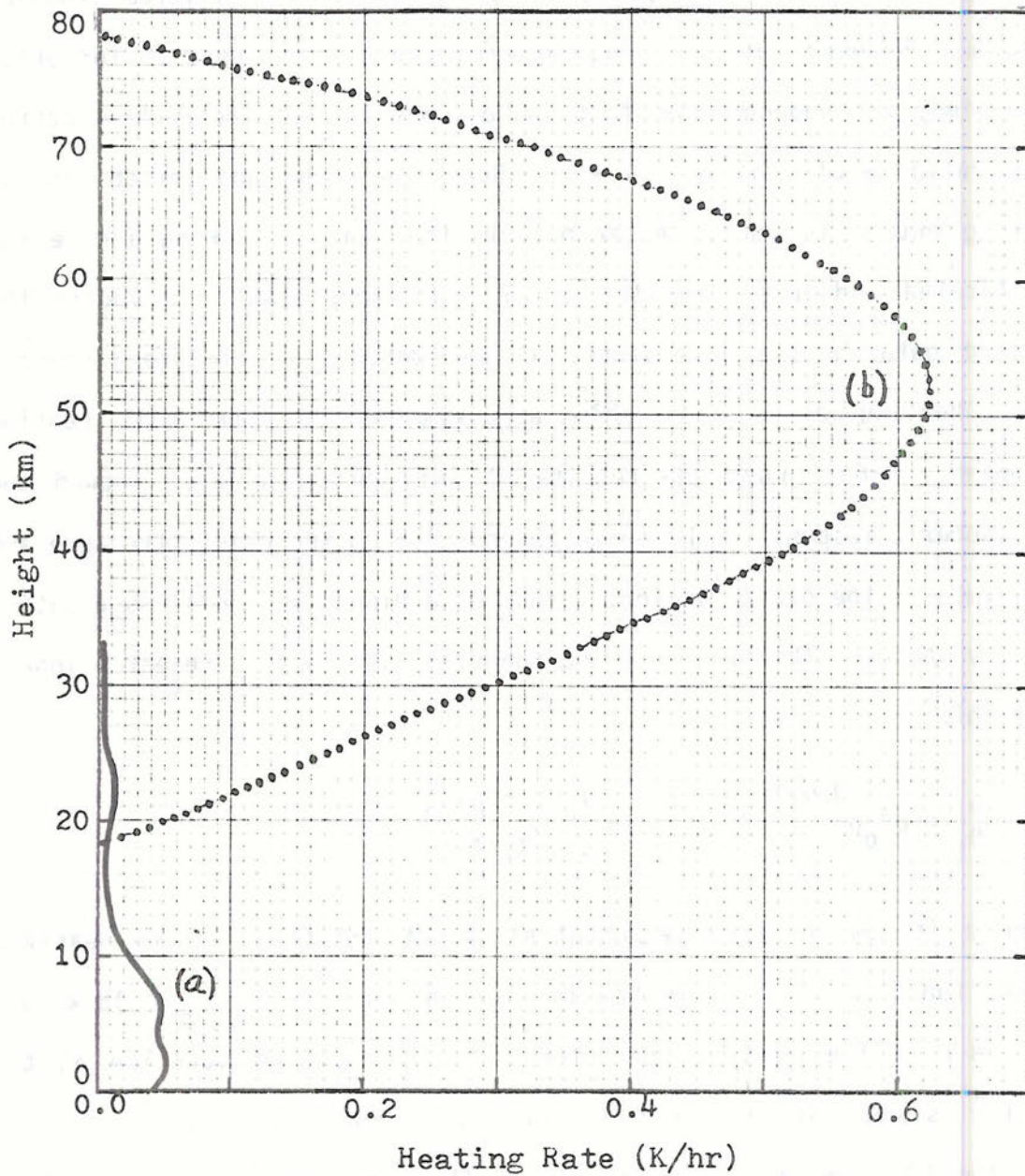


Fig. 3.7 Vertical profiles of the amplitudes of the diurnal components of the H_2O and ozone heating rates: (a) the smoothed H_2O heating profile derived from the radiative transfer routine, and (b) Lindzen's ozone heating profile. Both profiles are for equinox at the equator.

Finally, while discussing the improved tropospheric heating function, it would also be appropriate to discuss cumulus heating. It was hypothesized that diurnal variations in the rate of latent heat release might have a significant effect upon the amplitude and phase of the diurnal tide in the troposphere. To test this hypothesis, a very crude cumulus heating function was added to the SW heating. Like the ozone heating, the cumulus heating was assumed to be of a prescribed functional form separable in θ and z^* .

$$J_{CH}^{\sigma, s}(\theta, z^*) = A e^{bz^*} \sin \left(\pi \frac{z^* - z_B^*}{z_T^* - z_B^*} \right) e^{-\left(\frac{\theta}{30}\right)^2} e^{i\rho},$$

where $A = 1.23 \times 10^{-2} \text{ W/kg}$, $b = -0.806$, z_B^* is the bottom of the latent heat release at 95.1 kPa, z_T^* is the top at 10.0 kPa, and ρ is the phase of the cumulus heating. In a more recent paper, Lindzen shows a table of the amplitudes of the diurnal and semi-diurnal components of the rainfall rate for various tropical stations (Lindzen, 1978). The value based upon the data from Jacobson (1976), which was an average for a number of small tropical island stations, was chosen to be the value for the amplitude of the diurnal variation at the equator for the purposes of this research. At best, the assumed diurnal variation of the rainfall rate, with an amplitude of 0.126 cm/day and reaching a maximum at 0647 LT, is only approximate. The functional form of the latent heat release written above is an educated guess. The values of b and A were chosen so that when this function is integrated over the vertical extent of the layer in which the latent heat is released, it will yield a heating value equivalent to 0.126 cm of rainfall per day. The vertical

profile of this heating at the equator is shown in Fig. 3.6. The horizontal profile is just a Gaussian curve which falls off to a value of $1/e$ at 30° from the equator.

3.2 Improved Hough Mode Representation

In Lindzen's study of the diurnal tide, he projected the latitudinal structure of his heating function onto only five Hough functions -- the first three positive equivalent depth modes and the first two negative equivalent depth modes (Lindzen, 1968). The sum of these five projections makes a very rough approximation to the heating profile, as is shown on the left side of Fig. 3.8. Even in the tropics, the shape of the five mode representation does not very closely resemble the actual structure of the heating; while in middle and upper latitudes, the representation is quite poor. Presumably, these representation errors might be reflected in the response calculated by using this distorted heating function, thereby producing artificial and misleading features -- particularly in the detailed latitudinal structure which is investigated here, but which others have not examined.

In order to alleviate this problem, sixteen modes were used to represent the longitudinal structure of the heating and of the different tidal variable responses. Eight positive and eight negative equivalent depth modes were used. The improvement that is made in representing the heating is clearly shown on the right side of Fig. 3.8. Notice that the largest representation errors occur between 25 and 40 degrees from the equator and very near the pole. Somewhat unusual behavior in the calculated responses might be expected in these areas.

An extreme example of the difference that can occur in the calculated response of a particular variable is shown in Fig. 3.9. This

... of this ... the ... value of ...

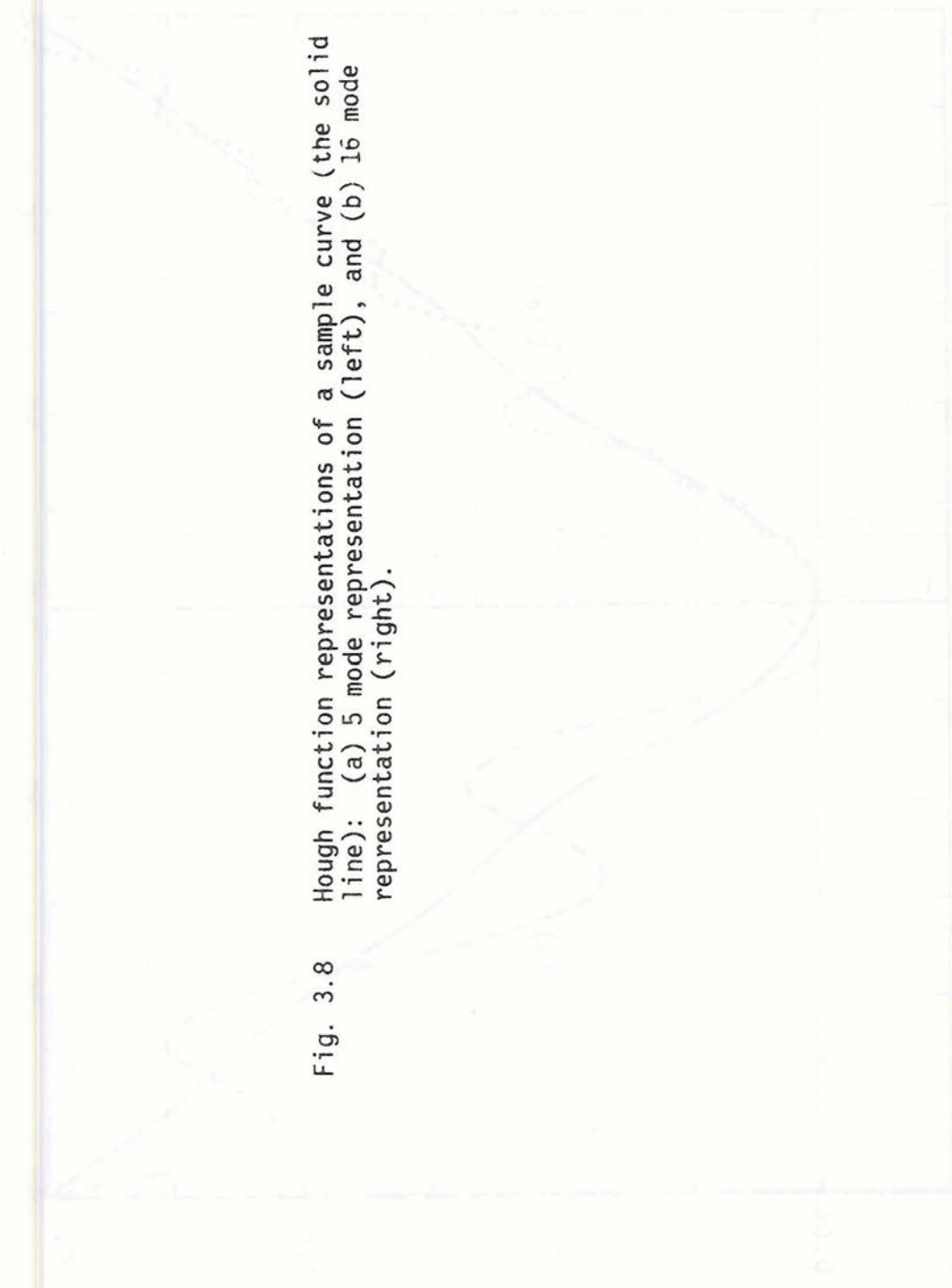
Experimental results and discussion

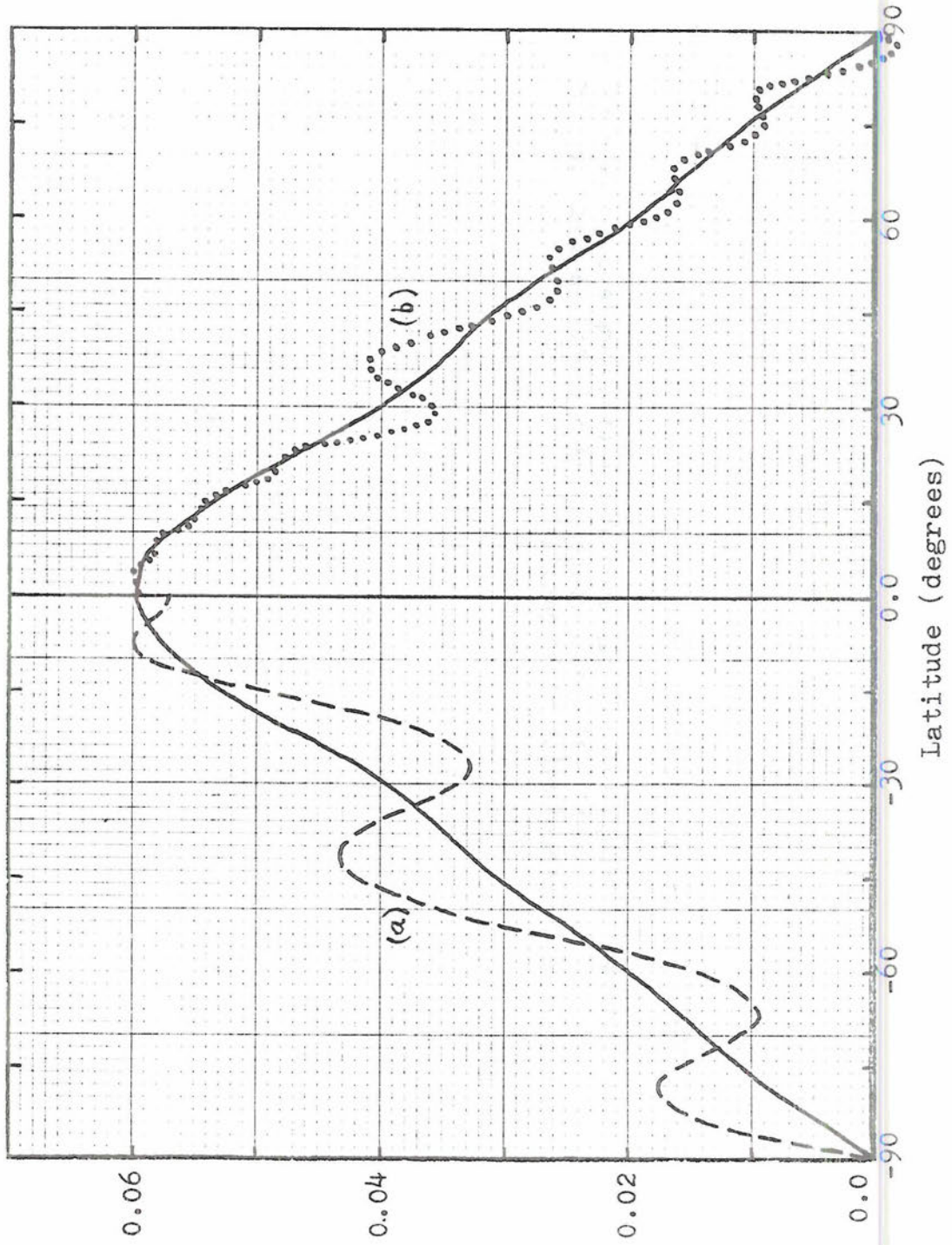
The ... of the ... the ... of the ...

In order to ... the ... of the ...

An ... of the ... of the ...

Fig. 3.8 Hough function representations of a sample curve (the solid line): (a) 5 mode representation (left), and (b) 16 mode representation (right).





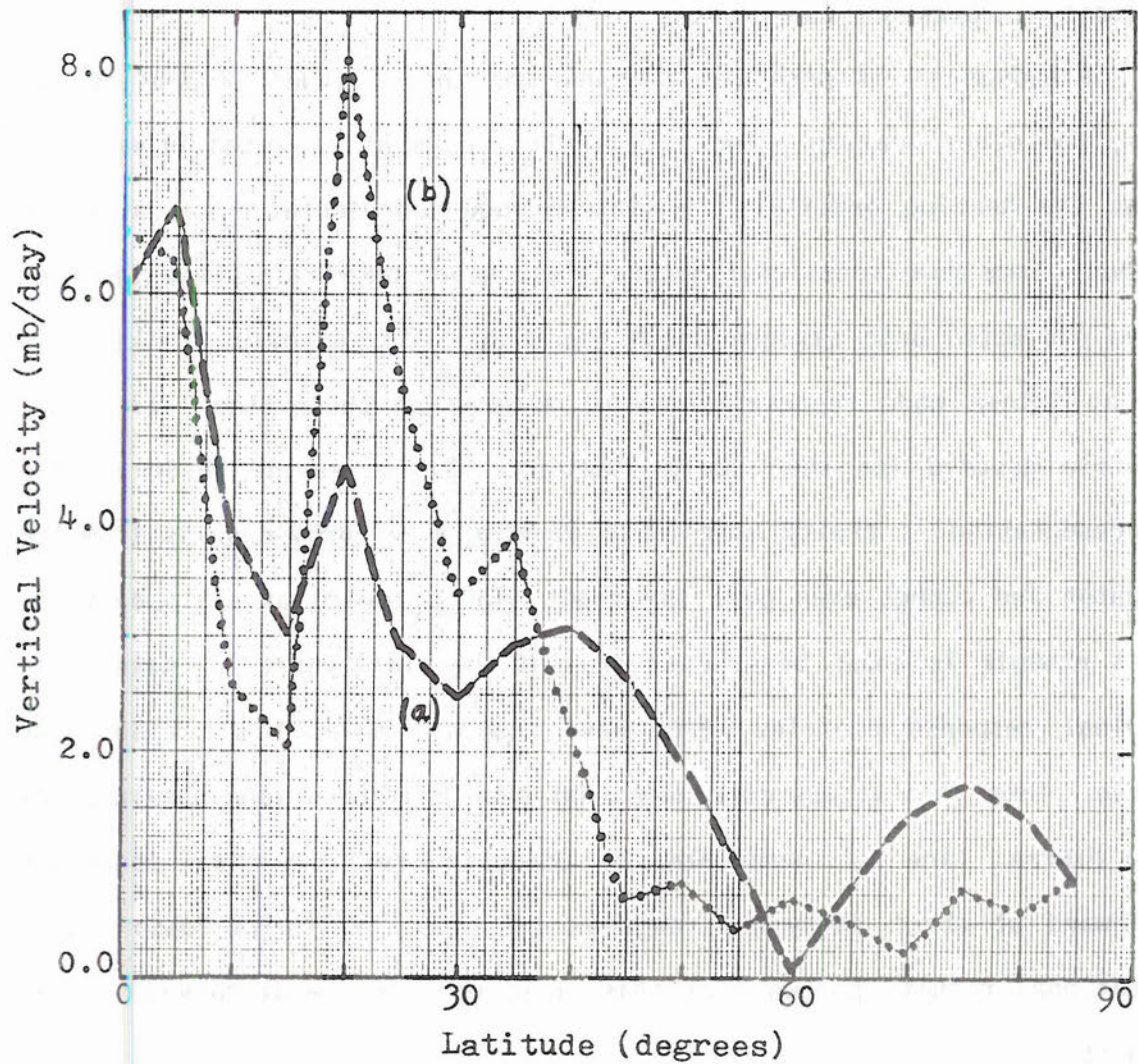


Fig. 3.9 Comparison of the horizontal (θ) structure of the amplitude of the tidal w response at 52.7 kPa using (a) five and (b) sixteen Hough modes to represent both the forcing and the response. (Data are plotted at 5° increments.)

example shows how the latitudinal profile of the w response produced by the five mode representation of the heating differs from the w response produced by the sixteen mode representation, where w is the vertical velocity in pressure coordinates.

Although it is possible to speak of the latitudinal profile of, say, the ozone heating being a cosine curve, what is actually meant is that the heating profile is a sixteen mode representation of a cosine curve. Some functional heating profiles cannot be well represented even when projected onto sixteen Hough functions. The example in Fig. 3.10 is a sixteen mode representation of a Gaussian curve--the latitudinal profile assumed for the cumulus heating. As is readily observed, the representation is pretty unreliable at more than forty degrees from the equator and cannot even give the right sign poleward of sixty degrees. This example is shown because several of the tidal variables have latitudinal response profiles which have shapes similar to this Gaussian curve. From this it was concluded that even a sixteen mode treatment of the diurnal tide is inadequate for computing reliable tidal responses poleward of about forty-five degrees latitude. For this reason, computational results poleward of this point will not be discussed in this report.

3.3 Improved Presentation of Results

Since the chief focus of this research is on the diurnal tidal variations in the tropical troposphere, it was imperative to obtain results with as fine a vertical and horizontal resolution as required to resolve the structure of the tide. Lindzen presented vertical profiles of the tidal response for several tidal variables at 15° increments of latitude. It was felt that this might be inadequate to resolve the

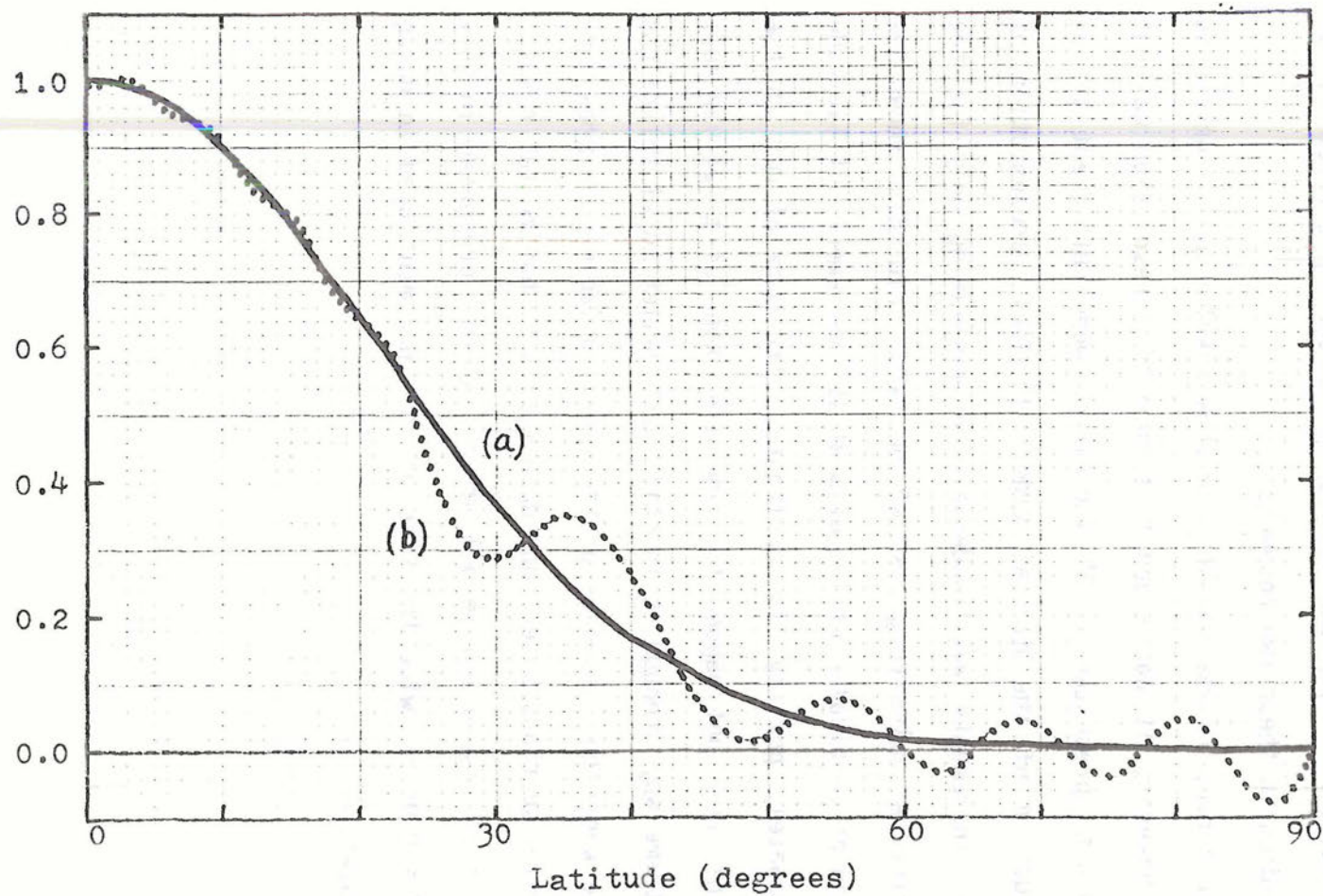


Fig. 3.10 (a) A Gaussian curve ($e^{-(\theta/30)^2}$) and (b) the sixteen Hough mode representation of that curve. This was the θ -structure of the cumulus heating.

latitudinal structure of the diurnal tide; and that, conceivably, one or more of the 15° increments could fall near nodes in the responses of some tidal variables. Thus, the results presented by Lindzen (1966) could be misleading in these two respects.

In this research, it was possible to show results at 1° increments of latitude. However, it was found that such fine resolution was not necessary. Results presented at 5° increments were sufficient to resolve the structure of the diurnal tide. In fact, presentation of results at 15° increments was inadequate or misleading only for the vertical velocity variables (e.g., w , w^* , ω , Γw^*). Fig. 3.11 shows how the presentation of vertical profiles of w at 15° increments of latitude would not adequately portray the horizontal structure of w . In the troposphere, this does not happen for any other kind of tidal variable in such an extreme way, though it is still much easier to visualize the tidal structure when the responses of the tidal variables are presented as contoured cross sections based upon data with a 5° horizontal resolution. The vertical resolution in all of the results presented in this report was $\Delta z^* = 0.04$ -- twice the size of the increment used in doing the tidal calculation.

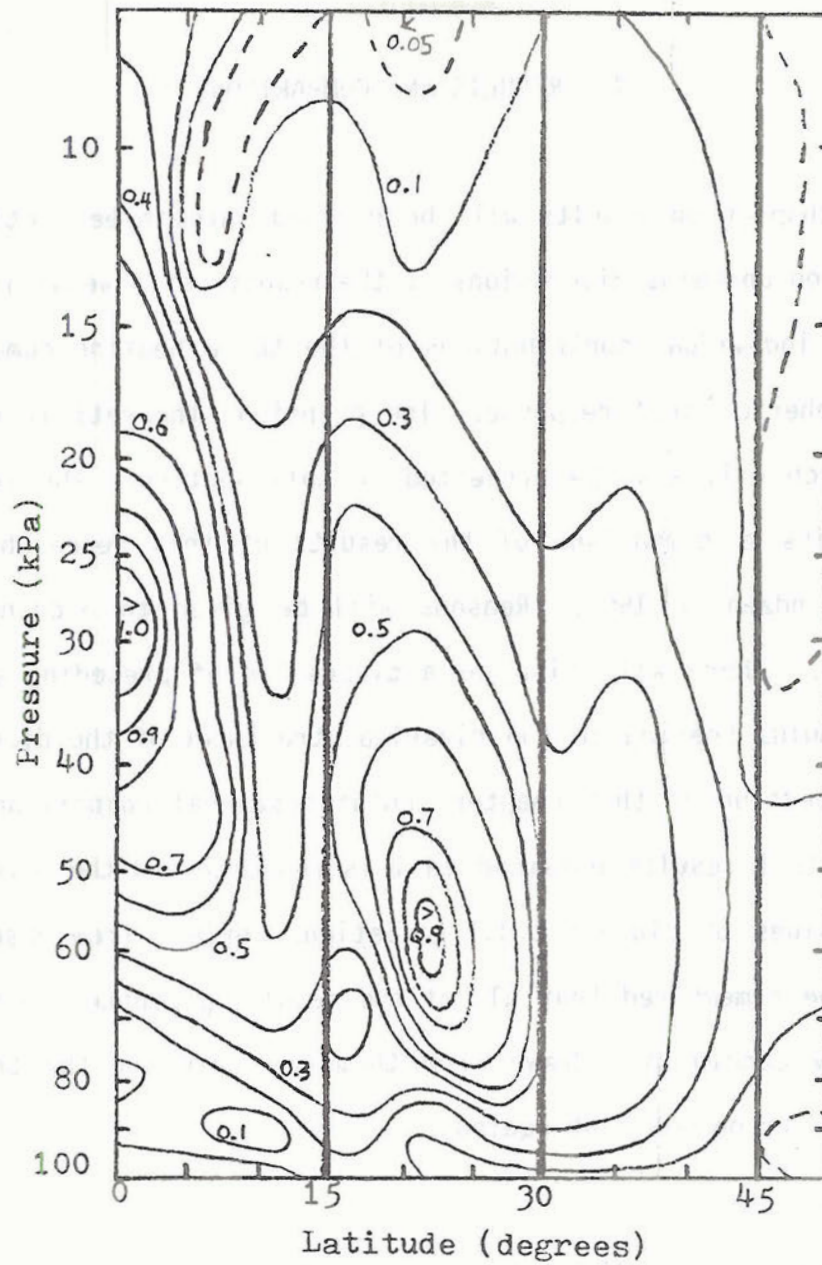


Fig. 3.11 A θ - z^* cross section of the amplitude of the tidal vertical velocity field forced by SW heating. Contour interval: 0.1 kPa/day. The 15° latitude increments are the latitudes for which Lindzen showed results.

4. RESULTS AND COMPARISONS

This chapter on results will be divided into three sections. The first section contains discussions of the results of a sensitivity study and of the individual contributions of the three heating components to the tropospheric tidal response. The principal theoretical results of this research will also be presented in this section. The second section contains a comparison of the results of this research to those shown by Lindzen in 1967. Reasons will be given to account for the differences. There will also be a discussion of preceding efforts to include cumulus heating in the classical treatment of the diurnal tide. The final section of this chapter contains several comparisons between the theoretical results obtained in this research and the more recently reported values of diurnal tidal variations derived from observations. It should be remembered that all of the results presented in this chapter and any conclusions drawn from them are only for the tropical or sub-tropical troposphere at equinox.

4.1 Results

Before presenting the principal results of this research, it would first be appropriate to discuss the sensitivity study and the study of the contributions of the three heating components which were carried out. This will aid in providing a better understanding of the numerical results presented later and in providing a greater confidence in their significance.

4.1.a Sensitivity study

In order to determine which parameters most sensitively influence the structure of the amplitude and phase fields of the diurnal tidal response, five parameters were varied individually in different runs of the tidal calculation. None of the variations produced order-of-magnitude changes in the amplitude fields; nevertheless, several produced significant changes in the results that should be noted.

In the first test, the number of Hough functions (or modes) used in the calculation was varied. One model run used the same five modes used by Lindzen, while the second run used an additional ten modes. In comparing the results, significant differences were noticed in both the vertical and horizontal structures of the responses. In the vertical direction, the fifteen mode response tends to oscillate (with height) around the vertical profile of the five mode response at the same latitude. This is a result of the contribution of the higher order positive equivalent depth modes with their shorter vertical wavelengths. There are also significant differences in the horizontal structures of the two tidal responses. Five modes not only provide a poor representation of the θ -profile of the heating, but they are also inadequate to capture the finer horizontal structure of the tidal response. In particular, the fifteen mode run tended to concentrate a greater fraction of the response in the tropics and subtropics than the five mode run did. At more than ten degrees from the equator, the differences between the vertical profiles of amplitude for the two runs were frequently 30 to 50 percent or more through much of the troposphere. The phase differences are generally less pronounced. It would be interesting to see what changes would occur if the number of modes were again tripled. Hopefully, the effects would be less observable.

The second test was to observe the changes caused by moving the level of the top of the model. Generally, the model calculation was terminated at the mesopause. However, in one case, realistic thermospheric temperature and static stability profiles up to 200 km were added to the top of the model domain, and the results were computed regardless of whether or not the thermospheric physics were correct. The results showed that this change generally produced fairly minor differences in the tropospheric response for both amplitude (less than 10%) and phase (less than one half hour). Also, the fractional size of the changes in both phase and amplitude were nearly constant with height.

The third test requires some explanation. In Laplace's tidal equation, there is a quantity $(\mu^2 - f^2)$ which appears in the denominator of the θ operator, where $\mu = \sin \theta$ and $f = \sigma/2\Omega$ is the angular frequency of the tidal component divided by twice the angular frequency of the earth's rotation. The quantity σ is determined from the length of the solar day, while Ω is dependent on the length of the sidereal day. Thus, f has a value of very nearly, but not quite 0.5. At 30° from the equator, $\mu = \pm 0.5$, and consequently the value of $(\mu^2 - f^2)^{-1}$ becomes quite large. In the Galerkin treatment of the diurnal tide, this quantity appears only at the end of the tidal calculation, when producing the graphical, two dimensional representation of the solution. Even then, this quantity only appears in the computation of the horizontal wind components. As a test, f was set equal to 0.5 in order to produce an apparent singularity at the grid point 30° away from the equator. The vertical profiles of the wind perturbations were not computed at this

point (though they could have been with an application of l'Hospital's rule). No significant change occurred in the wind fields away from this point.

In the fourth set of tests, the structure of the H_2O heating was varied. The two basic vertical structures used are shown (at the equator) in Fig. 2.6. The horizontal structure of the heating function derived from the radiative transfer routine varies with height. The horizontal structure of the other heating function was very nearly the same as that used by Lindzen (1967) and did not vary with height. Two versions of the heating function derived from the radiative transfer routine were used. One was a slightly smoothed function (in the vertical) of the other. A three point smoothing scheme was used, giving a 50% weighting to the center point and a 25% weighting to each neighboring point. (At the point in the calculation where the smoothing was done, the vertical spacing between data points was 0.5 km below 10 km and 1 km above 10 km.) This smoothed profile is what is shown in Fig. 2.6. The tidal responses to the smoothed and unsmoothed heating functions showed no significant differences. The smoothed function merely resulted in a slightly smoother response. Since the smoothed profile was considered to be a little more representative of the real atmosphere, it was used for producing the results shown later in this section.

Two runs were made using an exponential H_2O heating profile like Lindzen's, where in the second case the heating function was just multiplied by a constant value of 1.26. The ozone heating used in both cases was exactly the same. The result of making this change was just to

multiply the amplitude profile by nearly the same constant (1.26) throughout the troposphere while leaving the phase profiles very nearly identical. This provides evidence that the tropospheric response to the ozone heating must be small. The changes in amplitude and phase were much more significant in the stratosphere where the differing relative magnitudes of the two heating functions make a difference.

The greatest difference noted in this fourth set of tests was that between the response to the smoothed H_2O heating function derived from the radiative transfer routine and the response due to Lindzen's H_2O heating function. Examples of this are shown in Figs. 4.1 and 4.2. Notice in particular how radically different the vertical structures for the amplitude and phase profiles of the temperature perturbations are at fifteen degrees from the equator. The effects are much less pronounced for the amplitude and phase profiles of w at the equator, but they are still significant in the lower troposphere. Because of the fairly complicated structure of the smoothed H_2O heating function, it is not easy to find any consistent differences between the structures of the responses of the different tidal variables using the two heating functions. Suffice it to say that the differences can be substantial. Therefore, as stated before, in order to obtain an accurate portrayal of the diurnal tide in the troposphere, it is necessary to use a fairly representative tropospheric forcing.

It is also essential to use good temperature and static stability profiles. Varying these profiles was the fifth test of the sensitivity of this model. The results of this test indicate that the model results are quite sensitive to fairly small changes in the static stability

The first part of the report is devoted to a general survey of the situation in the country. It is followed by a detailed analysis of the economic and social conditions. The author then discusses the political situation and the role of the government. The report concludes with a series of recommendations for the future.

The author's analysis is based on a wide range of sources, including official statistics, interviews with government officials, and observations made during his travels in the country. He provides a clear and concise summary of the current situation, and his recommendations are well-founded and practical.

The report is a valuable contribution to the understanding of the country's development. It provides a comprehensive overview of the various factors that are influencing the country's progress, and it offers a clear path forward for the government and the people.

The author's analysis is based on a wide range of sources, including official statistics, interviews with government officials, and observations made during his travels in the country. He provides a clear and concise summary of the current situation, and his recommendations are well-founded and practical.

The report is a valuable contribution to the understanding of the country's development. It provides a comprehensive overview of the various factors that are influencing the country's progress, and it offers a clear path forward for the government and the people.

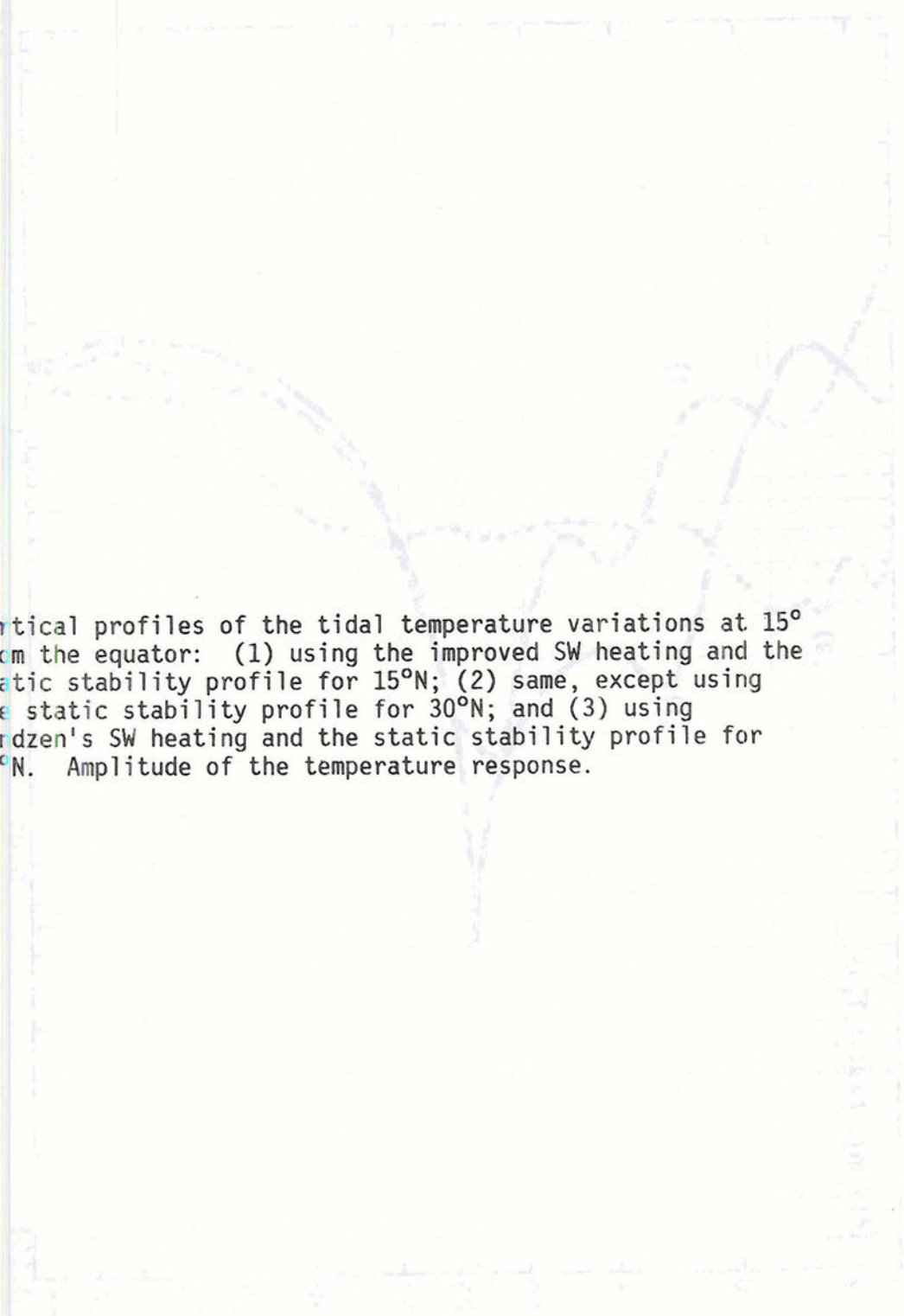
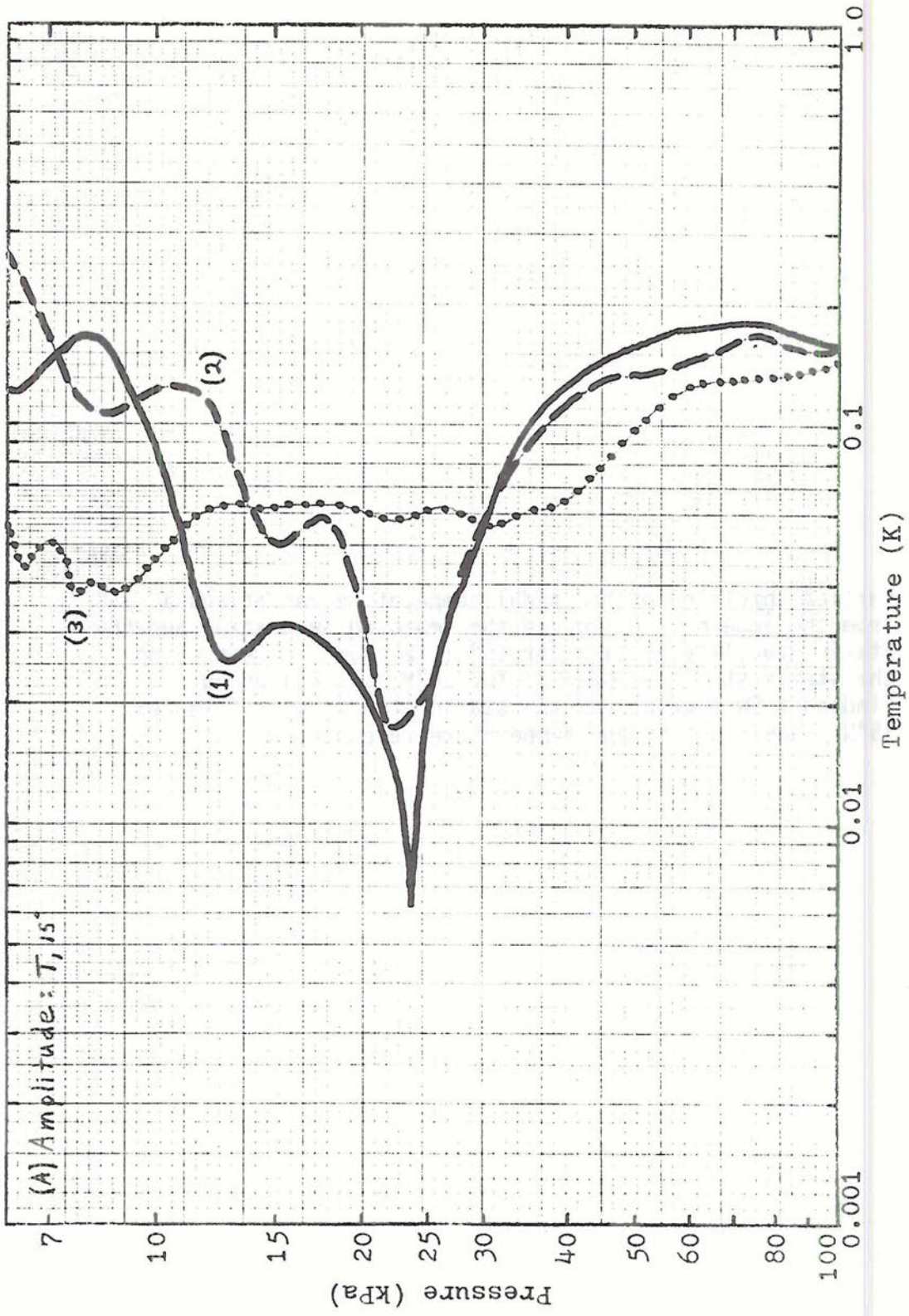


Fig. 4.1a Vertical profiles of the tidal temperature variations at 15° from the equator: (1) using the improved SW heating and the static stability profile for 15°N ; (2) same, except using the static stability profile for 30°N ; and (3) using Lindzen's SW heating and the static stability profile for 15°N . Amplitude of the temperature response.



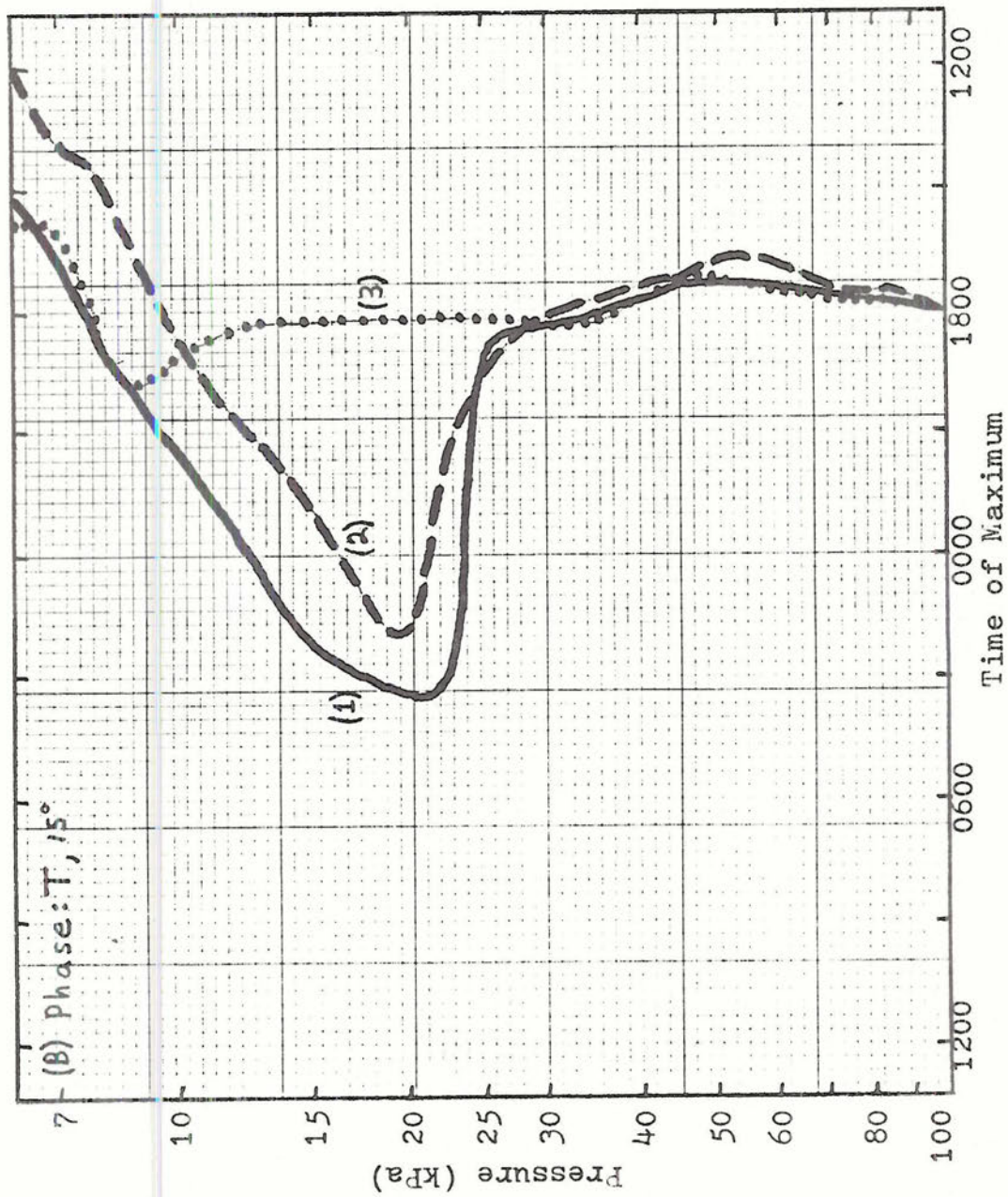
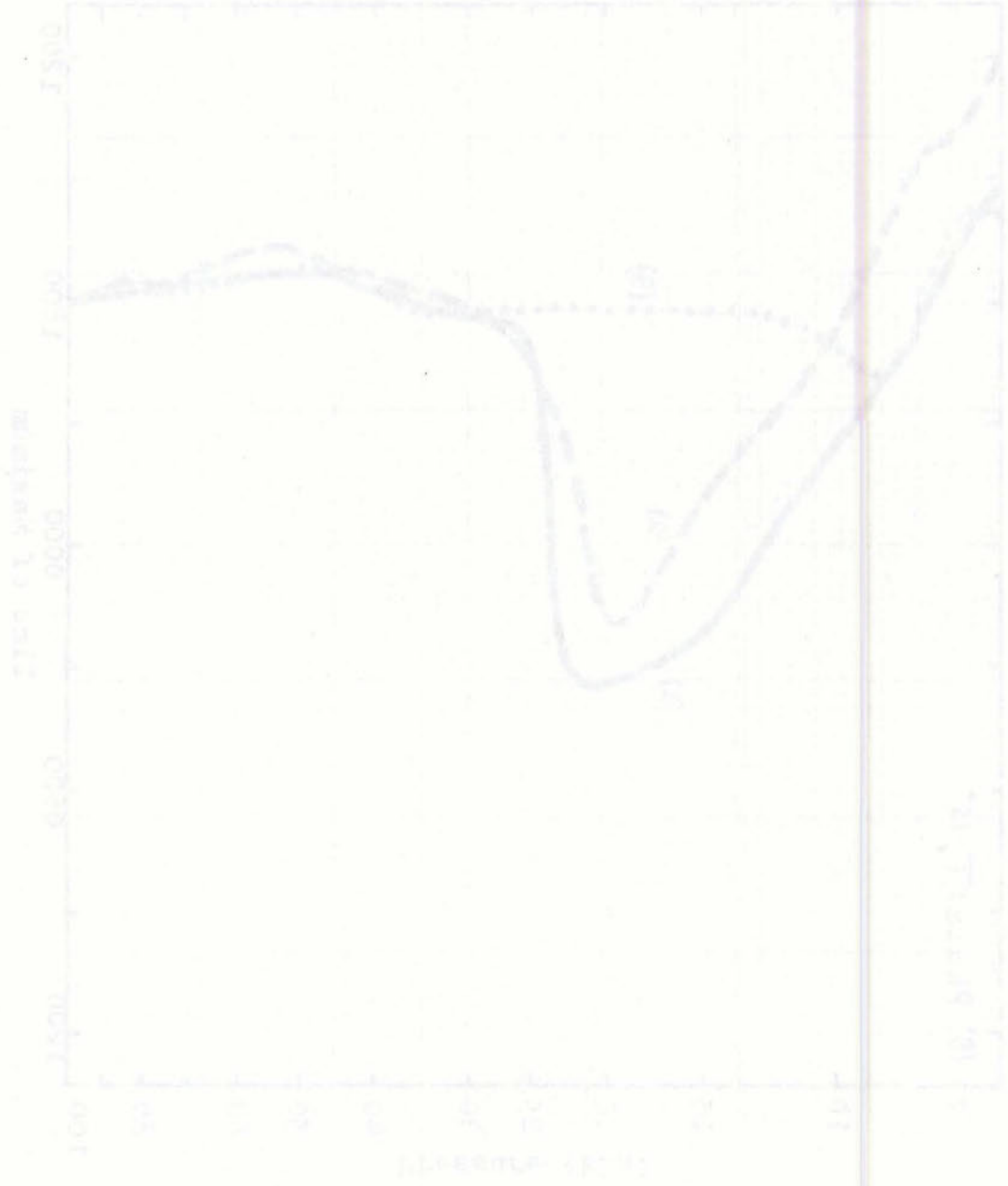


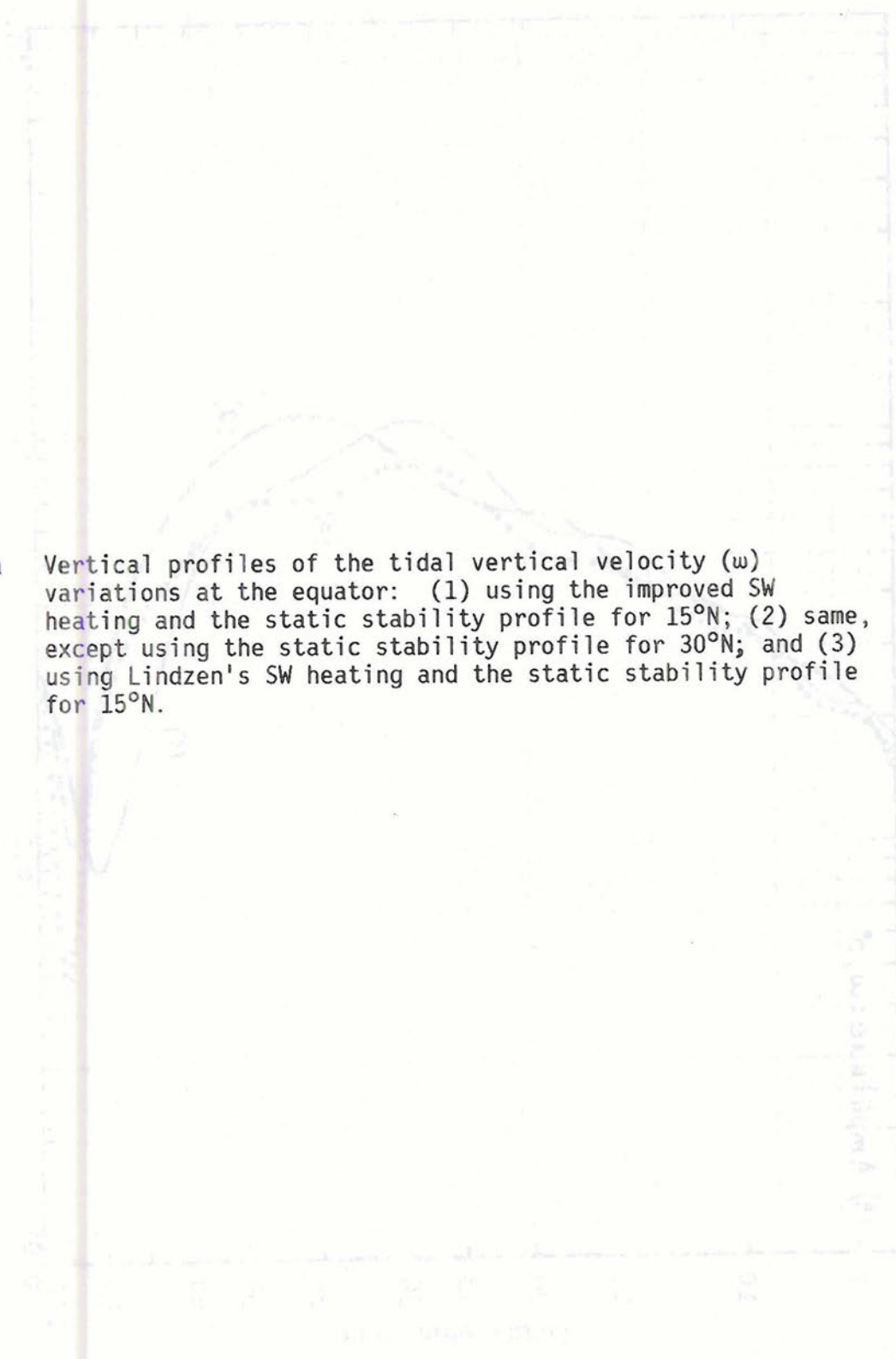
Fig. 4.1b Same as Fig. 4.1a, but for the phase of the temperature response.

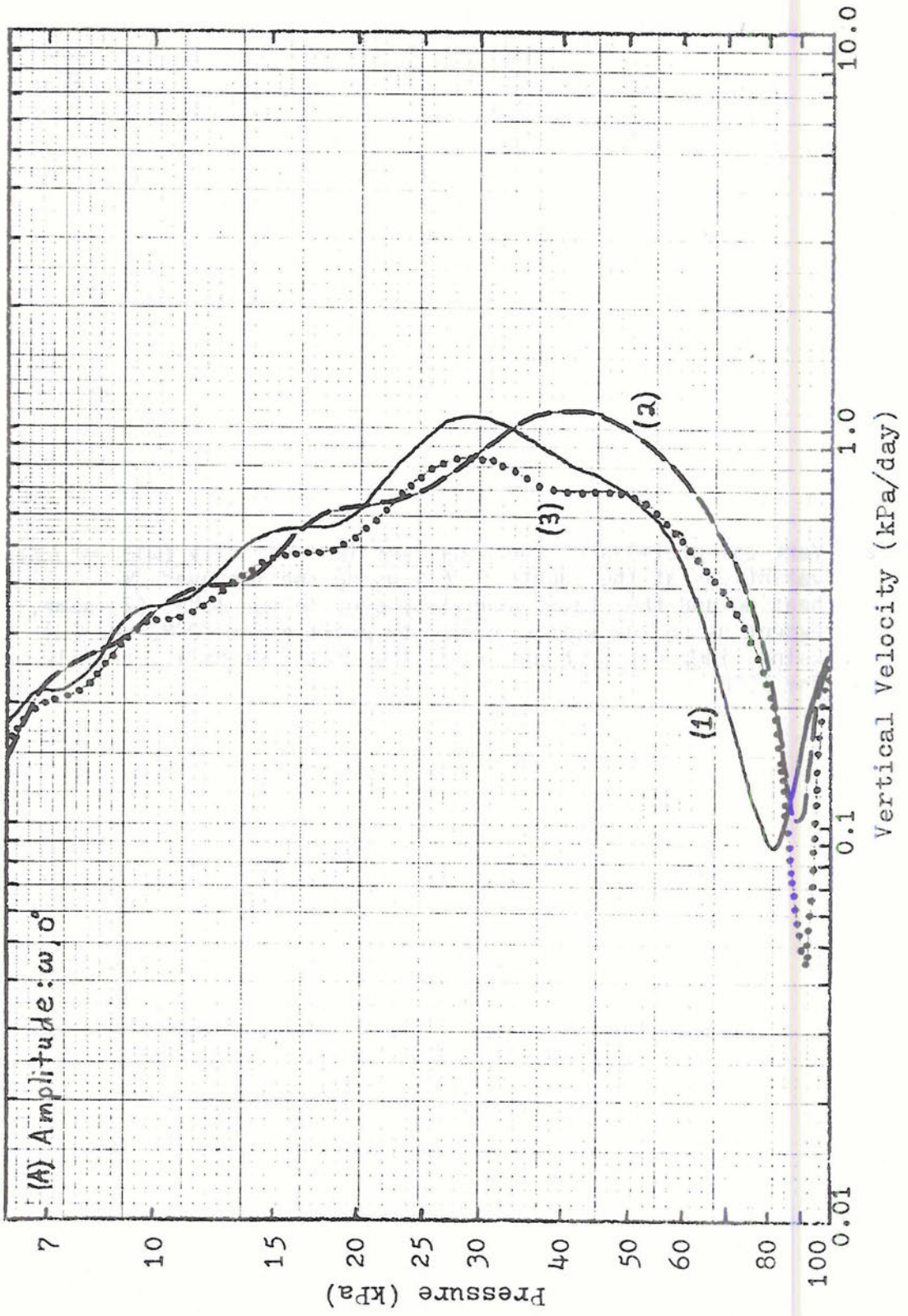
100 4 30 2000 4000 6000 8000 10000 12000



10, 10000, 12000

Fig. 4.2a Vertical profiles of the tidal vertical velocity (w) variations at the equator: (1) using the improved SW heating and the static stability profile for 15°N; (2) same, except using the static stability profile for 30°N; and (3) using Lindzen's SW heating and the static stability profile for 15°N.





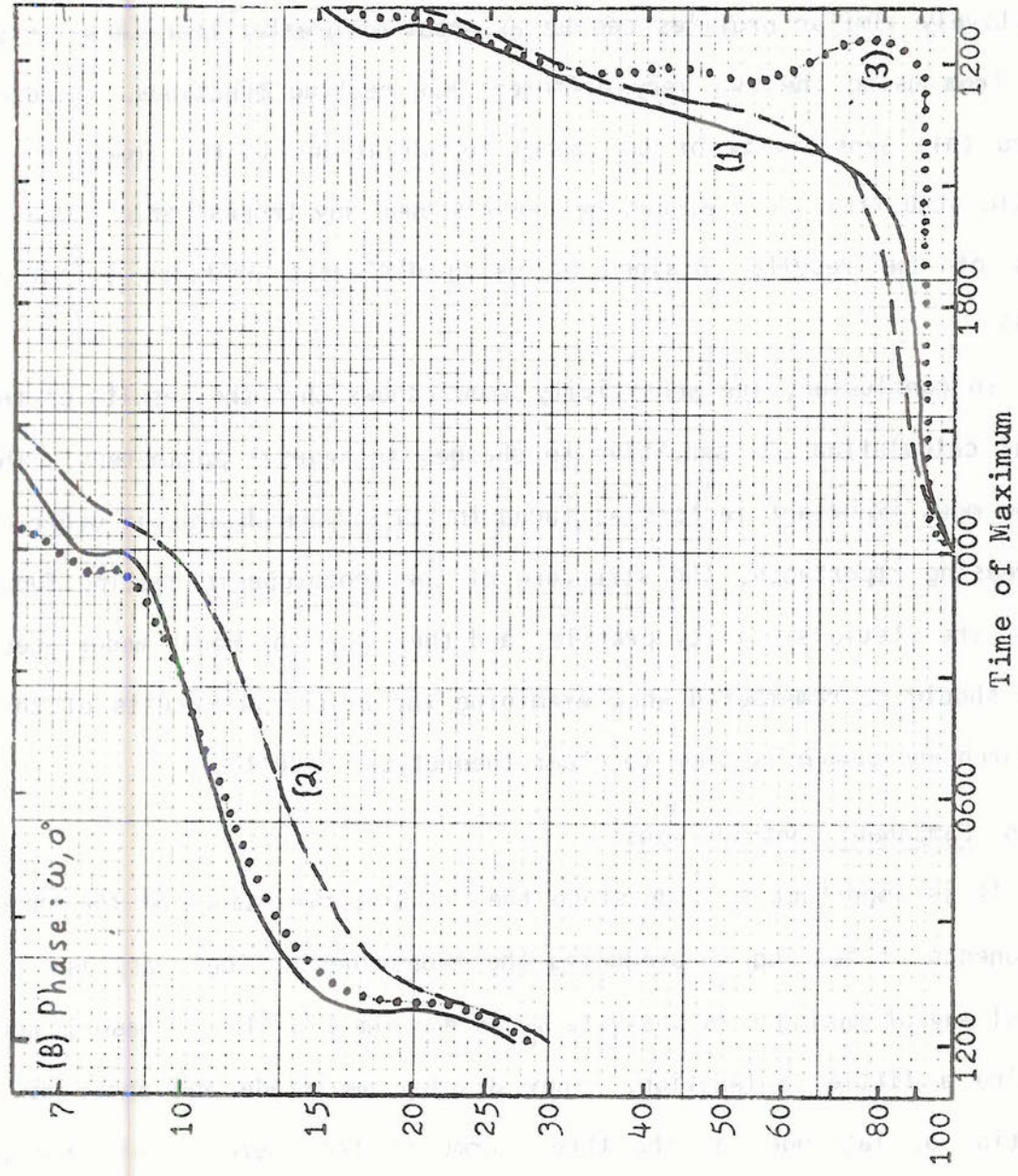


Fig. 4.2b Same as Fig. 4.2a, but for the phase of the vertical velocity response.

profile. Figs. 4.1 and 4.2 display the differences between using equinoctial static stability profiles at 15°N and 30°N. (The temperature and static stability profiles used are shown in Figs. 4.3 and 4.4.) The differences in both phase and amplitude which arise from using these relatively similar profiles can be as great or greater than those arising from using the two very different H₂O heating functions. Lindzen noted this sensitivity of the model to variations in the tropospheric static stability profile, but he never showed any tropospheric comparisons of the results obtained by using different profiles (Lindzen, 1968).

In conclusion, the sensitivity study shows that the results of the tidal calculation are sensitive to changes in several parameters. The three most important factors as found in this research are, in order of decreasing importance, the structure of the tropospheric heating function, the static stability profile, and the number of Hough modes used. This should be remembered when examining the principal results of this research and comparing them to other theoretical results.

4.1.b Component contributions

It is important to understand the relative importance of the three components of heating in producing the tropospheric tidal response. A useful way of making this analysis is to examine Fig. 4.5. These graphs require a little explanation. They display amplitude and phase as a function of latitude for the three terms of the thermodynamic energy equation:

$$i\sigma T^{\sigma,s} + \Gamma_w^* \sigma^{\sigma,s} = \frac{J^{\sigma,s}}{C_p}$$

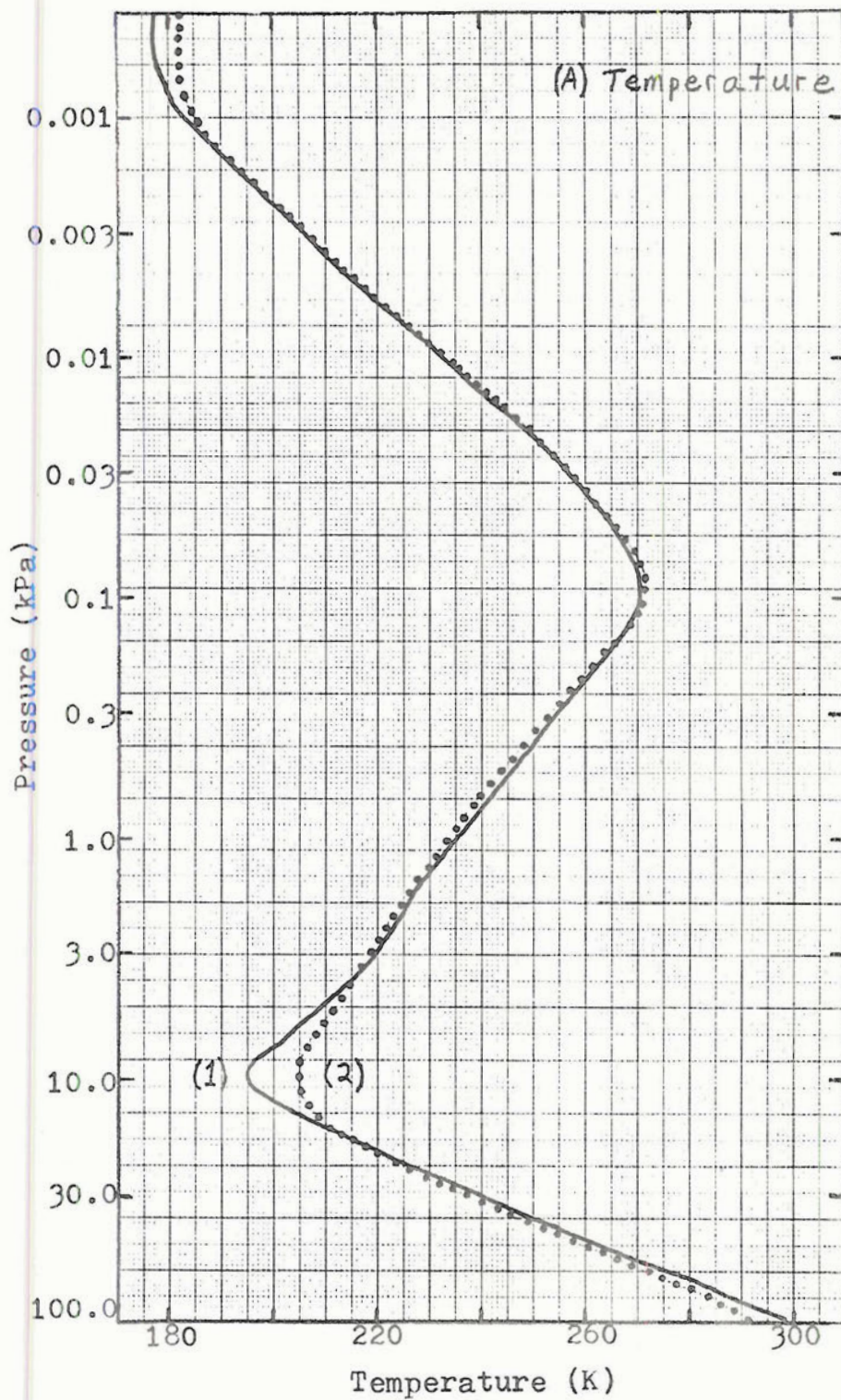


Fig. 4.3 Temperature profiles for (1) 15°N and (2) 30°N at equinox.

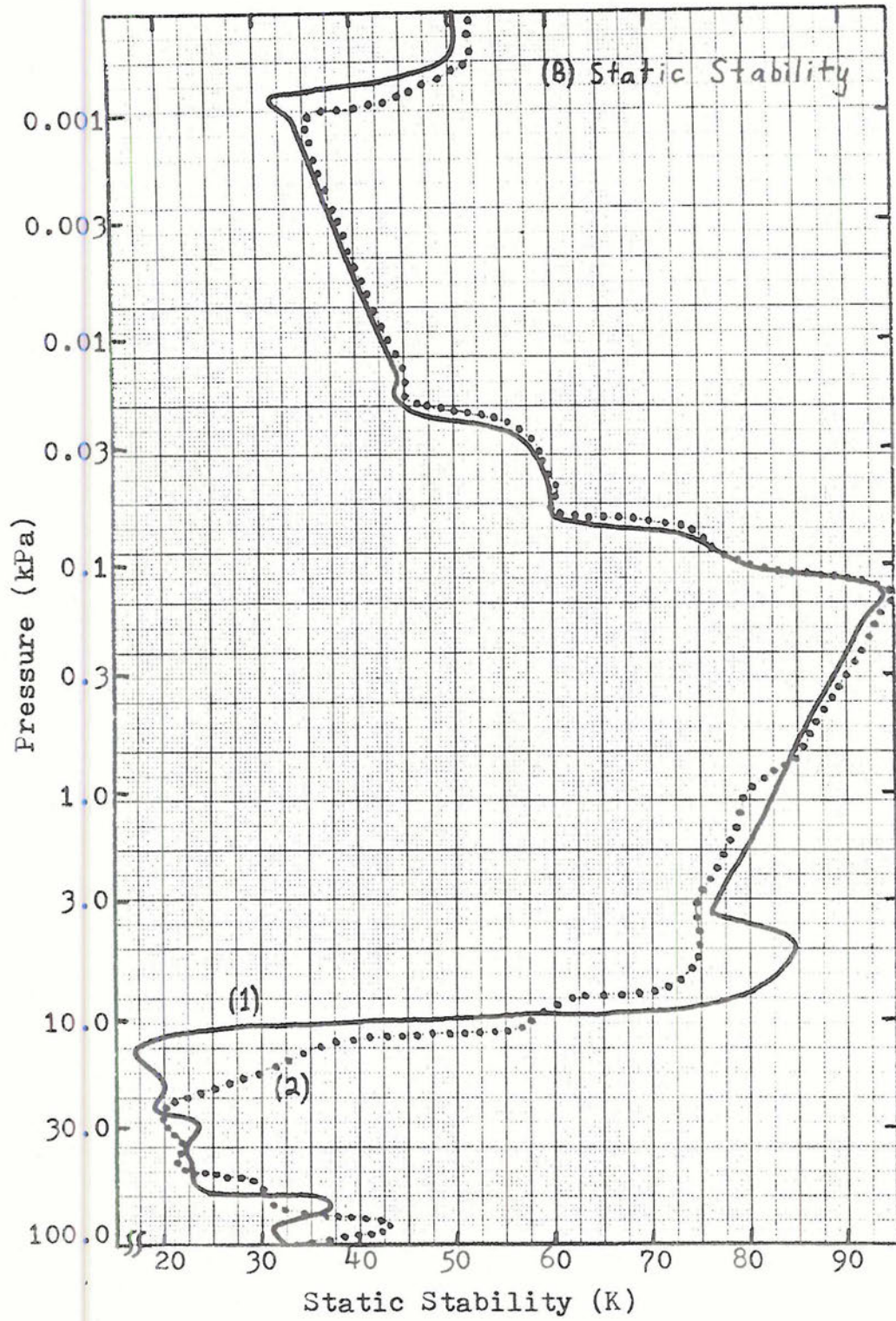


Fig. 4.4 Static stability profiles for (1) 15°N and (2) 30°N at equinox.



Handwritten text at the bottom of the page, possibly a signature or title, which is mostly illegible due to fading.

Fig. 4.5a Energy partitioning among the three terms of the thermodynamic energy equation averaged through the layer from 81.9 to 28.9 kPa: $J^{\sigma, S}/C_p$ (SW heating curve is indistinguishable from the H₂O heating curve). (1) Total (SW + Cumulus) heating, (2) SW heating, (3) H₂O heating, (4) cumulus heating, and (5) ozone heating. Note that the amplitude scale is different for all three terms.

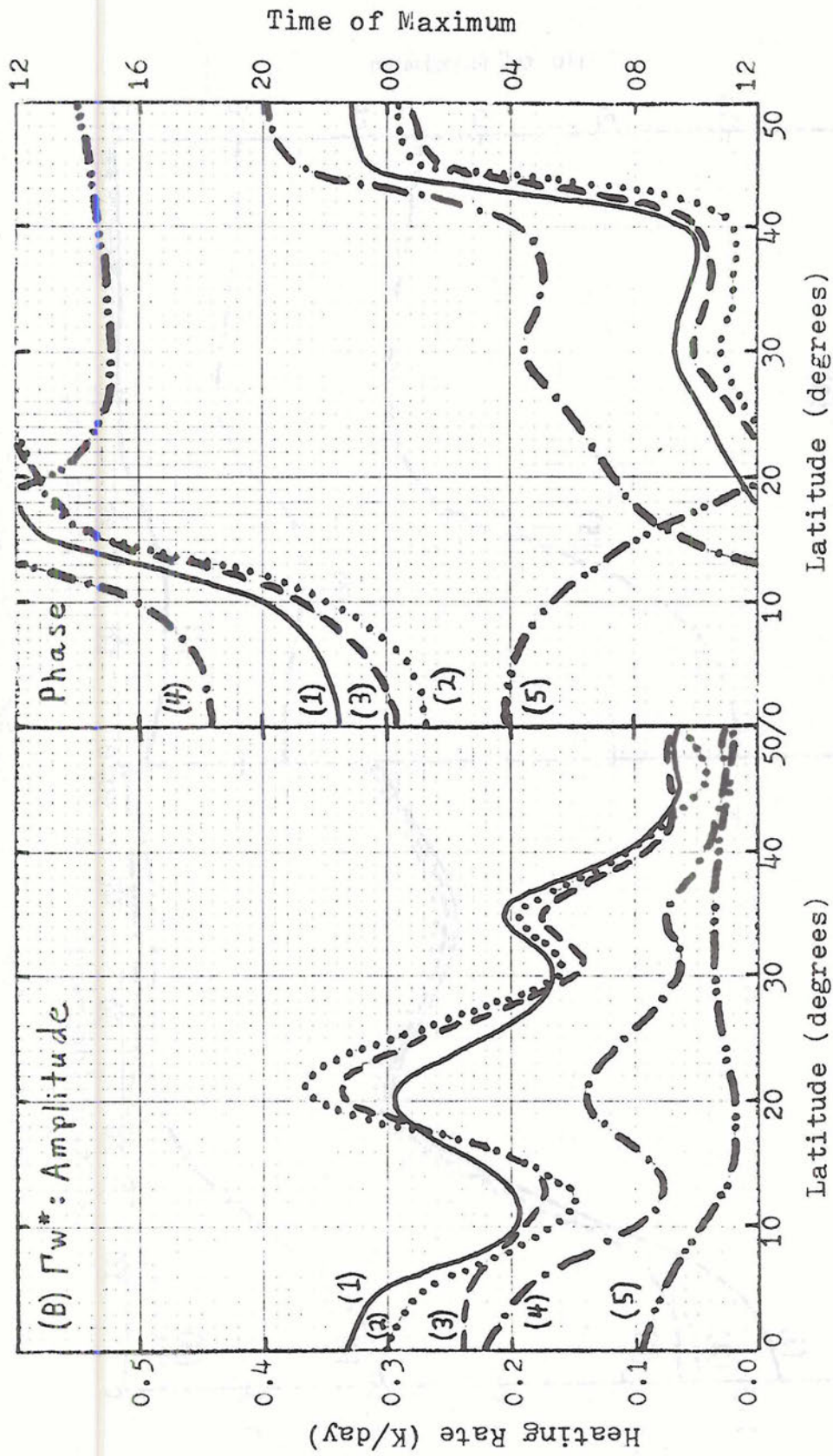


Fig. 4.5b Same as Fig. 4.5a, but for the term $\Gamma_w^{*0, s}$.

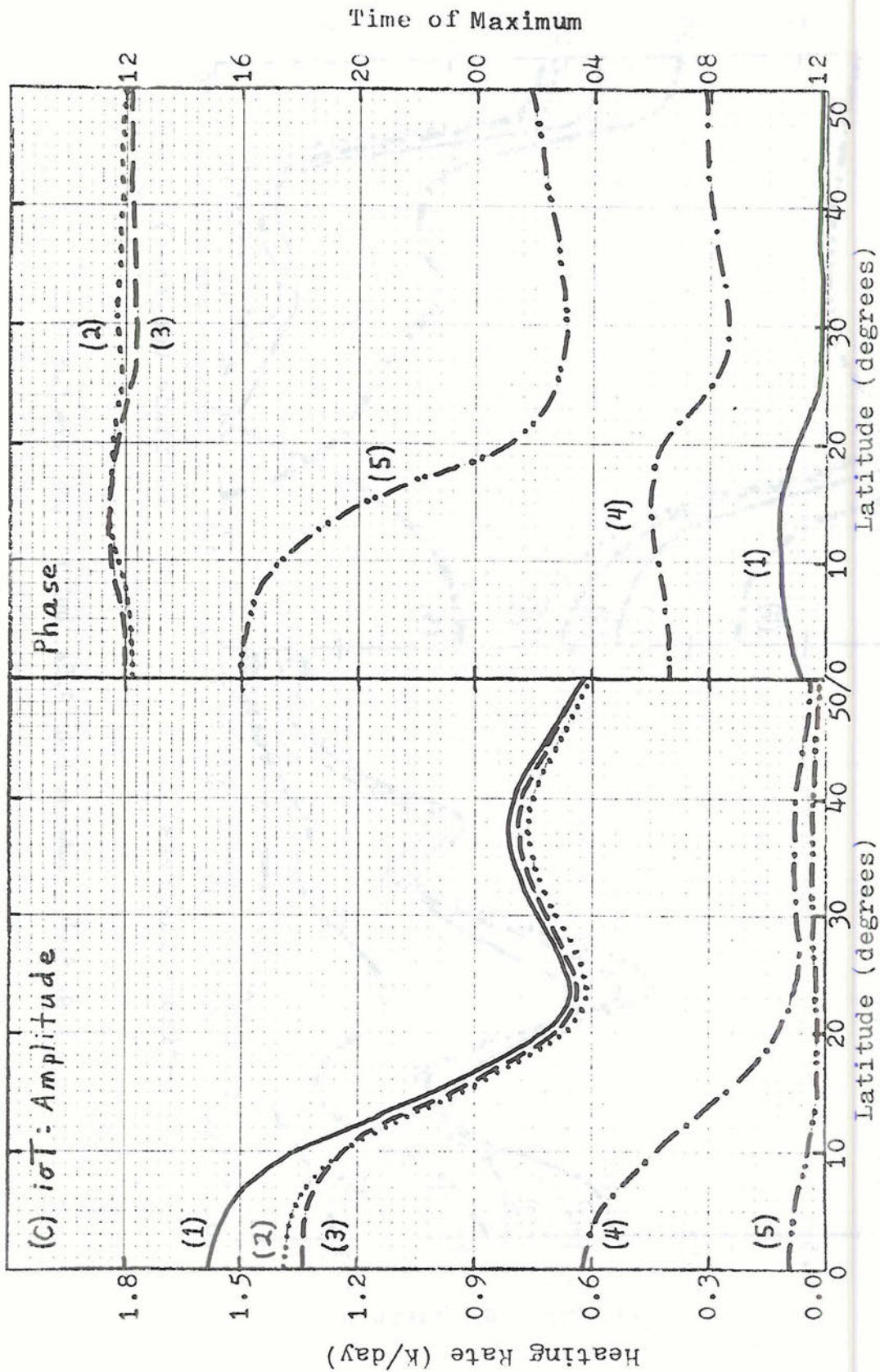


Fig. 4.5c Same as Fig. 4.5a, but for the term $i\sigma T^{\sigma}, s$.

Each curve is a pressure weighted average for that term in the TEE through a deep layer of the troposphere (81.9 to 28.9 kPa). The phase diagram shows the time when the maximum positive deviation occurs.

Fig. 4.5a displays the heating term, $J^{\sigma,S}/C_p$. Several things should be noted. First, there is no ozone heating in the troposphere. Second, the H_2O heating is much greater than the cumulus heating. Because the cumulus heating is 78° out of phase with the water vapor heating, the amplitude of the total heating (shortwave plus cumulus heating) is increased over the water vapor heating less than might otherwise be expected. Finally, the wiggles in the θ -profile of the heating curves due to the finite Hough mode approximation are plainly evident.

Fig. 4.5b displays the vertical motion term, $\Gamma_w^{*\sigma,S}$. (Note that the amplitude diagrams of parts b and c of Fig. 4.5 have different vertical scales than Fig. 4.5a.) Since $w^{*\sigma,S}$ is computed directly, using the heating curves in Fig. 4.5a, it would be expected that some of the wiggles in the θ profiles of $\Gamma_w^{*\sigma,S}$ are directly correlated to those in the $J^{\sigma,S}/C_p$ curves. The structure equatorward of 25° is probably significant, while that poleward of 25° is probably just a fictitious artifact stemming from the approximate Hough mode representation of the heating. The relative importance of the heating components in forcing adiabatic lifting is less clear cut. The response due to ozone heating is smallest, but it is still significant in shaping the total SW response near the equator. The vertical motion forced by cumulus heating is significant at all latitudes. However, being again nearly 90° out of phase with the vertical velocity forced by the SW heating (at most latitudes), the difference between the SW heating response and the total heating response is not very great.

Fig. 4.5c displays the temperature term, $i\sigma T$. The situation is quite distinct here. The stratospheric ozone forcing is almost completely incapable of directly producing temperature changes in the troposphere. The cumulus heating is also relatively much less effective in producing a temperature response than it was in producing a vertical motion response. Thus, the temperature response in the troposphere is almost entirely forced by the H_2O heating, except very near the equator. Notice two other things as well. First, the amplitudes of the temperature term responses are much greater than those of the vertical motion term, indicating that the great majority of the energy in the tropospheric diurnal tidal response goes into the temperature term. Second, in the process of subtracting the vertical motion term from the heating term to obtain the temperature term, most of the wiggles are lost.

Three conclusions can be drawn from this study. First, the H_2O heating is clearly the most important heating component in forcing the diurnal tide in the troposphere. This provides additional support for the assumption that the use of an approximate ozone heating function would provide reliable tropospheric results. Second, the cumulus heating, being much less than the H_2O heating and nearly 90° out of phase with the H_2O heating generally has only a small effect on the θ -profiles of the responses and shifts the phases by an hour or less. Third, by far the greatest fraction of the energy goes into the temperature term in the troposphere.

It is worthwhile to make a few more comments about this last conclusion. In the troposphere, the static stability, Γ , is low and the vertical motion forced by the heating is insufficient for there to be much response in the $\Gamma w^{*\sigma, s}$ term of the TEE. As a result, this term

behaves somewhat like a residual quantity, while the heating and temperature ($i\sigma T$) terms are more nearly equal in amplitude and have very nearly the same phase. This implies that the temperature response, $T^{\sigma, S}$, always tends to lag the heating by very nearly 90° (or six hours). Thus, if the heating reaches a maximum at noon (as the SW heating does), the temperature reaches its maximum value at 1800 LT. For a realistic static stability profile, the only way to achieve an earlier temperature maximum in this model is to add an additional source of heating which achieves its maximum at an earlier time than the SW heating does. The cumulus heating is able to do this to some extent; though, as noted, its effect was not very great. This will be important to remember later when examining the results shown in the next section and when comparing them to the observational results shown in section 4.3.

It was also observed that increasing the static stability in the troposphere increased the fraction of energy that went into the vertical motion term, and that the heating and temperature terms were then no longer so nearly in phase. However, even with an isothermal atmosphere, about 60% of the response energy went into the temperature term for this thick layer of the troposphere.

4.1.c Principal results of this research

There are many results that could be shown in this section -- many more than could feasibly be shown here. In order to try to obtain insight into the global structure of the diurnal tide, model results were obtained in three forms. First, amplitude and phase cross sections in the θ - z^* plane were obtained with resolutions of 5° in the θ -direction and 0.04 in the z^* -direction. Second, instantaneous θ - z^* cross sections were obtained for various times during the course of a day.

Third, instantaneous ϕ - z^* cross sections were obtained around several latitude circles with a 15° horizontal resolution. Cross sections were obtained for the following quantities: the three terms of the TEE; the perturbation fields of temperature, geopotential, horizontal divergence, and the horizontal wind components; and the perturbation vertical velocity fields in pressure, log-pressure, and geometric height coordinates.

The instantaneous cross sections were quite useful and illuminating. Certain features, like tilting axes and cellular structures, become very apparent in these sections. It was also fairly easy to confirm from these cross sections that the general features of the results are internally consistent and are consistent with the governing equations. However, because these instantaneous cross sections do not convey information in a concise form, they will not be shown in this report. Instead, only θ - z^* cross sections of amplitude for a number of variables will be shown here along with vertical profiles of phase at 0° , 15° , and 30° of latitude.

It was decided that the most representative results were obtained by incorporating the following features into the model: sixteen Hough modes, the static stability profile for 15°N , the same ozone heating that Lindzen used, and the slightly smoothed H_2O heating derived from the radiative transfer routine. The results of two model runs are shown here. The first run was driven only by shortwave heating (ozone and H_2O heating). The second run contained the additional forcing due to cumulus heating as well. The results are shown on the following pages in Figs. 4.6 to 4.12, and a comparison can be made between the tidal responses with and without cumulus heating.

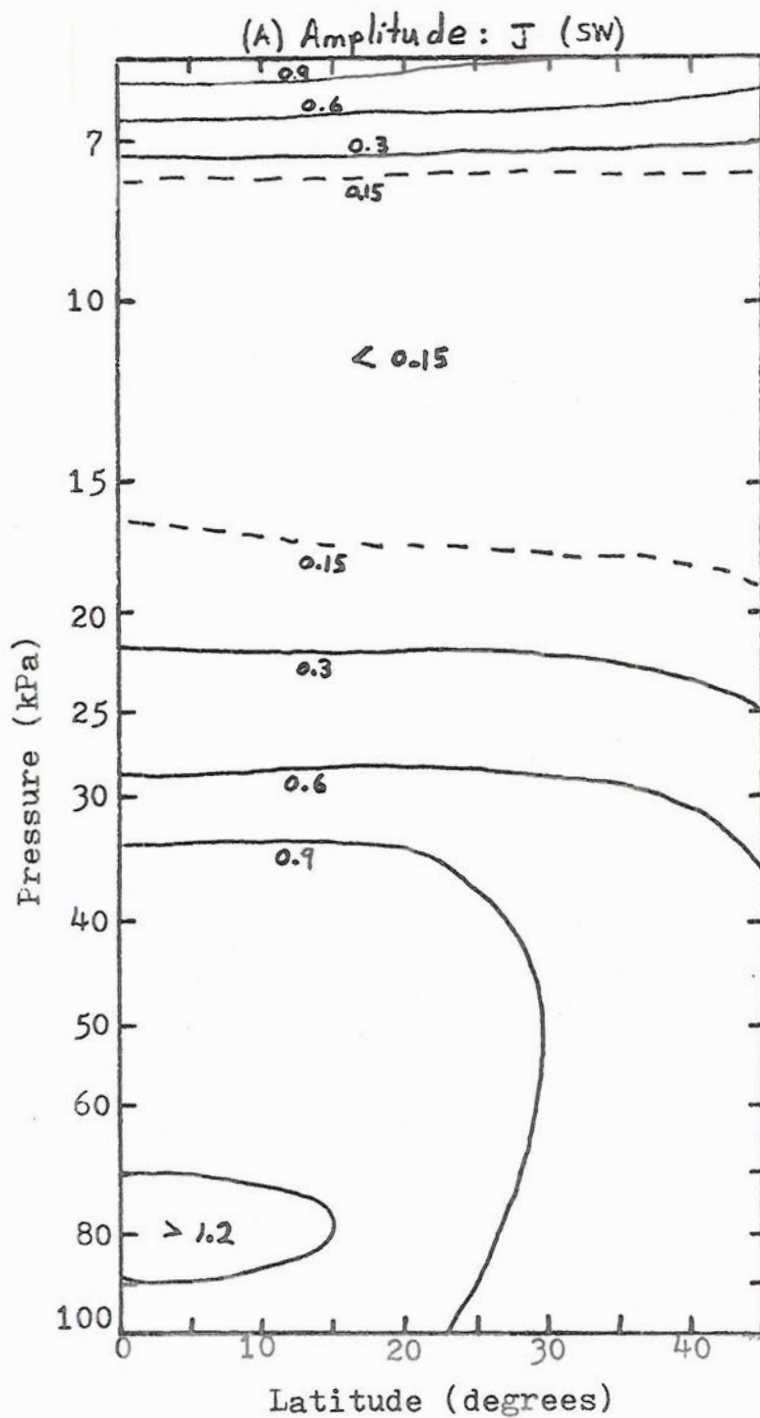


Fig. 4.6a Heating. Contour interval: 0.3 K/day. Amplitude of the SW (H_2O + ozone) heating.

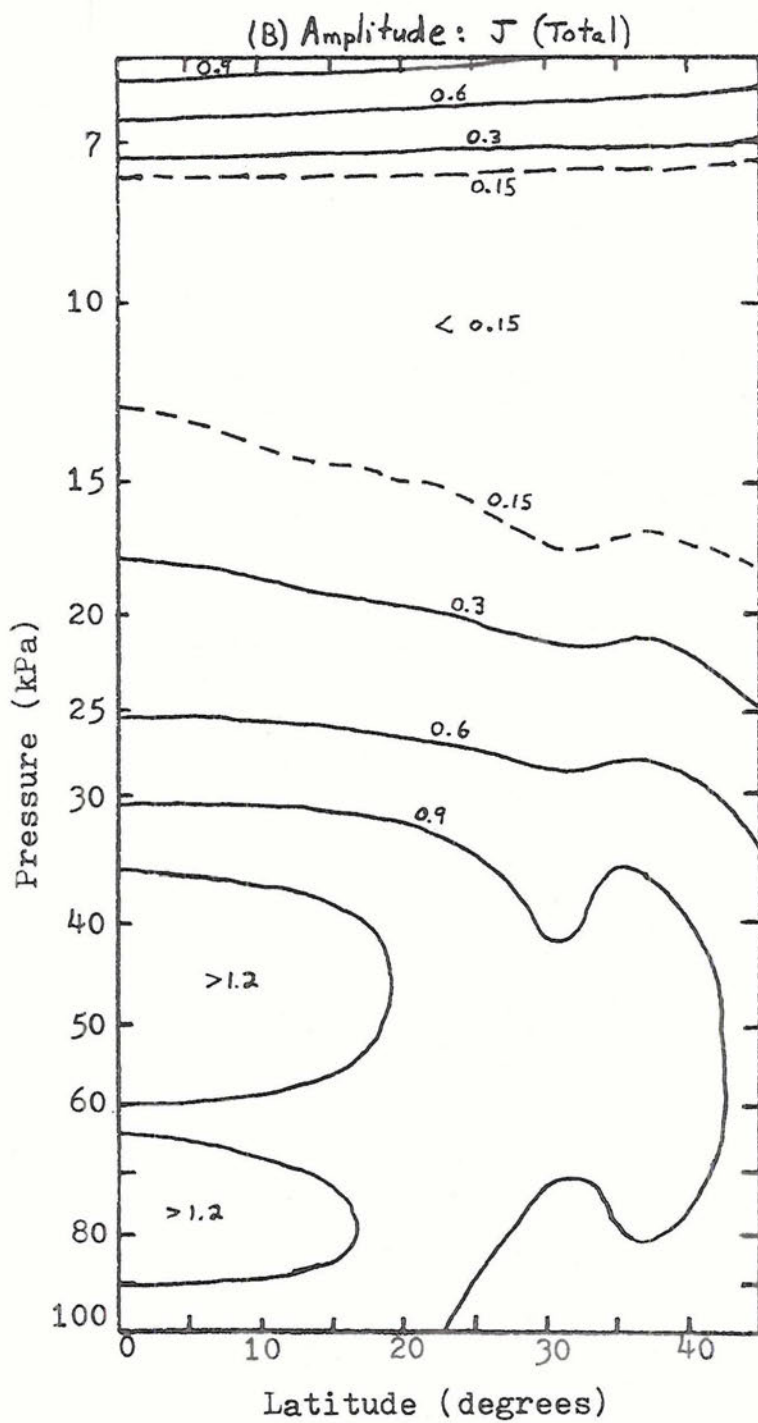
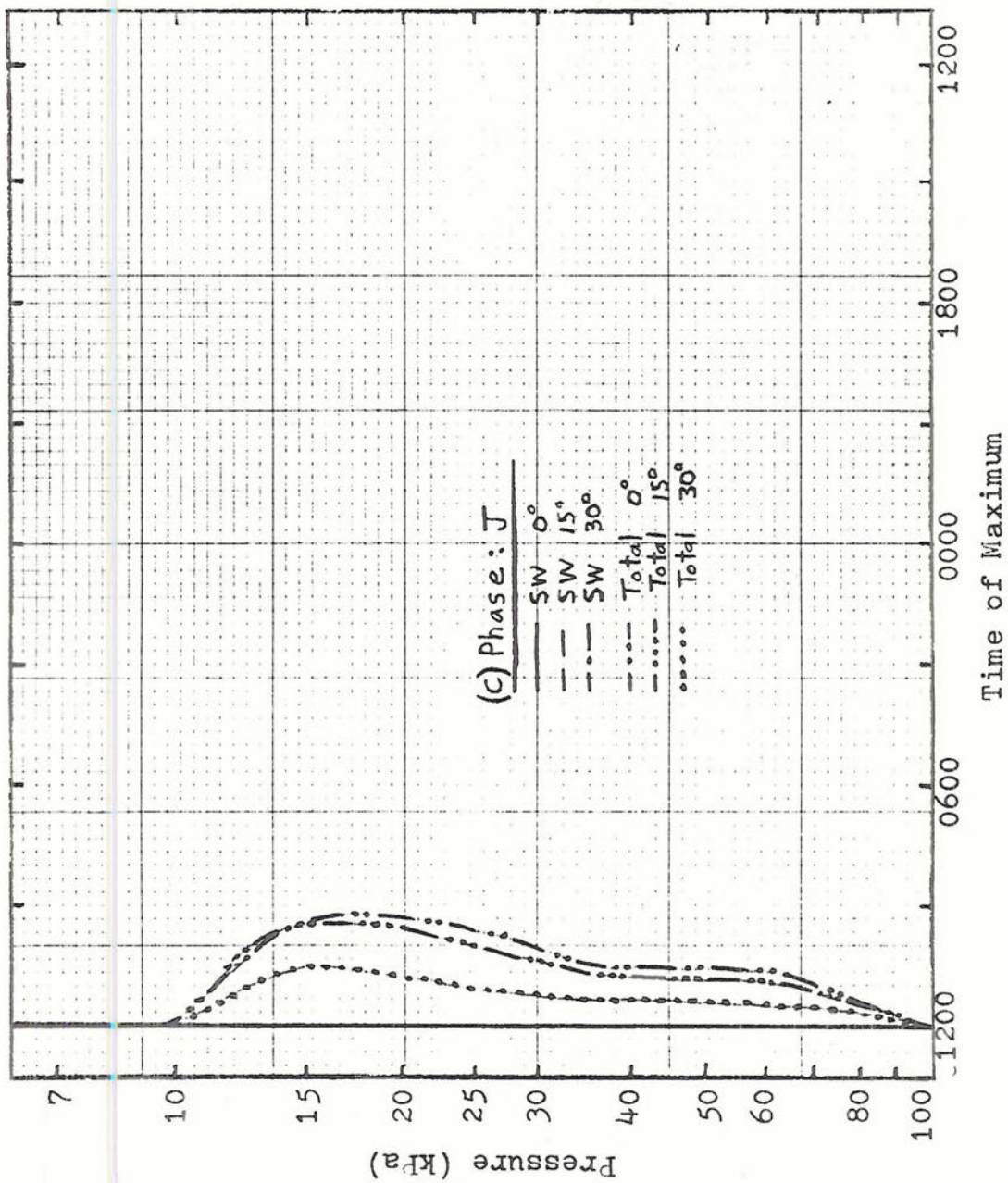


Fig. 4.6b Same as Fig. 4.6a, but for the amplitude of the total (SW + Cumulus) heating.



(a) $A_{total}(\theta)$ vs θ for the region of the total (2x) ...

Fig. 4.6c Heating. Vertical phase profiles at 0° , 15° , and 30° from the equator. The shortwave heating is maximum at noon at all latitudes.



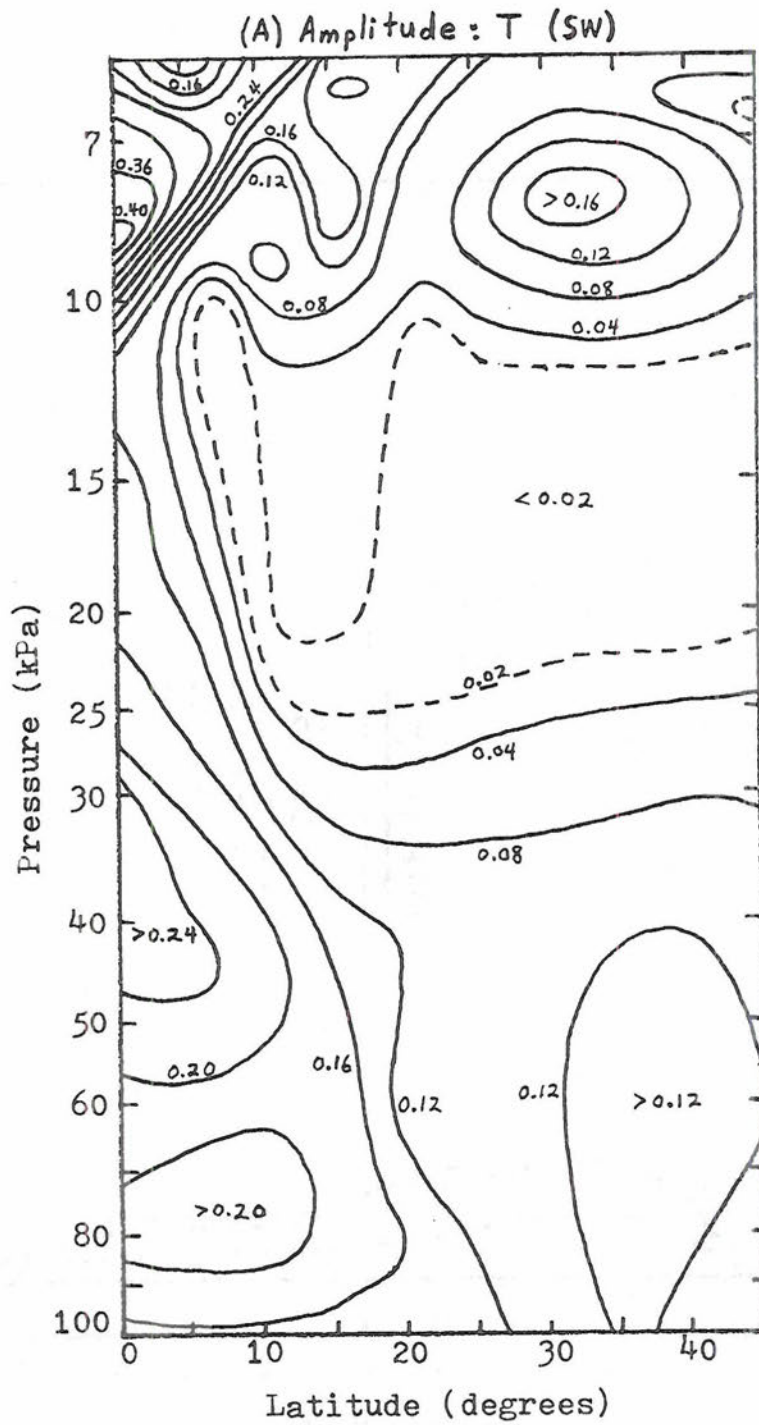


Fig. 4.7a Temperature response. Contour interval: 0.04 K. Amplitude of the response to SW heating.

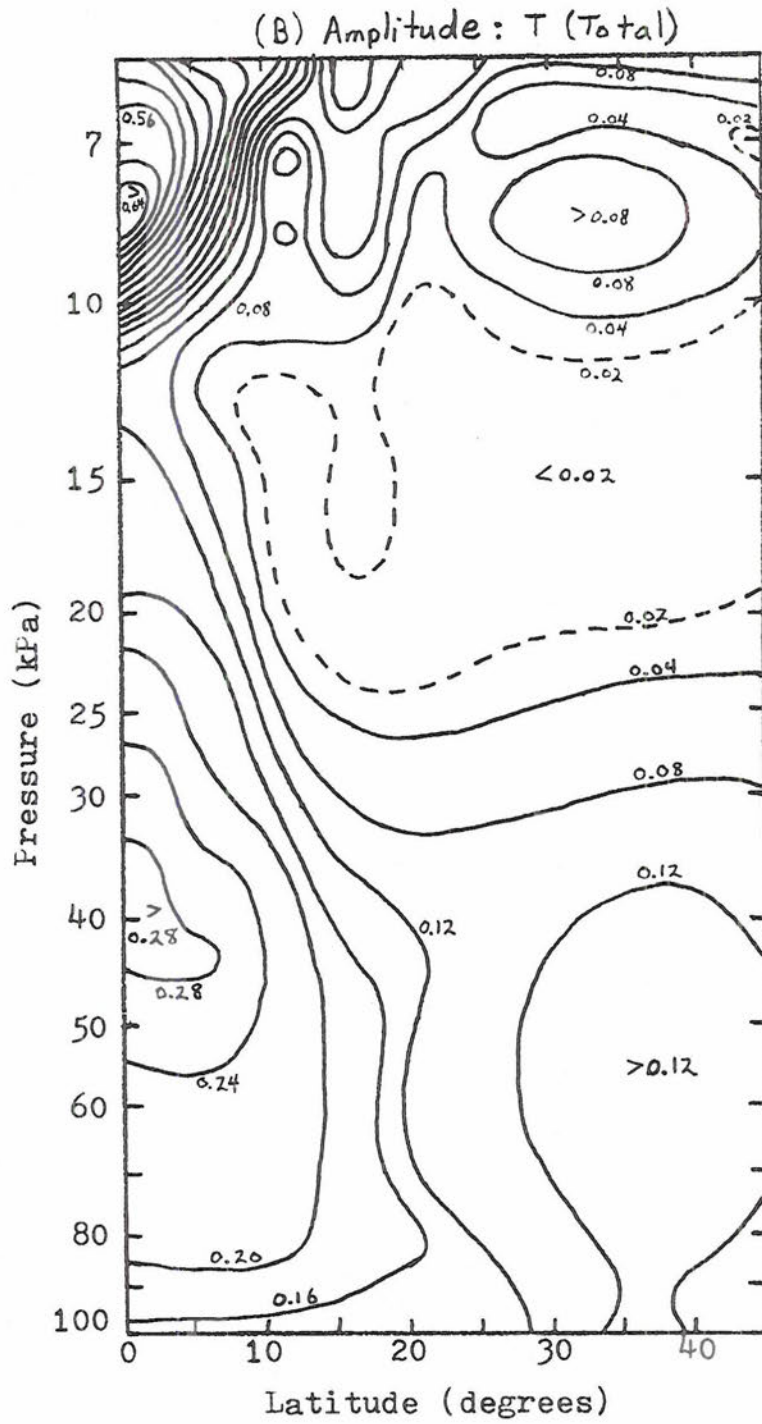
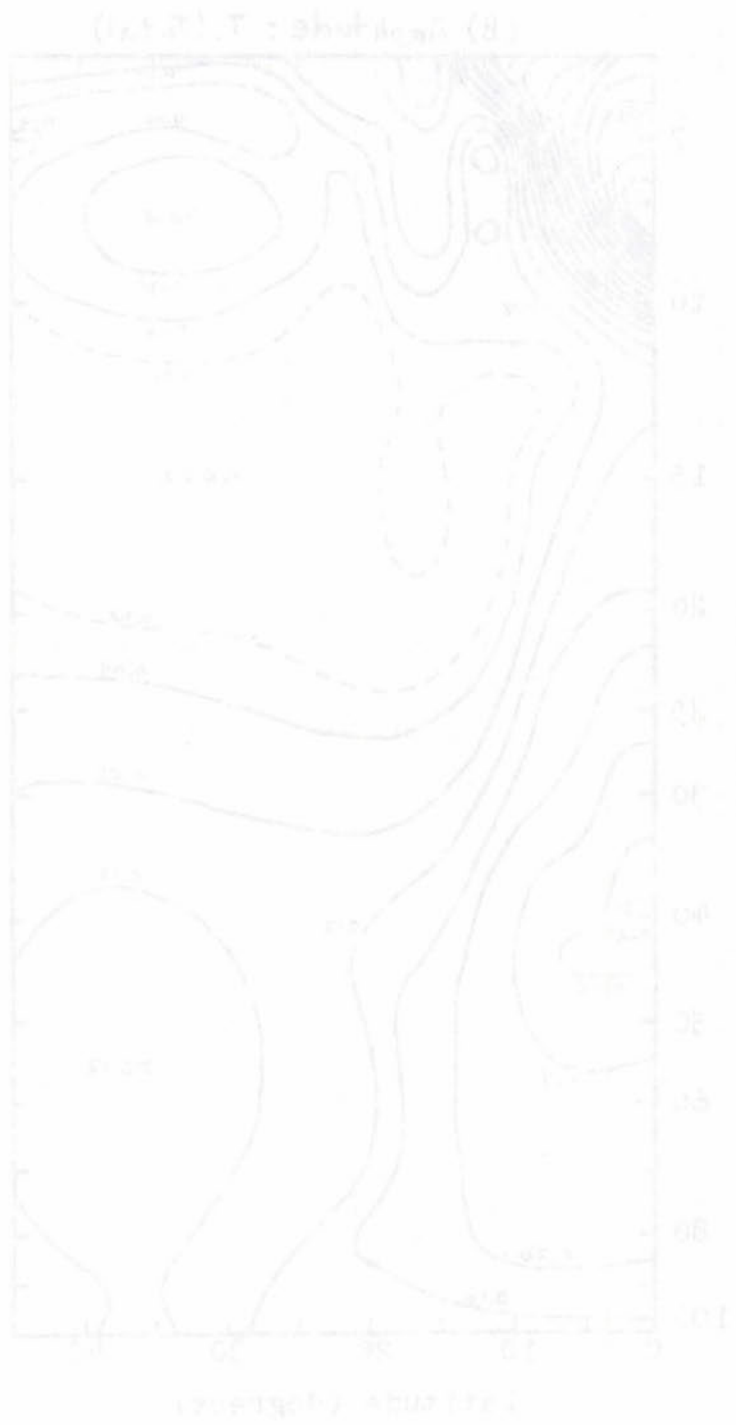
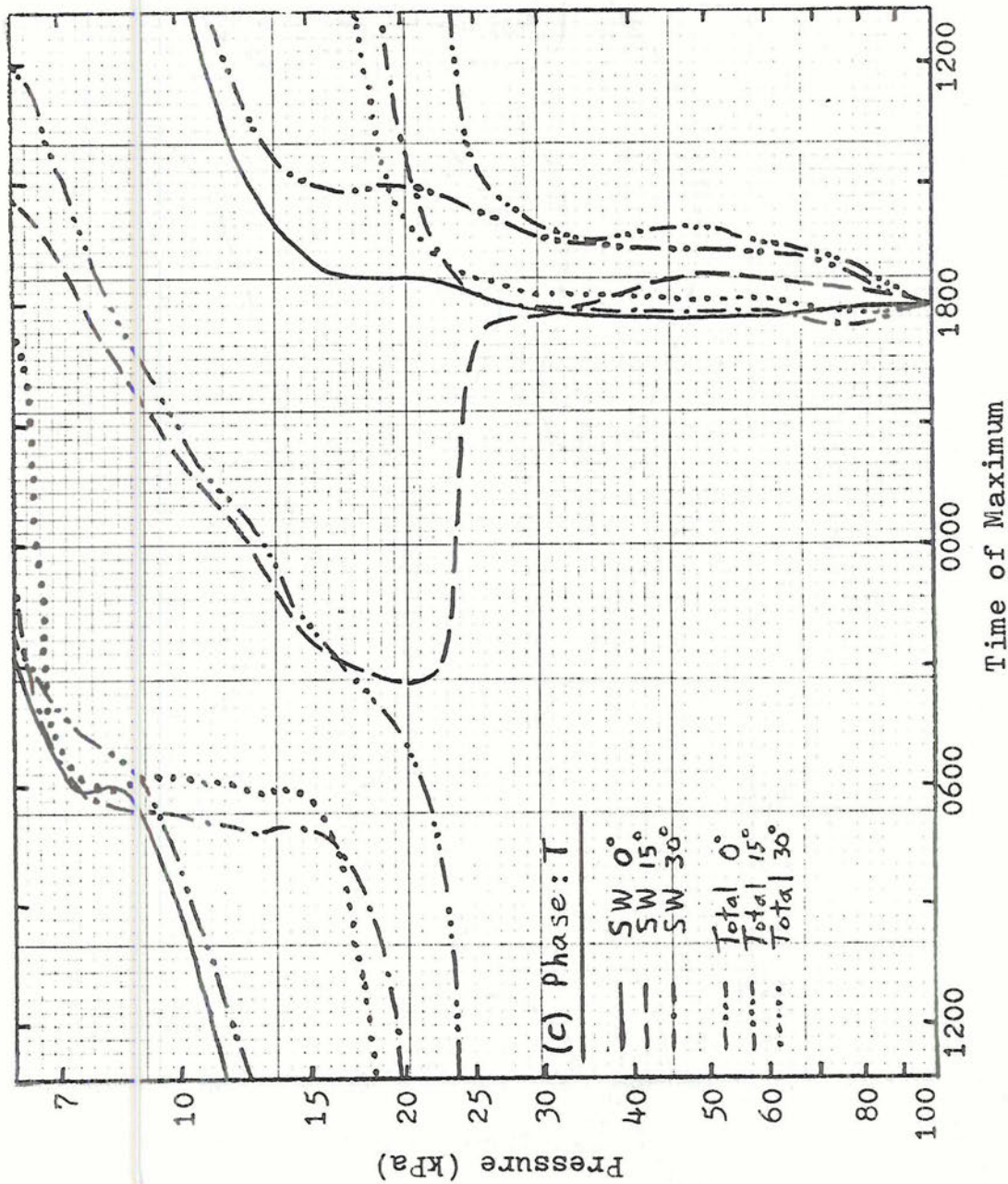


Fig. 4.7b Same as Fig. 4.7a, but for the amplitude of the response to total heating.



Amplitude: T (1.2, 1.4) is a function of the amplitude of the response.

Fig. 4.7c Temperature response. Vertical phase profiles at 0° , 15° , and 30° from the equator for responses to both SW heating and total heating.



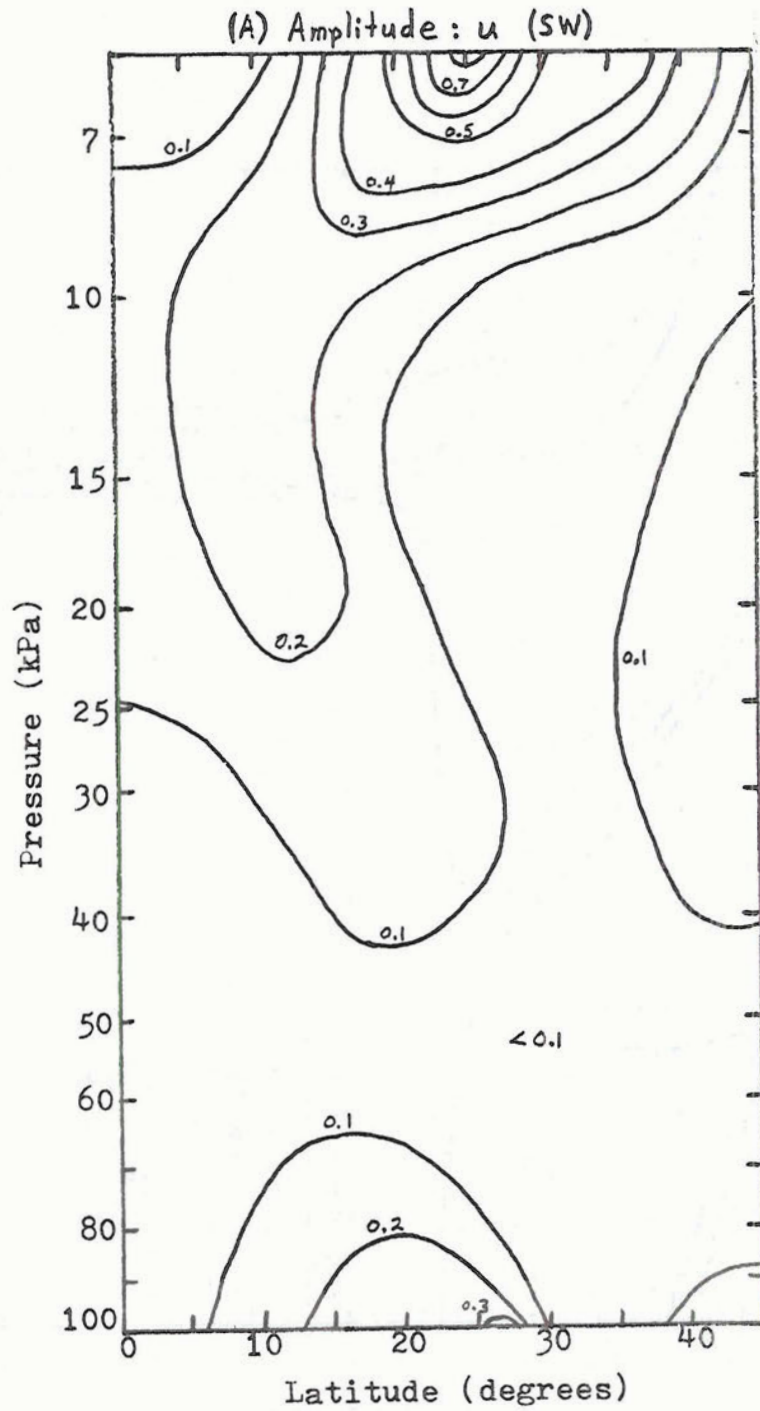


Fig. 4.8a Westerly wind response. Contour interval: 0.1 m/sec. Amplitude of the response to SW heating.

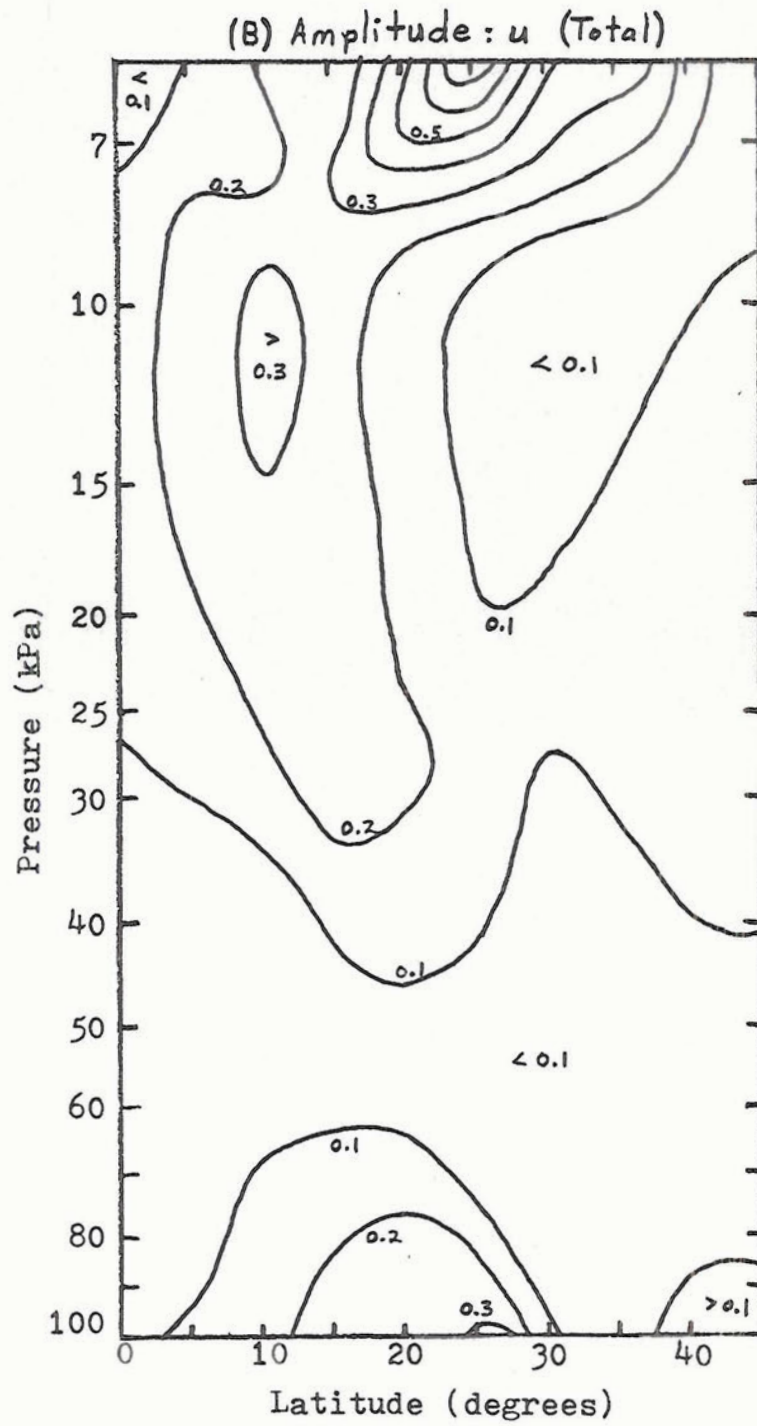


Fig. 4.8b Same as Fig. 4.8a, but for the amplitude of the response to total heating.

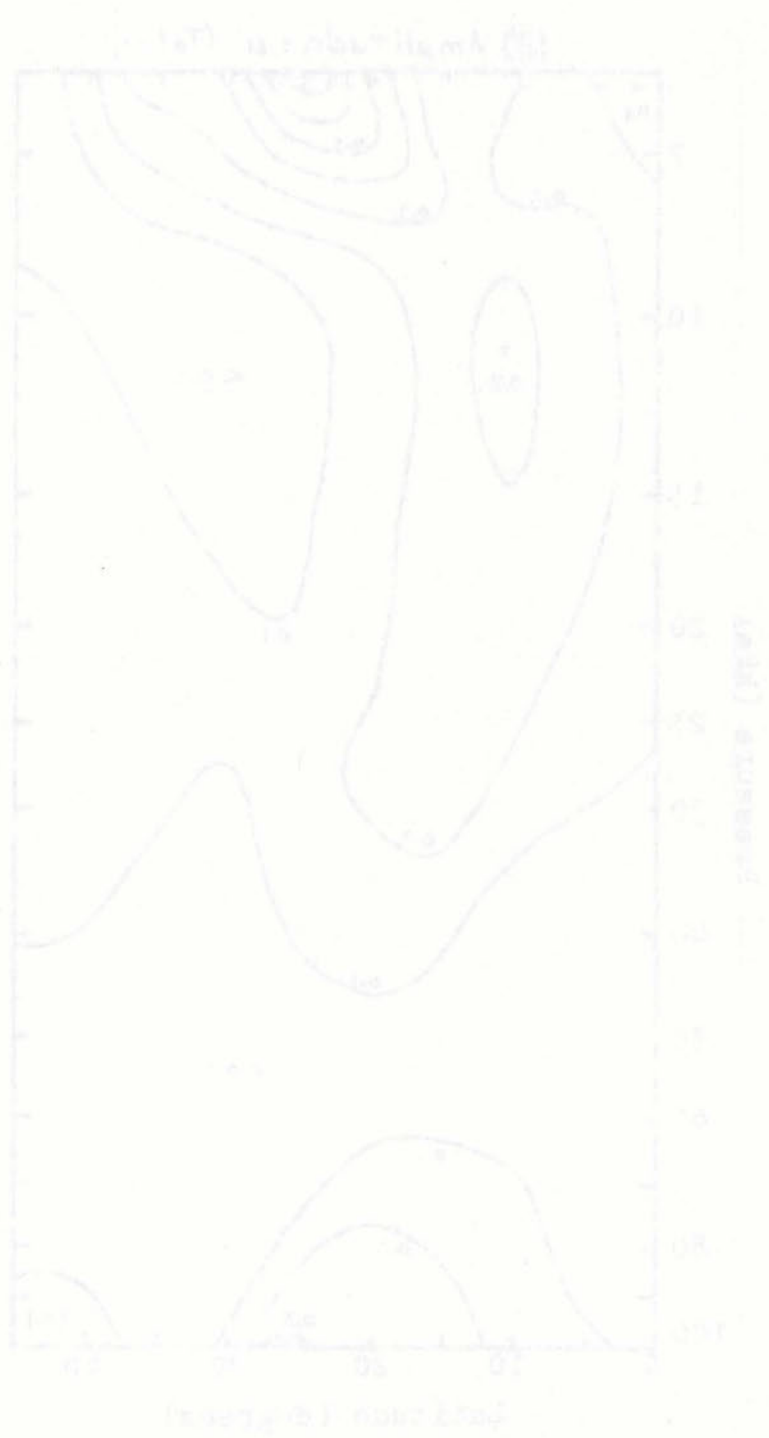
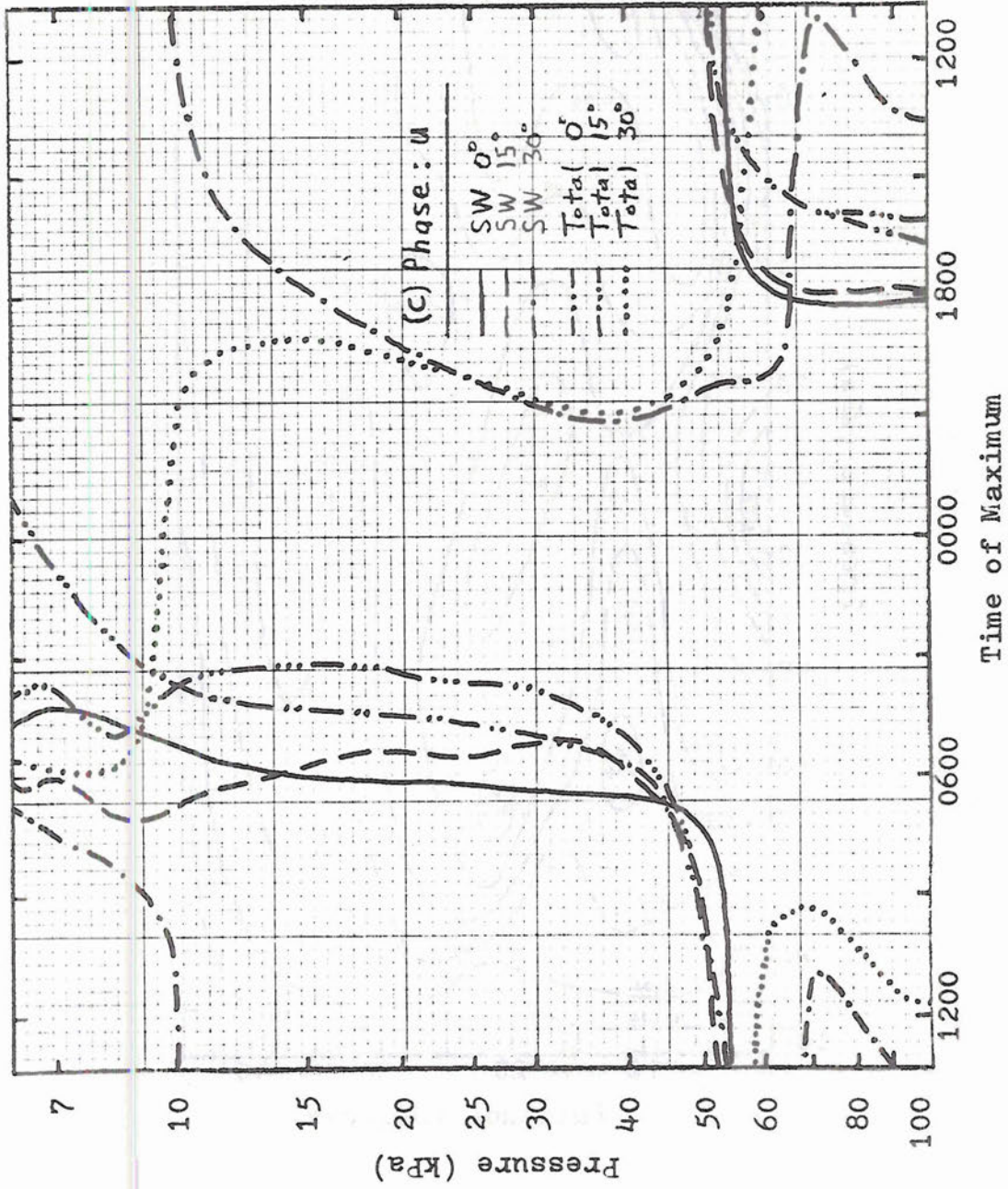


Fig. 4. The response surface for the response variable is shown in Fig. 4. The response surface is shown in Fig. 4. The response surface is shown in Fig. 4.

Fig. 4.8c Westerly wind response. Vertical phase profiles at 0° , 15° , and 30° from the equator for responses to both SW heating and total heating.



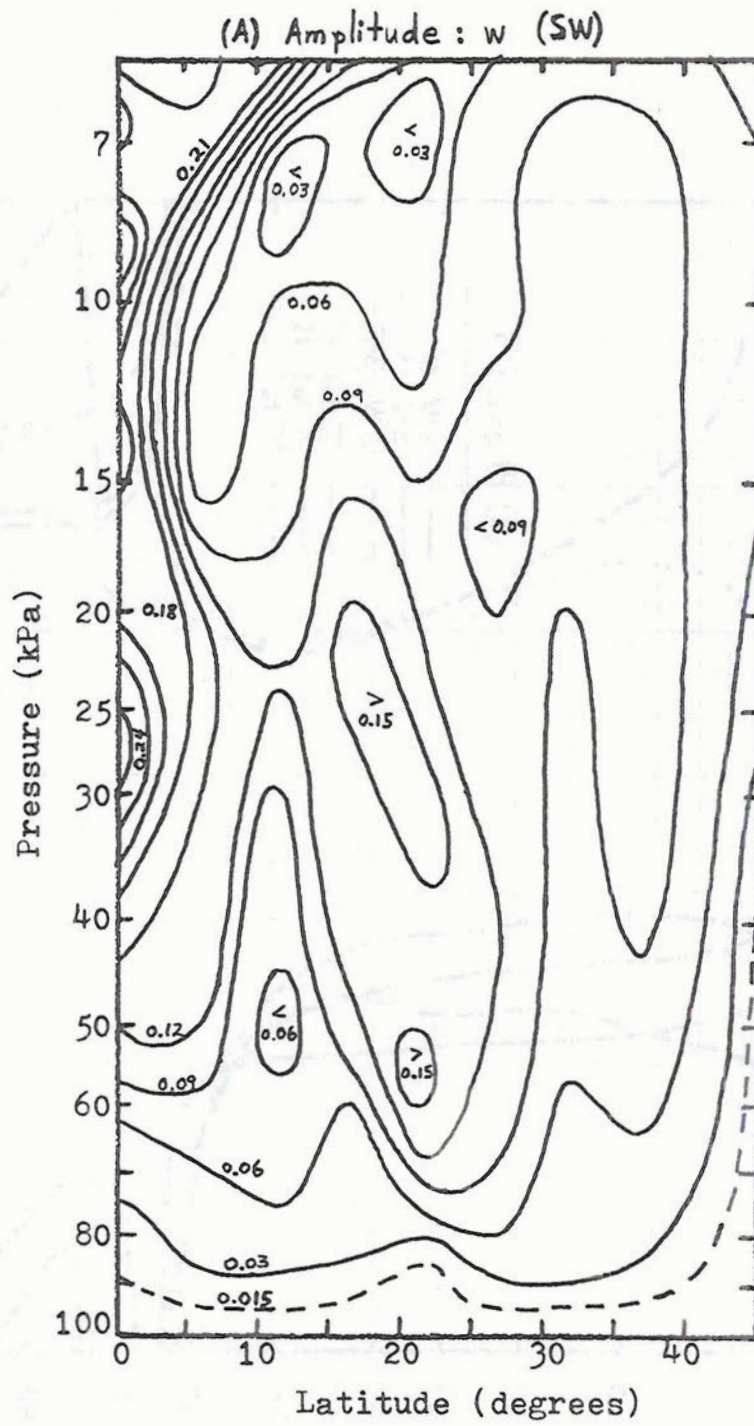


Fig. 4.9a Vertical velocity (w) response. Contour interval: 0.03 cm/sec. Amplitude of the response to SW heating.

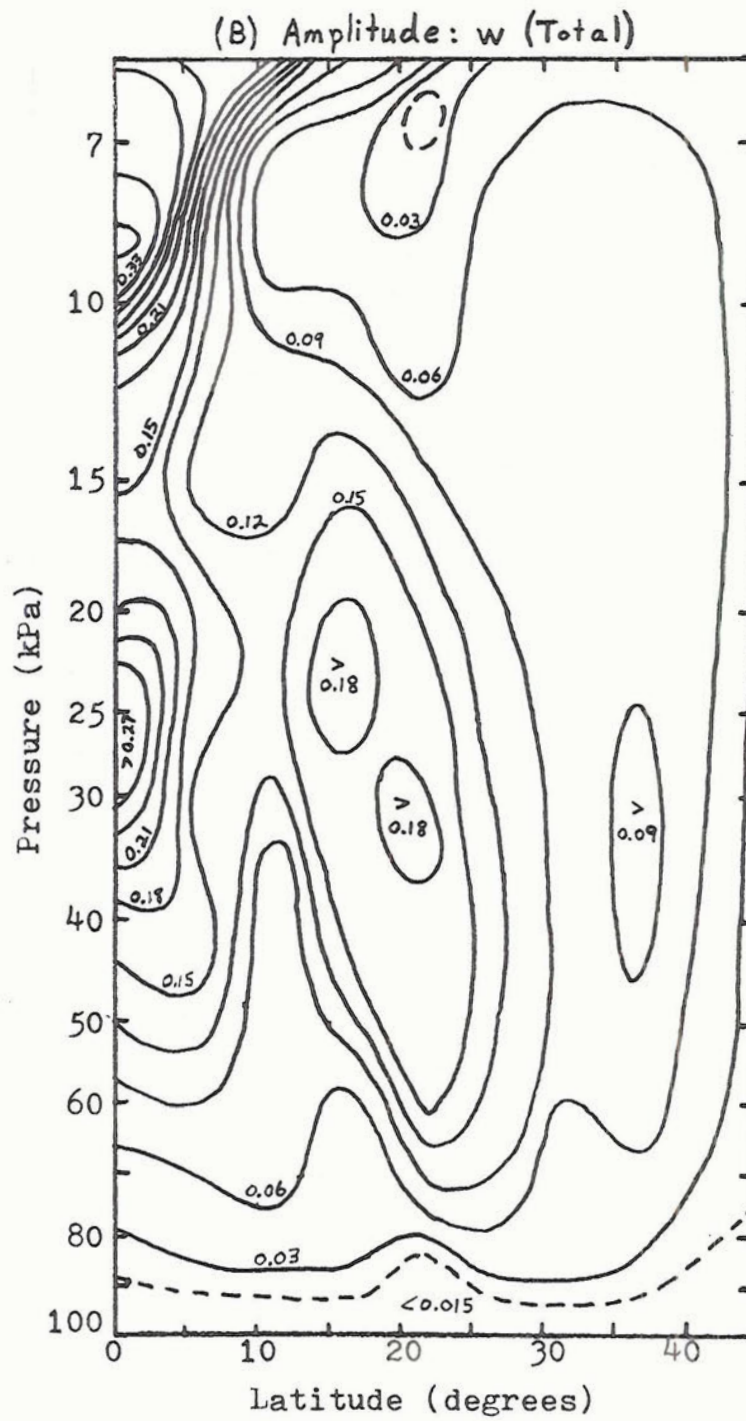
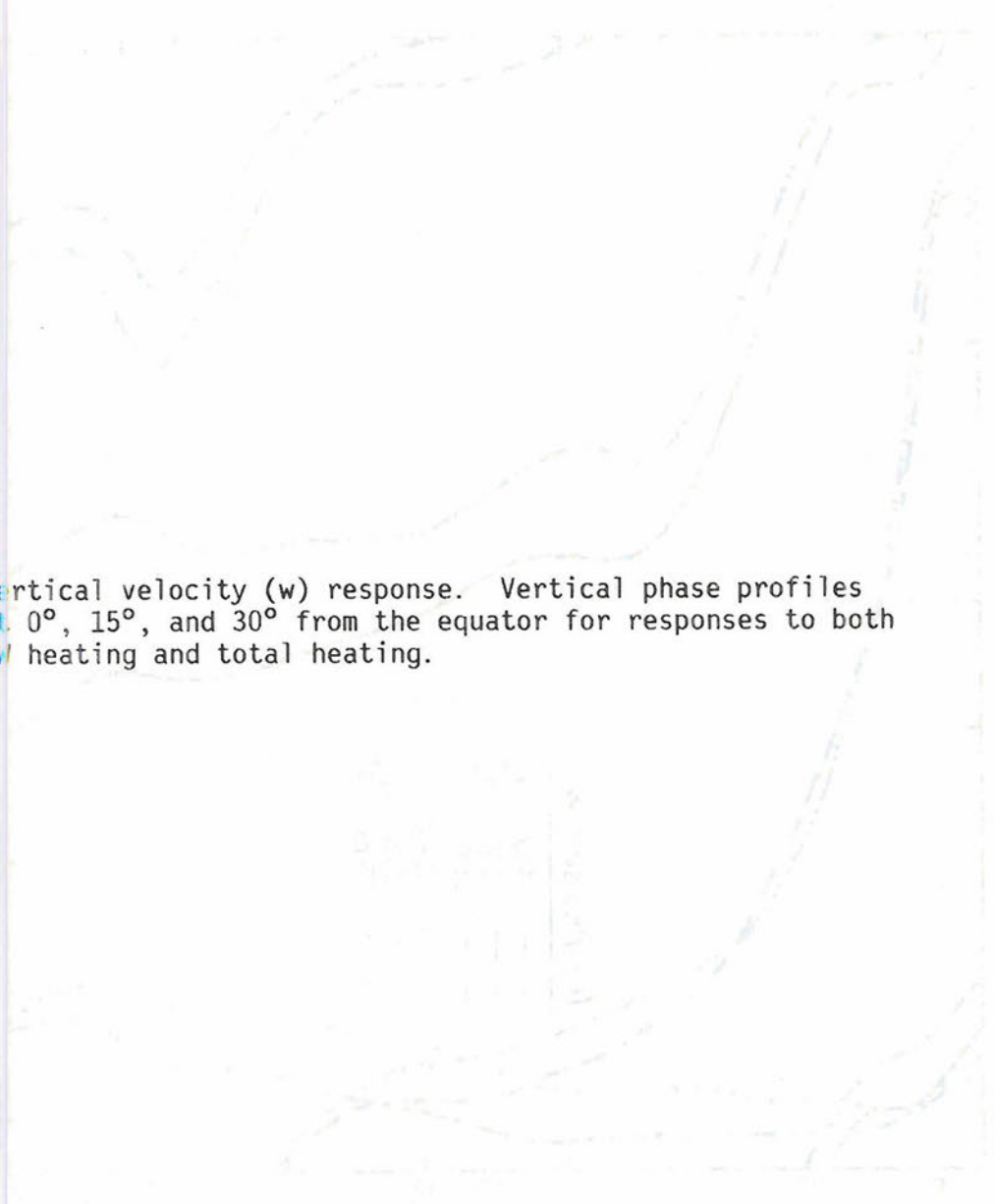


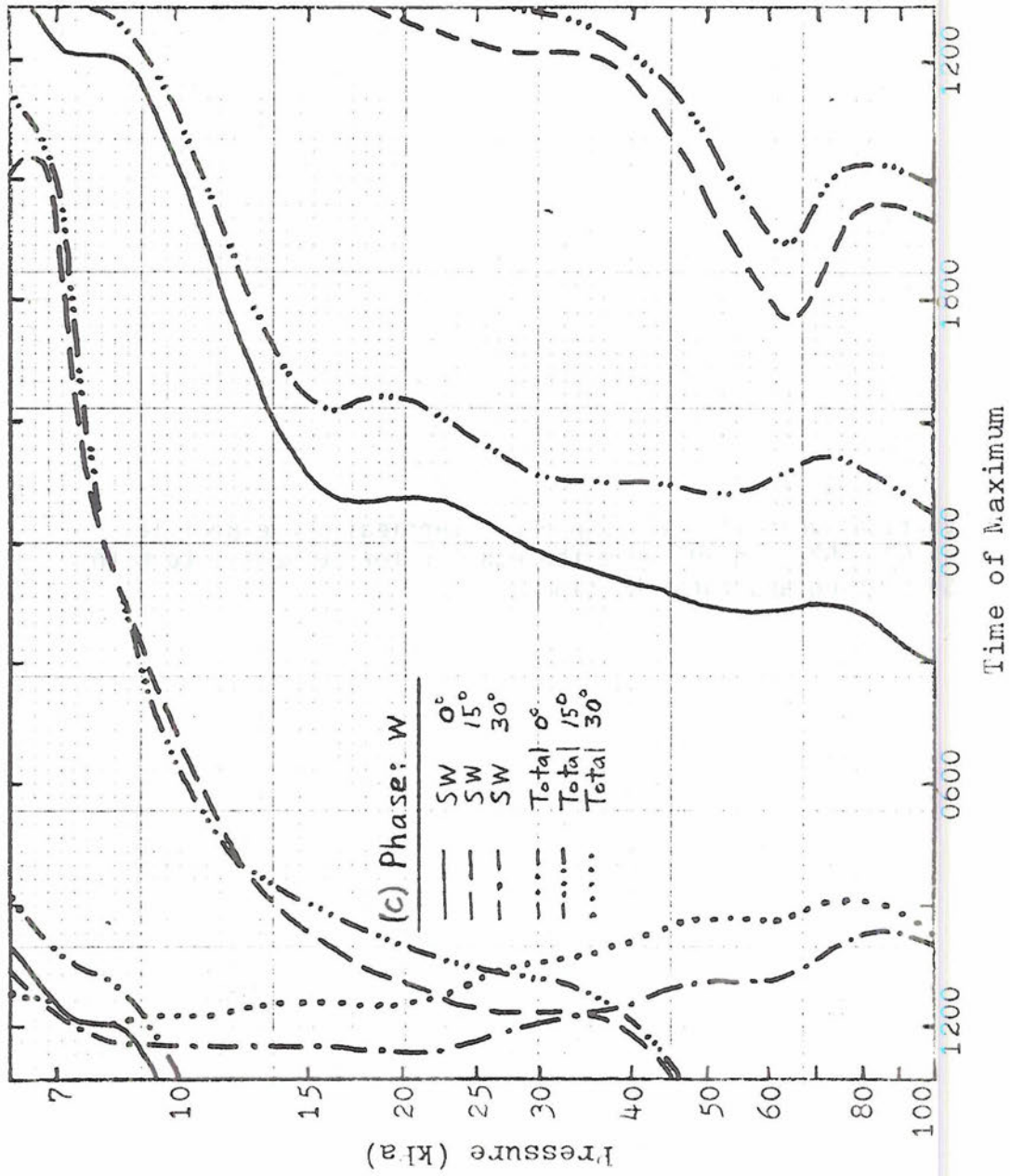
Fig. 4.9b Same as Fig. 4.9a, but for the amplitude of the response to total heating.



Some of the contours are shown in Figure 10, but for the amplitude of the response in each case.

Fig. 4.9c Vertical velocity (w) response. Vertical phase profiles at 0° , 15° , and 30° from the equator for responses to both SW heating and total heating.





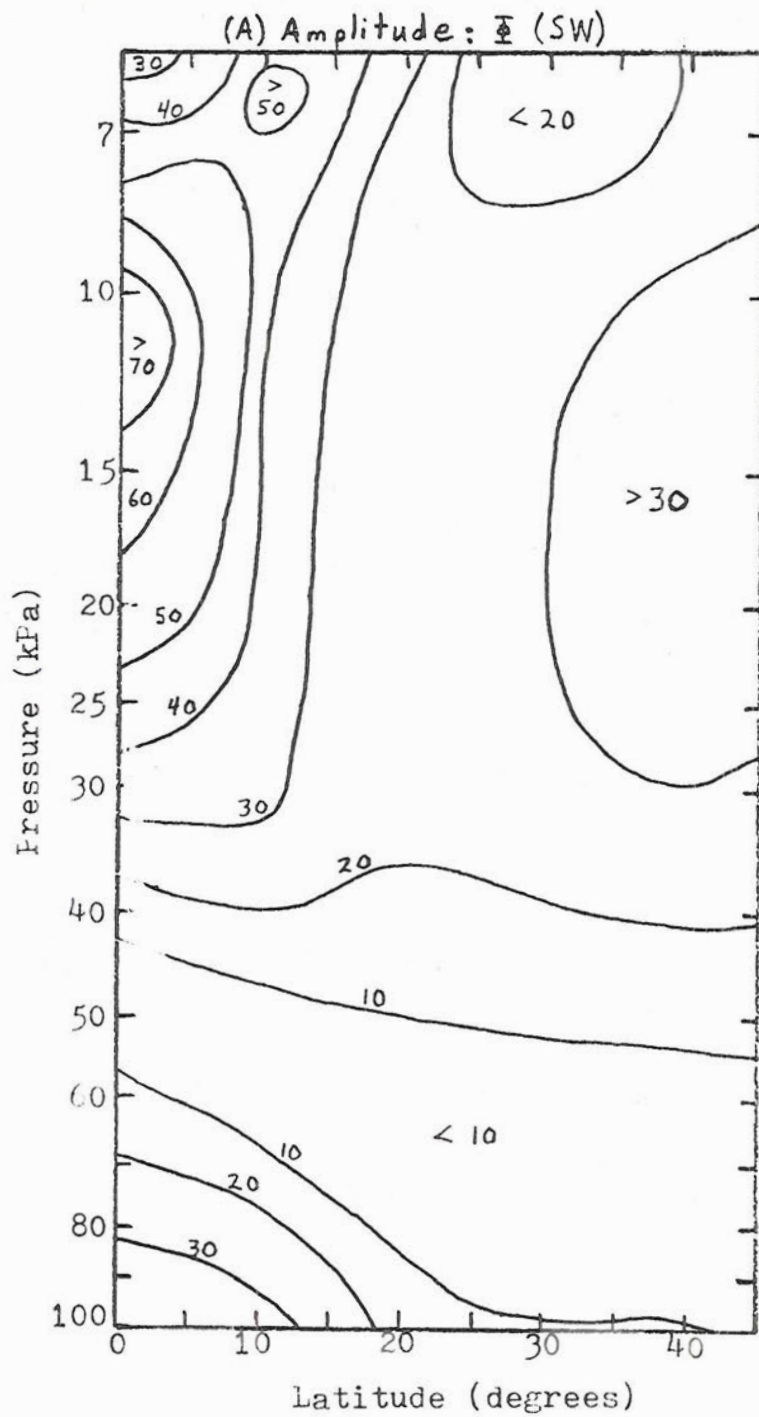
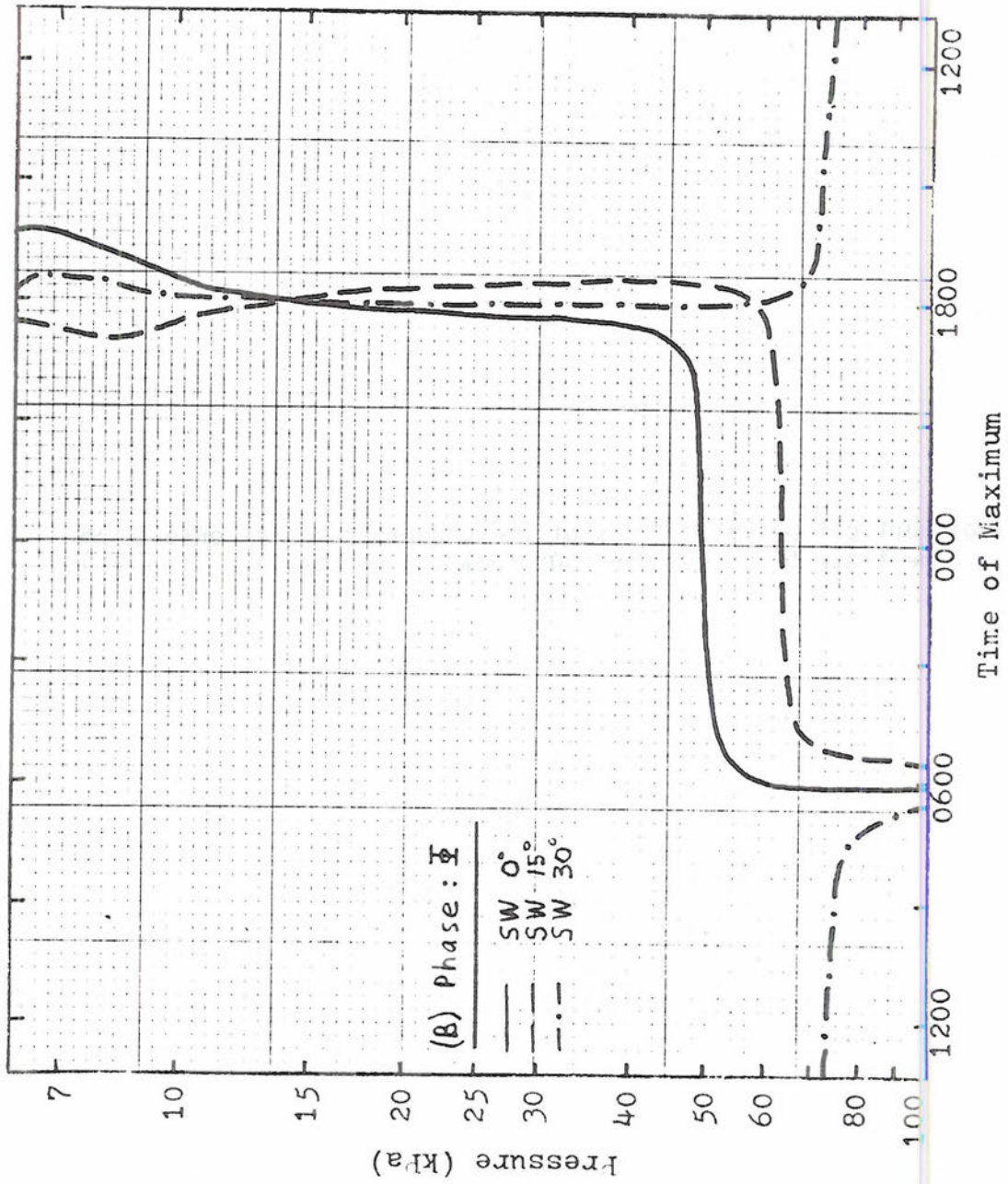


Fig. 4.10a Amplitude of the geopotential response to SW heating. Contour interval: $10\text{m}^2/\text{sec}^2$.



Fig. 4.10b Vertical phase profiles of the geopotential response to SW heating at 0°, 15°, and 30° from the equator.



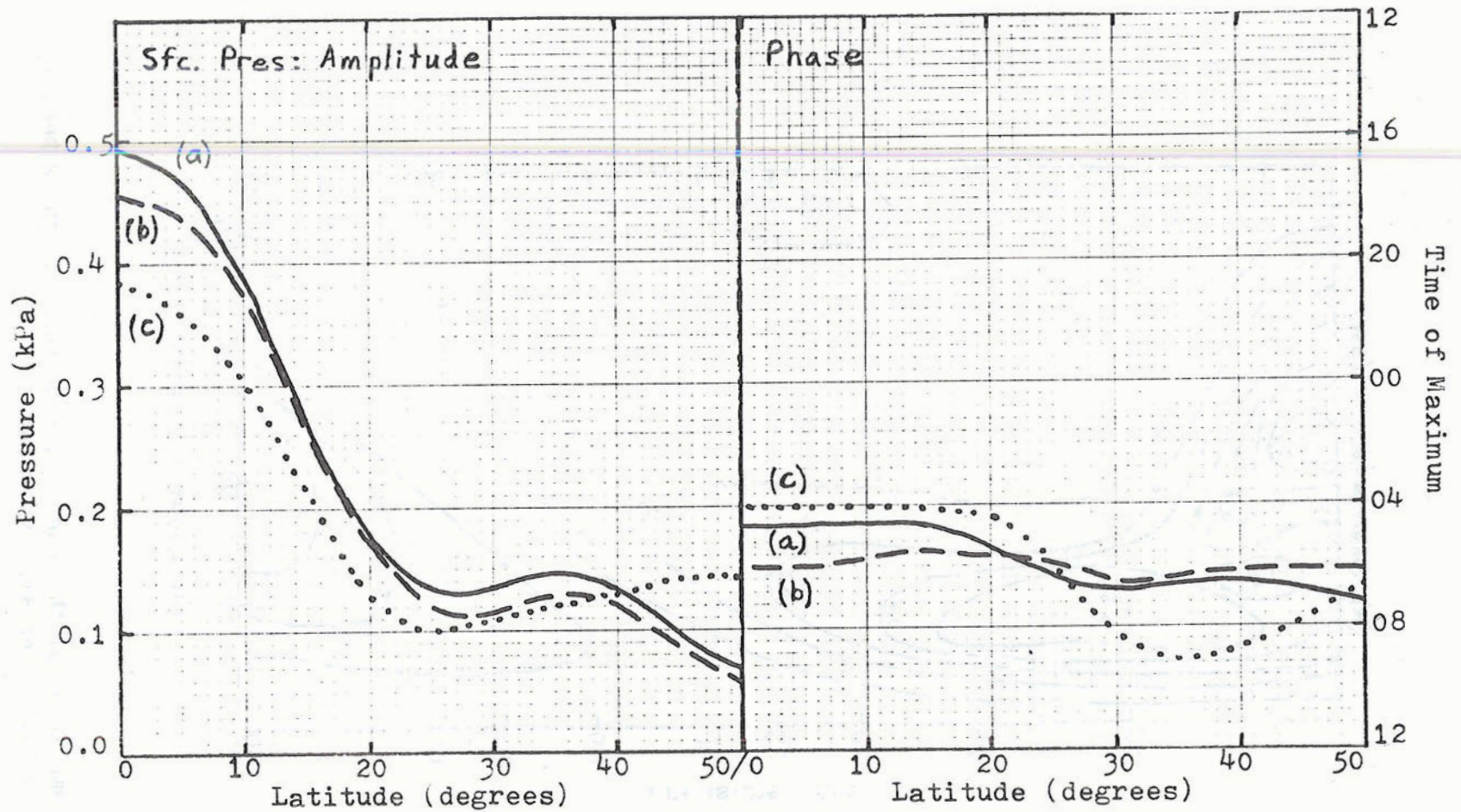


Fig. 4.11 Diurnal surface pressure variations due to (a) total heating and (b) SW heating. (c) The response calculated by Lindzen (1967) is given for comparison.

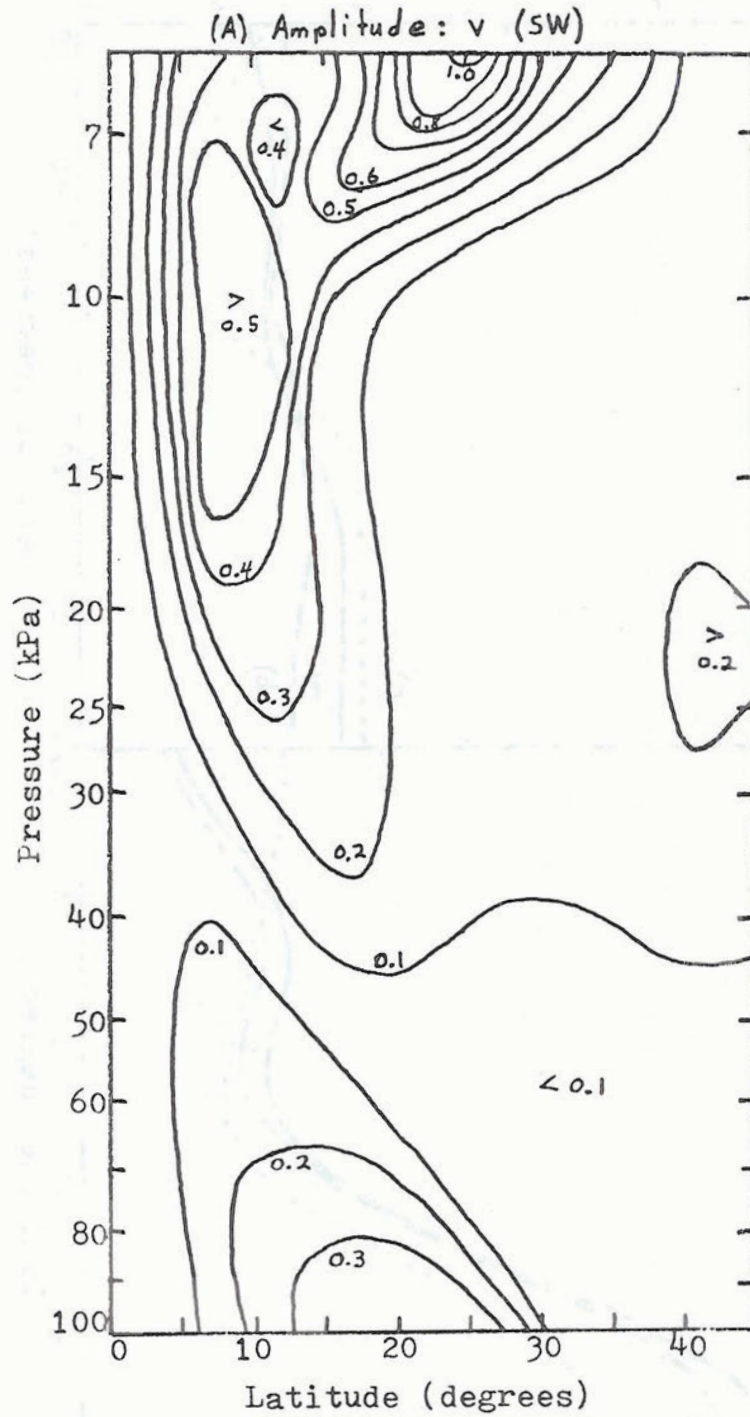


Fig. 4.12a Amplitude of the southerly wind response to SW heating. Contour interval: 0.1 m/sec.

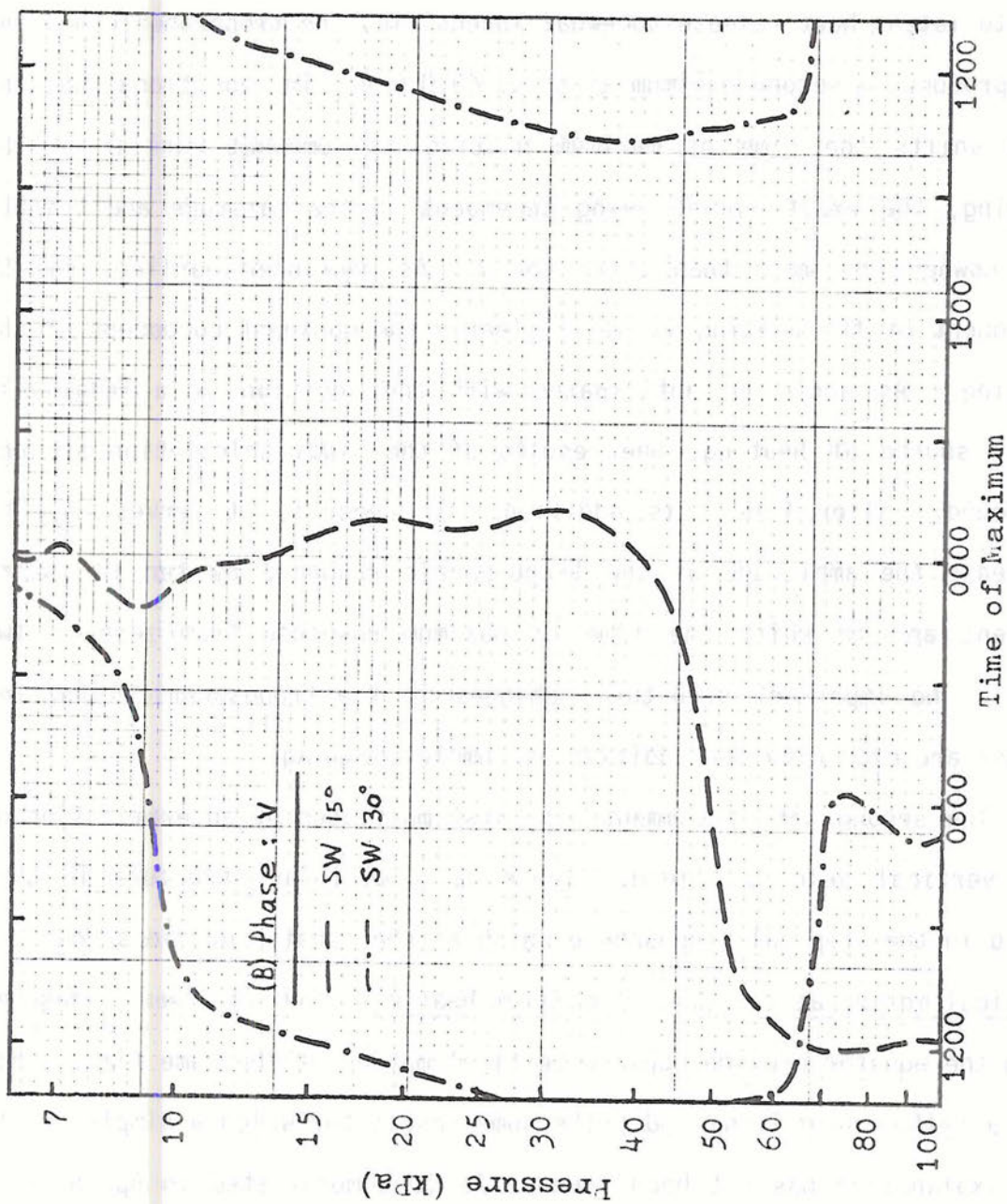


Fig. 4.12b Vertical phase profiles of the southerly wind response to SW heating at 0° , 15° , and 30° from the equator.

The results stand pretty much by themselves without requiring much explanation. Only a few features will be commented on here. The first set of comments pertains to the changes which occur with the addition of the cumulus heating. The amplitude and phase of the heating for the two runs are shown in fig. 4.6. It is evident that the additional heating due to latent heat release somewhat intensifies the tropospheric heating and produces a second maximum at about 45.0 kPa. The additional heating also shifts the time of maximum heating to somewhat earlier in the morning, the exact amount being dependent on the latitude and height, but nowhere by more than three hours. As mentioned earlier, the SW component of the heating is still clearly the dominant component of the heating. As would be anticipated with the addition of a relatively minor source of heating, the results of the tidal calculation are not profoundly altered by this addition. In general, it serves only to increase the amplitude of the tropospheric response by ten to twenty percent and to shift the time of maximum response from zero to two hours. No important structural changes in the tropospheric tidal response are caused by the addition of cumulus heating.

The second set of comments is first motivated by an examination of the vertical velocity field. There is a cellular structure in this field in the tropical troposphere which at the equator provides downward vertical motion at the time of maximum heating, and at twenty degrees from the equator provides upward vertical motion at the same time. This was a rather surprising and bothersome result for which a simple physical explanation has not been found. As is demonstrated in Appendix 3, even the mathematical explanation for this phenomenon is not very

straightforward. However, the mathematical veracity of the solution has been confirmed by two completely independent analytic solutions, and the phenomenon appeared to be quite persistent, even when fairly radical changes were made in the shapes of the forcing and the static stability profile. Apparently, even with the assumption of fairly simple structures for the atmosphere and the forcing, the problem of computing a tidal response in a thin atmosphere on a rotating sphere is still so complex that a simple physical or intuitive explanation for the results cannot easily be found.

The net circulation driven by the tidal forcing is diagrammed for the time of maximum heating in Fig. 4.13. The tidal response takes the form of a cellular circulation in the tropics. Thus, a diurnal variation is superimposed on top of the tropical Hadley circulation which tends to oppose the Hadley cell during the day and enhance it at night. (Though, of course, for the purposes of this problem, a resting basic state was assumed. But if the computed tidal response is at all characteristic of the real atmospheric tidal response, this is the effect that the computed response would display.) More will be said about this later when these results are compared to the results derived from observations.

4.2 Comparison with Earlier Theoretical Results

It seems that Lindzen is the only one who, using classical tidal theory to compute diurnal tidal variations in the troposphere, has recently shown a fairly complete set of results (Lindzen, 1967). Figs. 4.14 to 4.16 show Lindzen's amplitude and phase profiles at 0° , 15° , and 30° of latitude for the perturbation fields of temperature, westerly velocity, and vertical velocity. The corresponding results obtained

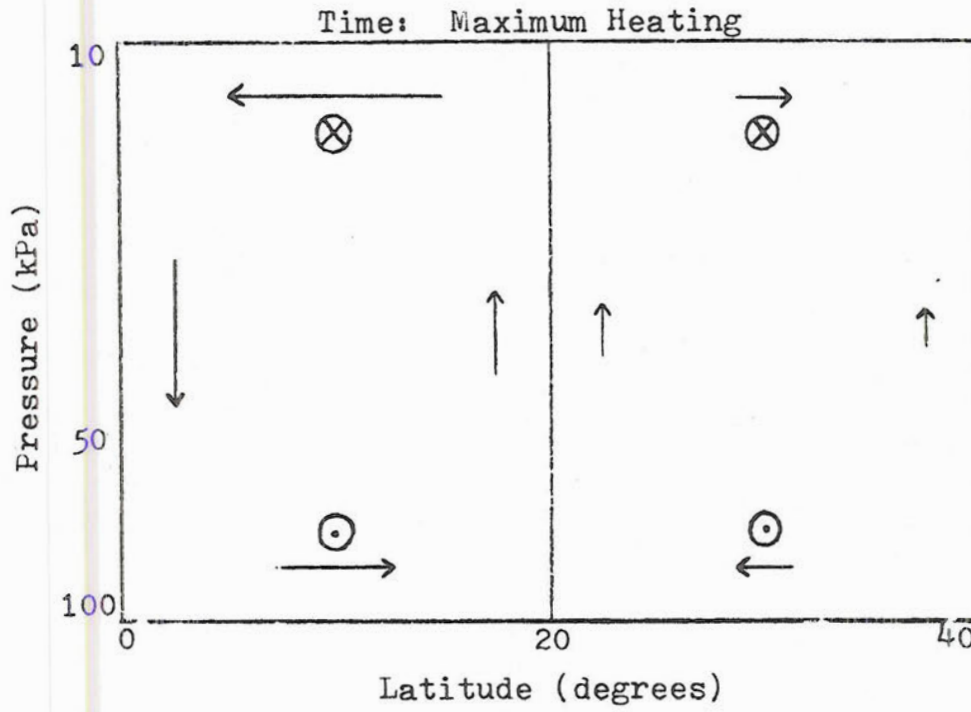
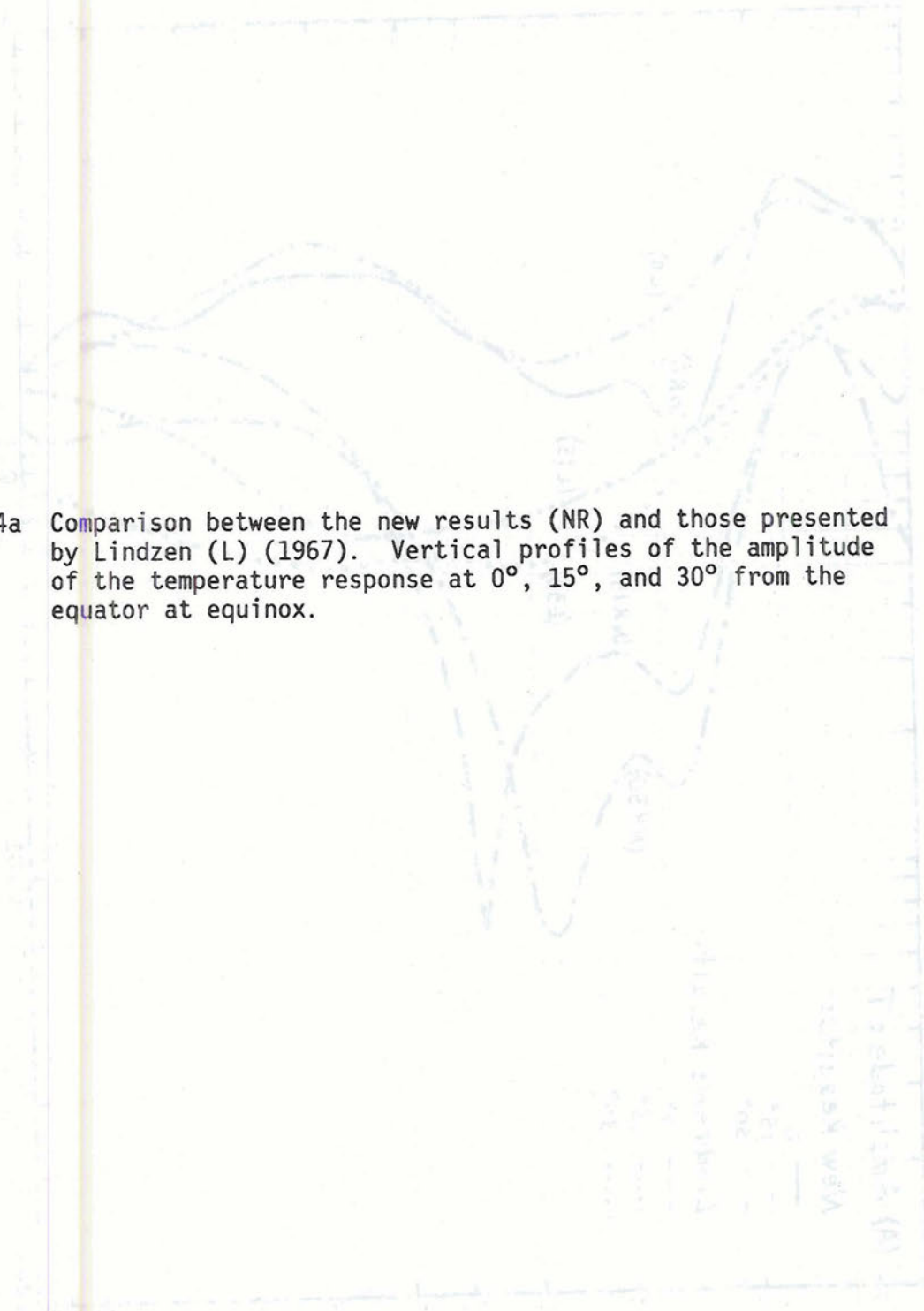


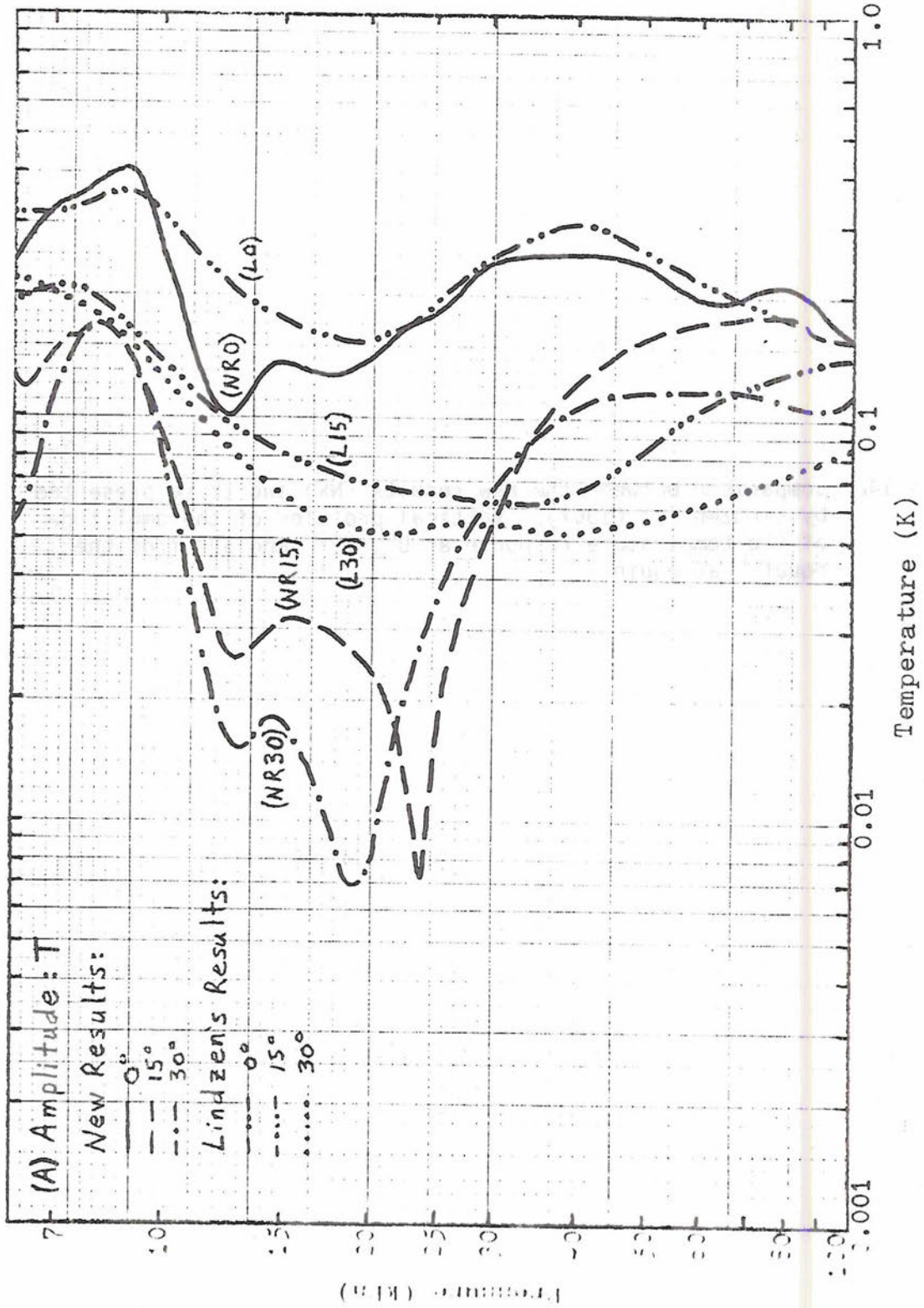
Fig. 4.13 Schematic θ - z^* cross section of the tidal wind circulation at the time of maximum heating.



At the end of the first part of the experiment, the following results were obtained:

Fig. 4.14a Comparison between the new results (NR) and those presented by Lindzen (L) (1967). Vertical profiles of the amplitude of the temperature response at 0°, 15°, and 30° from the equator at equinox.





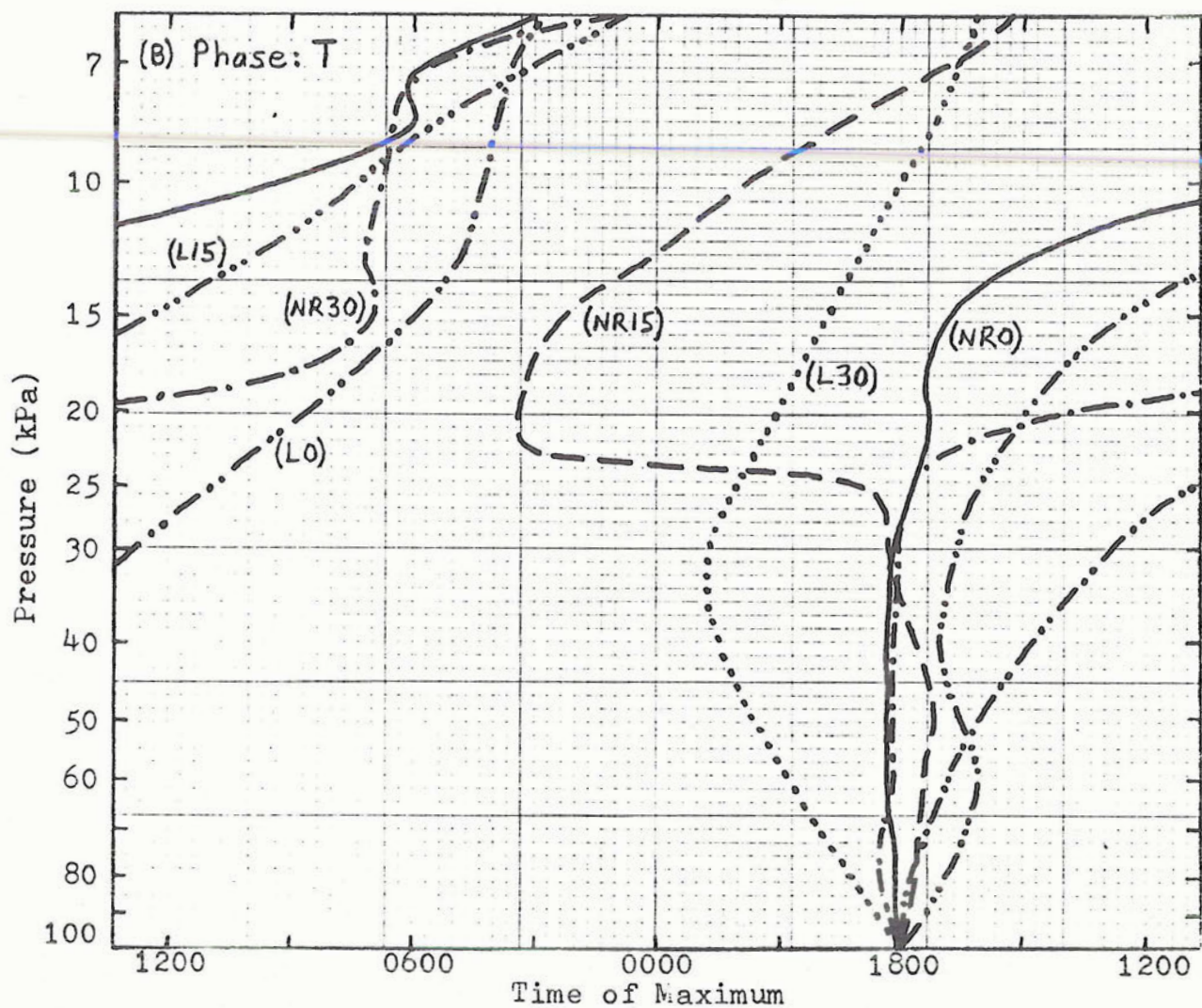


Fig. 4.14b Same as Fig. 4.14a, but for the vertical profiles of the phase of the temperature response.

1. 1000
 2. 1000
 3. 1000
 4. 1000
 5. 1000
 6. 1000
 7. 1000
 8. 1000
 9. 1000
 10. 1000
 11. 1000
 12. 1000
 13. 1000
 14. 1000
 15. 1000
 16. 1000
 17. 1000
 18. 1000
 19. 1000
 20. 1000
 21. 1000
 22. 1000
 23. 1000
 24. 1000
 25. 1000
 26. 1000
 27. 1000
 28. 1000
 29. 1000
 30. 1000
 31. 1000
 32. 1000
 33. 1000
 34. 1000
 35. 1000
 36. 1000
 37. 1000
 38. 1000
 39. 1000
 40. 1000
 41. 1000
 42. 1000
 43. 1000
 44. 1000
 45. 1000
 46. 1000
 47. 1000
 48. 1000
 49. 1000
 50. 1000
 51. 1000
 52. 1000
 53. 1000
 54. 1000
 55. 1000
 56. 1000
 57. 1000
 58. 1000
 59. 1000
 60. 1000
 61. 1000
 62. 1000
 63. 1000
 64. 1000
 65. 1000
 66. 1000
 67. 1000
 68. 1000
 69. 1000
 70. 1000
 71. 1000
 72. 1000
 73. 1000
 74. 1000
 75. 1000
 76. 1000
 77. 1000
 78. 1000
 79. 1000
 80. 1000
 81. 1000
 82. 1000
 83. 1000
 84. 1000
 85. 1000
 86. 1000
 87. 1000
 88. 1000
 89. 1000
 90. 1000
 91. 1000
 92. 1000
 93. 1000
 94. 1000
 95. 1000
 96. 1000
 97. 1000
 98. 1000
 99. 1000
 100. 1000



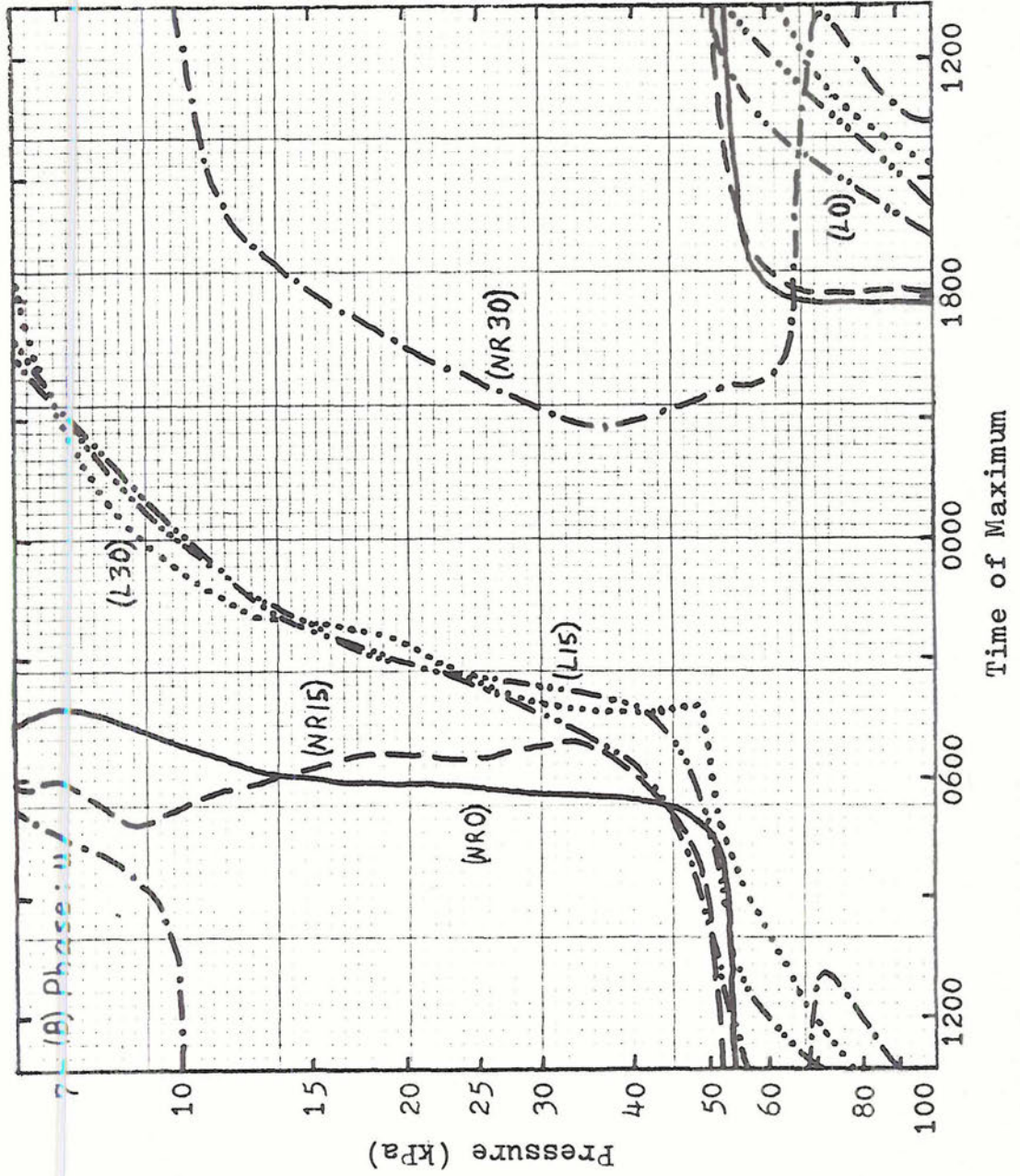
Fig. 4.15a Comparison between the new results (NR) and those presented by Lindzen (L) (1967). Vertical profiles of the amplitude of the westerly wind response at 0° , 15° , and 30° from the equator at equinox.

THE UNIVERSITY OF CHICAGO
DIVISION OF THE PHYSICAL SCIENCES
DEPARTMENT OF CHEMISTRY
5708 SOUTH CAMPUS DRIVE
CHICAGO, ILLINOIS 60637



Fig. 4.15b Same as Fig. 4.15a, but for the vertical profiles of the phase of the westerly wind response.

These are the only two responses
to the question, "What is the
purpose of the study?"



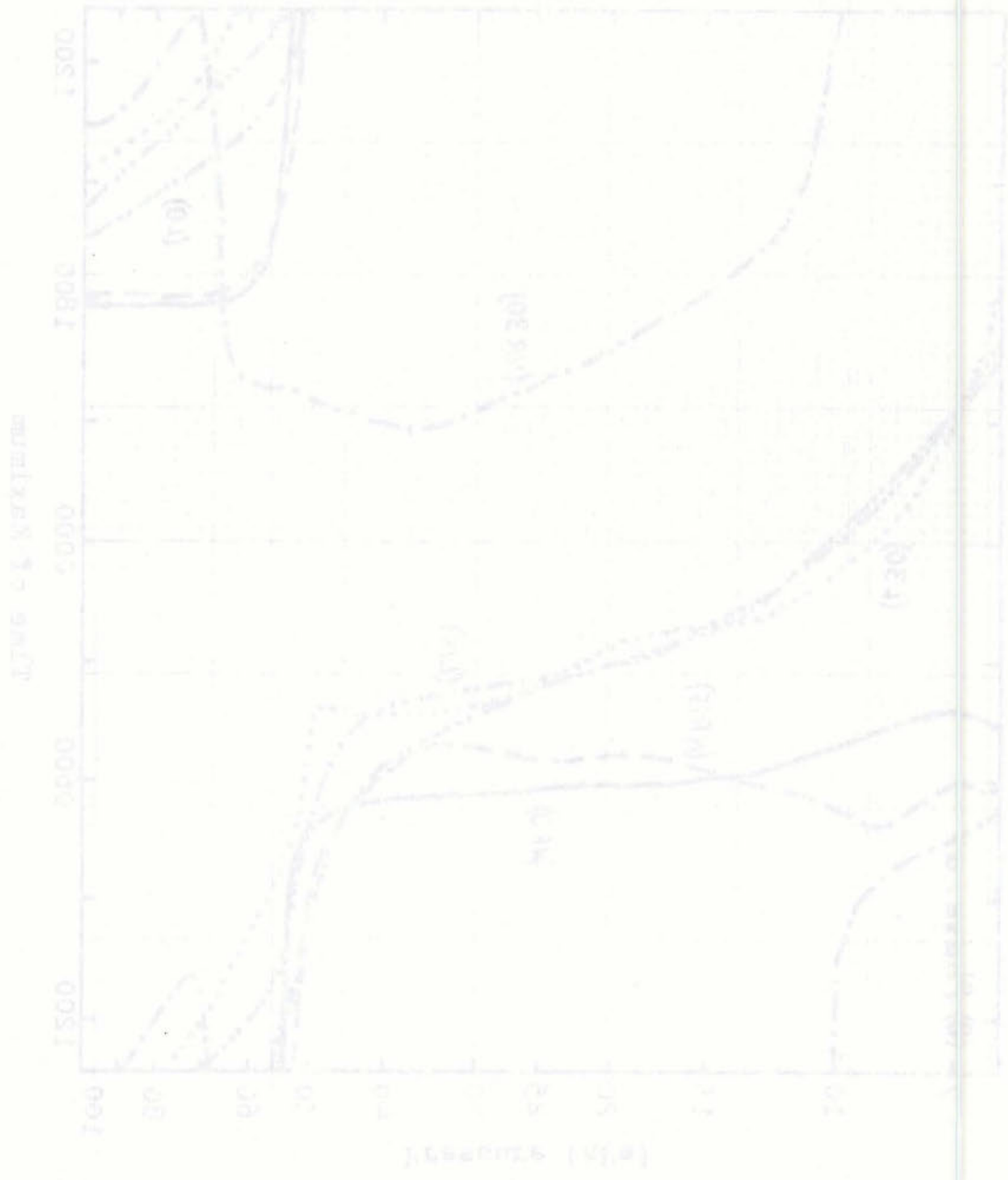
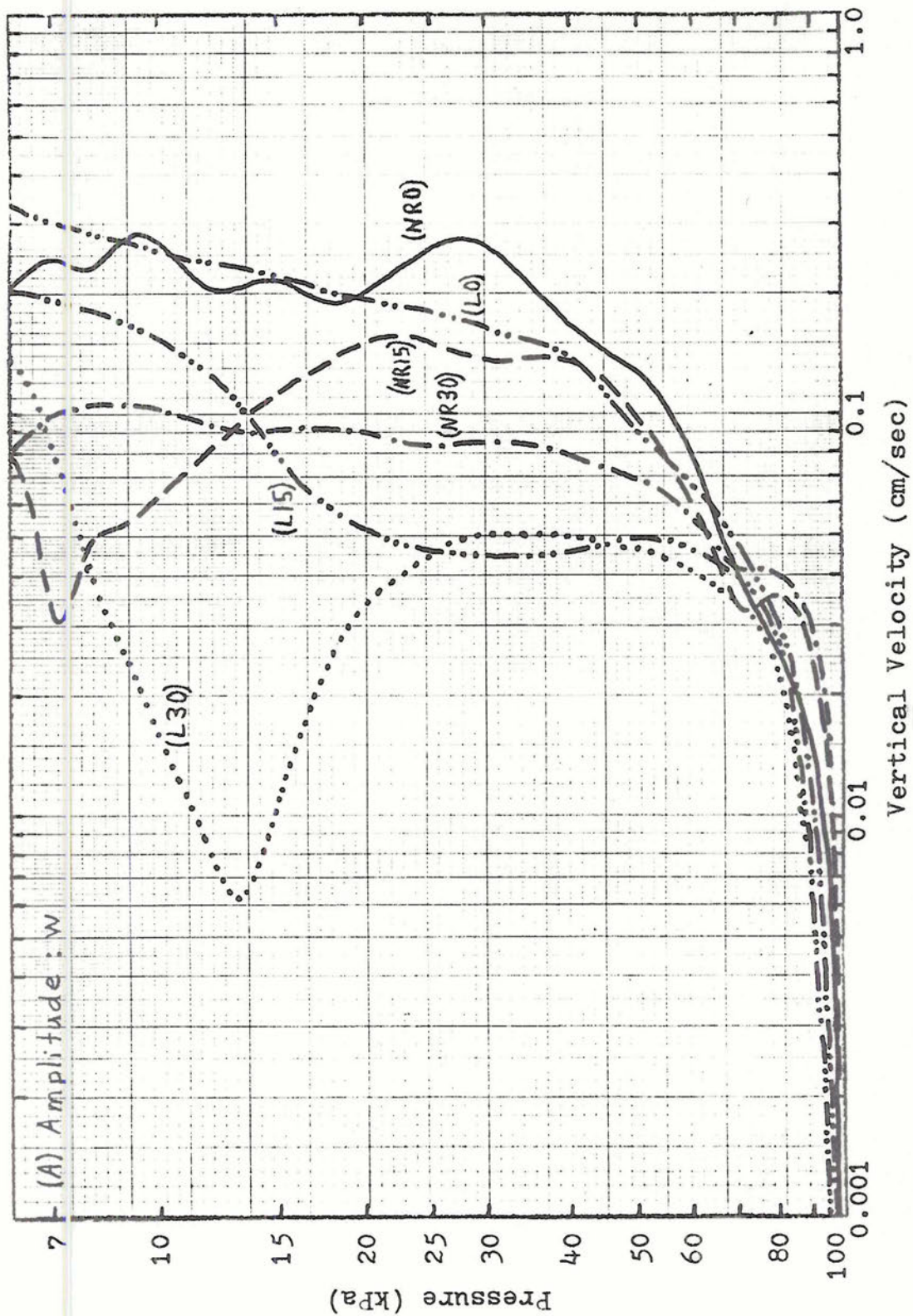


Fig. 4.16a Comparison between the new results (NR) and those presented by Lindzen (L) (1967). Vertical profiles of the amplitude of the vertical velocity (w) response at 0° , 15° , and 30° from the equator at equinox.

...the ... of ...
...the ... of ...
...the ... of ...





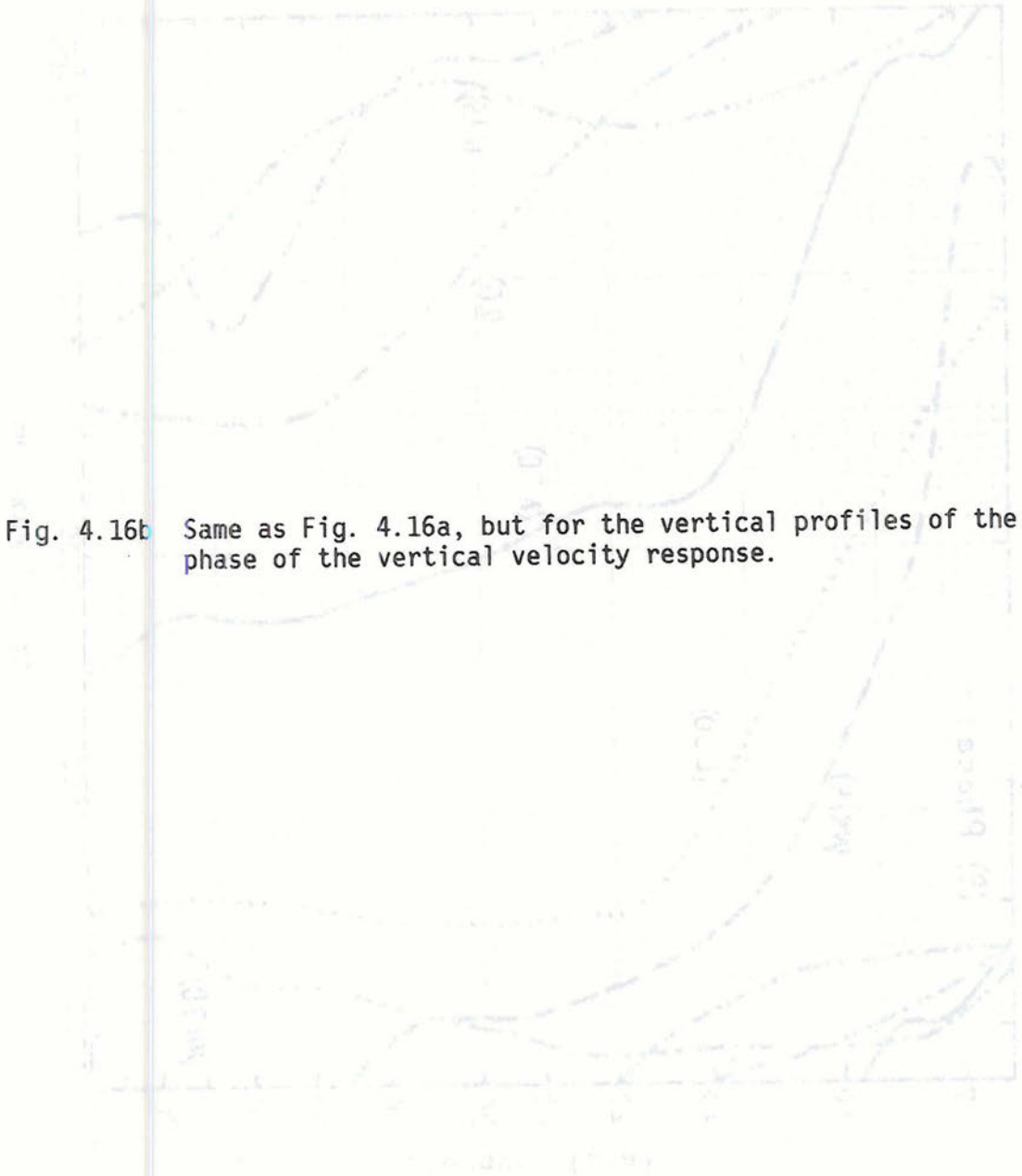
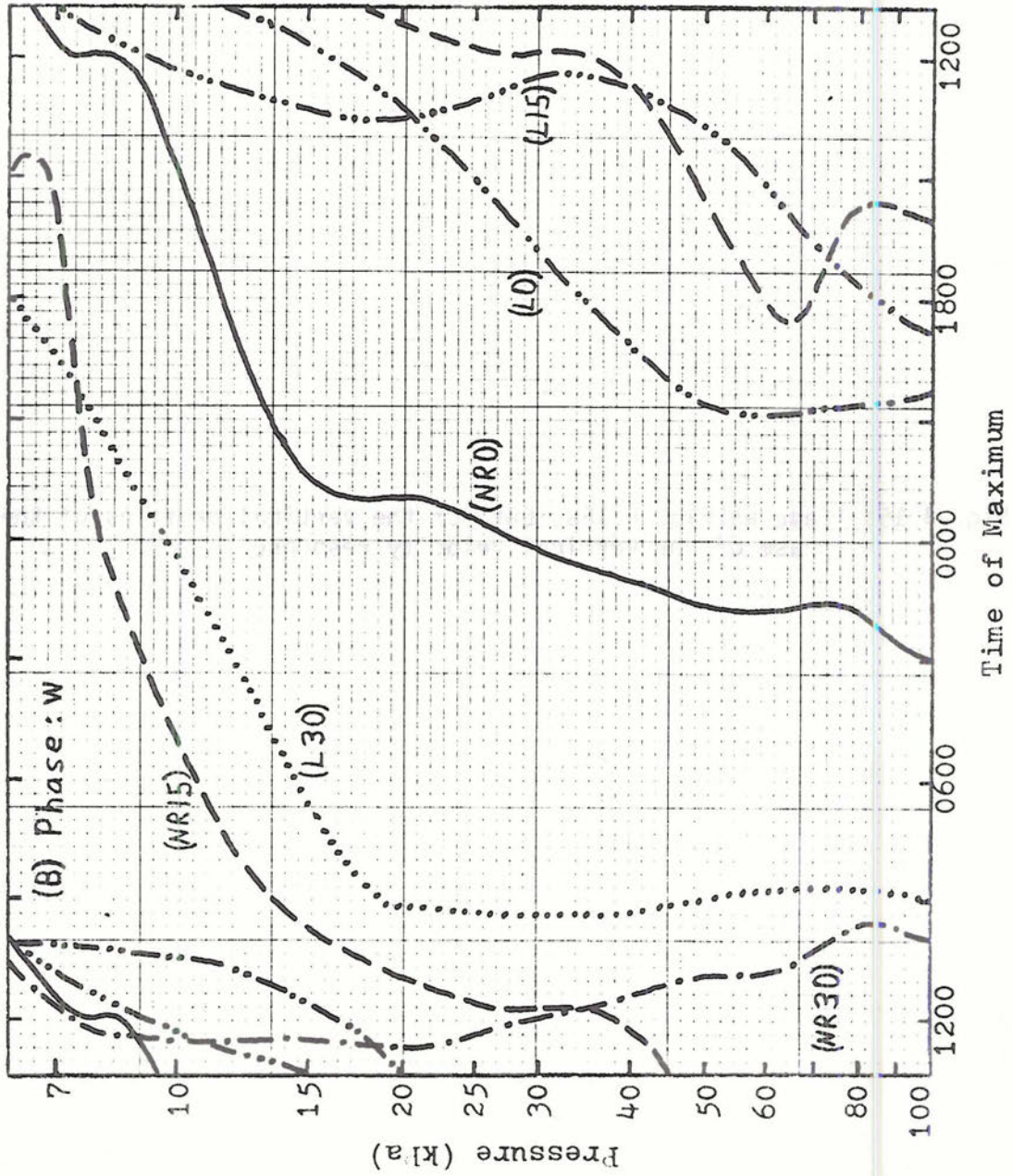


Fig. 4.16b Same as Fig. 4.16a, but for the vertical profiles of the phase of the vertical velocity response.



from this research are also shown. Both sets of results were obtained using only SW heating.

It is difficult to find any consistent differences between the two sets of results. About all that can be said is that the differences are frequently quite large through most of the troposphere. The vertical structures of both the amplitude and phase profiles are quite different at all three latitudes and for all three variables.

Three factors are responsible for the differences between these sets of results. First, Lindzen used only five Hough modes in his calculations, whereas 16 were used here. Second, the two sets of results were obtained using very different H₂O heating functions (see Fig. 3.6). However, the most significant contributor to the difference is the fact that all of the results which Lindzen shows were obtained using an isothermal atmosphere (260 K). This assumption especially affects the vertical profiles of phase. In light of the sensitivity of the model to changes in the static stability profile, it is quite surprising that no one has published complete results using a more realistic profile.

Lindzen did compute the diurnal tidal response using more realistic static stability profiles, but he showed no results below 30 km (Lindzen, 1968). He makes the observation that variations in the tropospheric static stability profile are the most effective factor in modifying the tidal fields throughout the atmosphere. However, nothing was published showing the changes that occur in the tropospheric tidal response as a result of using these different profiles. Consequently, most subsequent observational studies have made comparisons to the

inadequate theoretical results obtained by using an isothermal atmosphere. Hence, the need to show the results given in this report is made plain.

Hong and Wang (1980) used classical tidal theory with realistic H_2O and ozone heating functions and with a realistic static stability profile to determine the dynamic tidal responses in the atmosphere. Their primary objective was to obtain a better agreement between theory and observations for the semi-diurnal tide, and consequently they were concerned mostly with the ozone heating function which is much more effective in producing the semi-diurnal tropospheric response. However, they also looked at the diurnal tidal responses in the surface pressure field and the northerly component of the wind. It is unfortunate they did not present more results for other perturbation variables. As it stands, the forms in which they present their results provide little enlightenment into the nature of the tropospheric diurnal tidal response.

In the same paper, Hong and Wang also consider the effect of latent heat release in forcing tidal oscillations. They compute the amount of cumulus heating required to account for the difference between observed surface pressure variations and the predicted surface pressure oscillations using only SW heating. Assuming a particular vertical profile of latent heat release, they then compute the diurnal variation in rainfall rate implied by this amount of cumulus heating and compare this value to observed diurnal variations in rainfall rate. They show results only for the semi-diurnal tide. They make the valid observation that computing the diurnal component of latent heat release from rainfall data probably substantially underestimates the magnitude of this diurnal heating component. The droplets which reach the ground as rain account

for only a fraction of the amount of water which is condensed in a cloud, and many clouds may form without ever producing rain that reaches the ground. Water droplets which do not fall out of clouds may later evaporate and extract heat from the atmosphere. Thus, this process does not contribute to the net heating of the atmosphere, but it does contribute to the oscillations of the atmospheric heating. Diurnal variations in cloudiness or cloud water content may be of the same order of importance as diurnal variations in rainfall, and therefore the simple parameterization of latent heat release used in this research may significantly underestimate the total latent heat release.

Hong and Wang further point out that latent heat is released at the time of condensation -- not at the moment the rainfall reaches the ground. Consequently, the maximum heating due to latent heat release should occur sometime before the maximum rainfall. However, Lindzen (1977) suggests that this time delay should only be a few minutes. In light of the many other factors which introduce inaccuracies into the tidal calculation, it seems useless to quibble about small phase differences (less than about 1 hour) between theory and observations for whatever reason they may arise.

In any case, for the semi-diurnal tide, Hong and Wang determined that cumulus heating probably produces a larger tropospheric response than H_2O heating and less than ozone heating. This is contrary to the case for the diurnal tide. However, it is possible that latent heat release could produce more significant changes in the tidal responses than have been shown in the results of this research.

Earlier, Lindzen (1977) studied the role of cumulus heating in forcing the semi-diurnal tidal response by using a similar technique.

Concerning the diurnal tide, Lindzen only notes that the diurnal component of rainfall seems to be rather incoherent in phase around the globe, and that, relative to the SW heating component, the cumulus heating is fairly small. He assumed, therefore, that tropical latent heat release would not contribute significantly to the migrating diurnal tide. Lindzen also notes the great difficulty of computing the diurnal rainfall component from real data and the large uncertainties in the results of such analyses. (This, by the way is a crucial problem which generally arises in all attempts to compute tropospheric tidal variations from observational data, though the problem is particularly acute in computing rainfall variations.) The results of this research tend to confirm Lindzen's conclusion that the cumulus heating is small relative to the SW heating; though it was found in this study that, even in the possibly underestimated form used here, the cumulus heating can produce a significant response.

Hamilton (1981) tried to examine the effects of the geographic distribution of latent heat release in forcing tidal oscillations. Again, most of his work investigated the impact of this factor on the semi-diurnal tide. However, he did also briefly examine the effects on the diurnal tidal response. Unfortunately, he made a critical assumption which, in light of the observational results presented by Gray and Jacobson (1977), appears to be quite poor. Gray and Jacobson discovered that globally, the diurnal component of deep convection and rainfall is predominant -- especially over the oceans. Hamilton, using data mostly from continental and coastal stations concluded that the diurnal component of latent heat release is much more important (both in terms of amplitude and in terms of phase coherence among stations) over land

areas than it is over the oceans, and that it is the semi-diurnal component of latent heat release which dominates over the oceans. Considering the highly variable effects of topography and sensible heat transfer over continents, one would hardly expect to find the diurnal tide to be more coherent over land than over the oceans (see Wallace and Hartranft, 1969). In any case, Hamilton proceeded to postulate a global cumulus heating function which was equal to zero over the oceans and had a functional form over land with an unphysical discontinuity at cloud top. As would be expected from ignoring the diurnal variation of latent heat release over 70% of the earth's surface, he found the diurnal tidal response in the perturbation field of the southerly wind component to be quite small.

As has been shown here, the most recent theoretical calculations of the tropospheric diurnal tidal variations using classical tidal theory are inadequate. The work that has been done has tended to focus on the semi-diurnal tide. Since Lindzen's work in 1967, no one has given a detailed presentation of significantly improved values for diurnal tidal variations in the troposphere. The role of latent heat release as a forcing mechanism for the diurnal tide has also been discussed in the past. However, no adequate presentation has been given to compare the diurnal tidal responses which are produced with and without the inclusion of this additional forcing. The results obtained in this research differ significantly from Lindzen's results. The need to update his results and to present new results showing the effects of cumulus heating is evident.

4.3 Comparison with Observations

In order to achieve advancement in the understanding of the atmosphere, there must be interplay between theoretical and observational analyses of the same phenomenon. This section focuses on this aspect of scientific inquiry. The theoretical results of this research will be compared to a number of recent observational studies of diurnal tropospheric variations.

4.3.a General remarks about observed diurnal variations

Before making individual comparisons, it would be well to make a few general comments about how the theoretical results compare to the observational results. Unfortunately, even with the improvements incorporated into this treatment of classical tidal theory, it was found that the agreement between theoretical and observational results was not improved as much as had been hoped. Usually, the difference in amplitude was still a factor of two or three or more, while the phase structures of the theoretical tidal responses still did not agree well with the observed phases either.

Obviously, some way must be found to account for this discrepancy. Two factors can be mentioned here at the outset. First, it is apparent either that the magnitudes of the forcing components used in this research must be underestimated or that some of the neglected effects must be important. Second, there is still a pretty large amount of uncertainty in the observational analyses.

With regard to the second factor, it is always tempting in a theoretical treatment of a phenomenon to blame the discrepancy with the observations on the poor quality of the observations. This should not be done unless the fault in the observational techniques can be clearly

elucidated. However, several things should be said about how diurnal tidal variations are deduced from observations. All tropospheric diurnal variations have been computed from rawinsonde data or from surface pressure measurements. The possibility of inherent and systematic errors in rawinsonde measurements of wind and temperature are well known. It has been argued by some that improved technology and accurate schemes to account for systematic errors have sufficiently reduced these sources of error to the point that the diurnal variations observed in the data are clearly significant (Foltz and Gray, 1979; Wallace and Patton, 1970). It should be remembered though that even with all instrumental error removed, it would still be difficult to discover the amplitudes and phases of diurnal variations in the troposphere. This is the most variable and complex part of the atmosphere in many respects, and the signal which is being sought is very small. Consequently, large amounts of data over long periods of time and at frequent time intervals during the day are required in order to obtain statistically significant values of the diurnal tropospheric variations. The necessary quantity of data is seldom (if ever) available for a single station -- much less for a large region. As a result, most observational studies report large margins of error. Often these error bounds, being as great as 30, 50, or 100 percent or more, are sufficiently broad to allow agreement with the theoretical results through much of the atmosphere. However, the fact that almost all observational studies are consistent in reporting larger amplitudes for the diurnal variations than the theory would allow seems to be significant.

The possibility that neglected effects are important is the other factor which must be considered. Numerous observational analyses have

argued for the significance of surface sensible heat flux, continent/ocean distributions, topography, the mean wind field, and longitudinally dependent heat sources (see for example Nitta and Esbensen, 1974; Wallace and Tadd, 1974; and Yoshida and Hirota, 1979). It appears from observations that there are local and regional effects everywhere around the globe that have the net effect of increasing the amplitudes of diurnal variations while significantly altering the phase structures from what theory would predict. However, one point should be remembered. This research focused exclusively on that migrating component of the diurnal tide which has zonal wavenumber one in the assumption that this should be the clearly dominant diurnal component and that these neglected factors would not contribute much to this component (see Chapman and Lindzen, 1970). If it is still true that these neglected factors do not contribute much to this component, it is then quite evident that the component with zonal wavenumber one is not the single dominant component.

So, in light of these factors, what kind of data should provide the best comparison to the theoretical results in this research? Single station observational analyses are not likely to be very enlightening, especially if they are over or anywhere near to a continent or some other relevant surface inhomogeneity (such as a warm ocean current) or atmospheric irregularity (such as a regional variation in water vapor content). Regional analyses utilizing data from a number of stations over a large area are less likely to be subject to local effects and inhomogeneities, but larger scale effects (particularly continent/ocean effects) are still likely to be important. If data could be collected

at small islands, atolls, or ships far from any continent, these regional effects could be minimized. However, the migrating diurnal tide is a global effect, and (as is typically suggested by idealistic theorists) probably only a global collection of data would be sufficient to obtain cancellation of regional and local effects so as to yield a data set which could be analyzed for the amplitude and phase of the diurnal component with zonal wavenumber one -- a pretty tall order.

From the observations, it appears that the nature of the diurnal tropospheric variations is not simply or adequately explained by the classical tidal theory as treated in this report. However, without the global analysis mentioned above, it is also difficult or impossible to ascertain whether or not this treatment is adequate for quantifying the characteristics of this one component of the diurnal tide -- the migrating zonal wavenumber one component. As will be shown, though, there appears to be a fairly significant phase discrepancy of some three or four hours which could be explained in more than one way, but which may indicate that a significant tropospheric forcing mechanism has been neglected in this treatment.

4.3.b Observational comparisons

Keeping these precautions in mind, comparisons will be made between the theoretical results of this research and the results derived from observations which are shown in six papers. In addition, the observational results presented in several other papers will also be commented on. It should be noted that comparisons will be made here between the theoretical results at equinox and observational results obtained in the tropics regardless of the season in which the observations were collected. The added assumption made here is that, in the tropics, the

seasonal variation of the diurnal tide is negligible. Certainly the SW heating will not vary a great deal in the tropics during the course of a year, and thus the tidal response would not be expected to vary significantly either.

The first comparison will be made to results presented by Foltz and Gray (1979). They analyzed rawinsonde data from five tropical experiments (GATE, ATEX, LIE, Operations Redwind and Hardtack, and BOMEX) in order to compute the diurnal temperature variation in the 85.0 to 45.0 kPa layer. Each of the five curves of the daily temperature cycle had very nearly the same character and phase (to within two hours), though the amplitude of the daily variation varied by about a factor of three among the experiments. When the five curves were averaged together, they produced the daily temperature curve shown in Fig. 4.17, which shows a peak-to-peak amplitude of 0.58°C and which reaches a maximum at 1400 LT. This is a nice result with which to make a comparison because these five experiments were spread out around the globe, were located in different parts of the Atlantic and Pacific Oceans relative to the continents, were located either on small islands or ship arrays, and were all within about $\pm 5^{\circ}$ of latitude from 10°N . So, a good comparison might be expected. Using SW heating only, the calculated temperature variation in the same layer at 10° from the equator has a peak-to-peak amplitude of 0.42°C and reaches a maximum at 1800 LT -- a delay of four hours from the observed time of maximum. Adding the cumulus heating increases the peak-to-peak amplitude at 10° away from the equator to only 0.44°C and only pulls the time of maximum back to 1630 LT. Thus, the theory predicts a response about $3/4$ as large as what is observed with a phase that implies a maximum several hours later. One conclusion

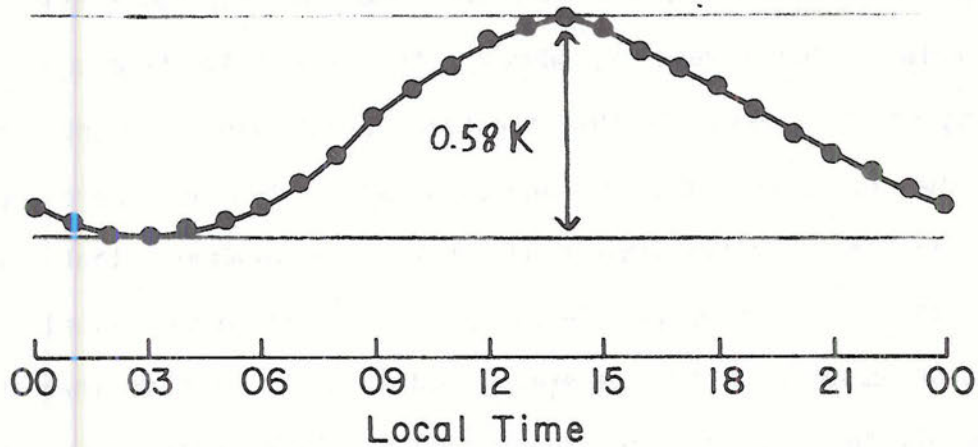


Fig. 4.17 Mean hourly temperature deviation in the 85.0 to 45.0 kPa layer for the five tropical experiments (GATE, ATEX, LIE, Operations Redwind and Hardtack, and BOMEX). (Adapted from Foltz and Gray (1979).)

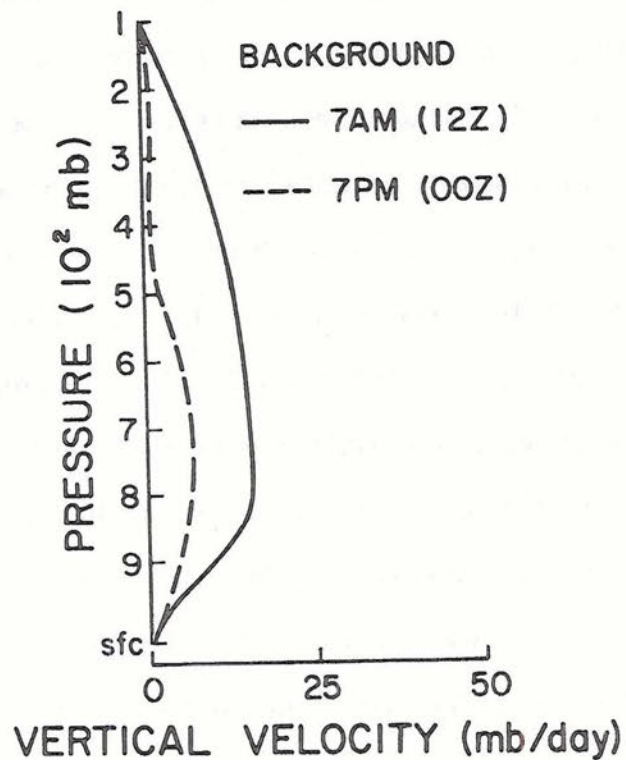


Fig. 4.18 Vertical velocity profiles for the western Atlantic background composite. (Adapted from McBride and Gray (1978).)

that could be drawn from this comparison is that quite a significant additional amount of heating would be required to produce exact agreement between these results, whether this might be from a source of heating not considered in this treatment or whether it might just mean that the additional heating source (cumulus heating) here has been underestimated. On the other hand, it must be remembered that Foltz and Gray stated that the magnitude of the instrument error caused by solar radiation absorption "is generally believed to be less than 0.2 K". Presumably this implies that the value of 0.58 K could be in excess by as much as 0.2 K and that, therefore, the theoretical result lies within the error bound of the observational result.

A second comparison can be made to a result given by McBride and Gray (1978) which is shown in Fig. 4.18. They show vertical velocity profiles at 0700 LT and 1900 LT for a background composite over the western Atlantic. By background composite they mean a composite over many years of summer months of data for this region and a composite over all weather conditions. The twelve hour difference between these curves is shown as the solid curve in Fig. 4.19. In making this twelve hour difference, all of the contributions by even (temporal) tidal harmonics in the ϕ -direction will automatically be eliminated, and the assumption is made that the diurnal component is of much greater importance than all higher order odd harmonics. The objective was to reproduce this curve. Initially, it was assumed that the theoretical results at 20° from the equator would be most representative of this region. As is shown in Fig. 4.19a, several different twelve hour difference curves were computed to compare with the result shown by McBride and Gray. It seemed that the closest fit was the theoretical twelve hour difference

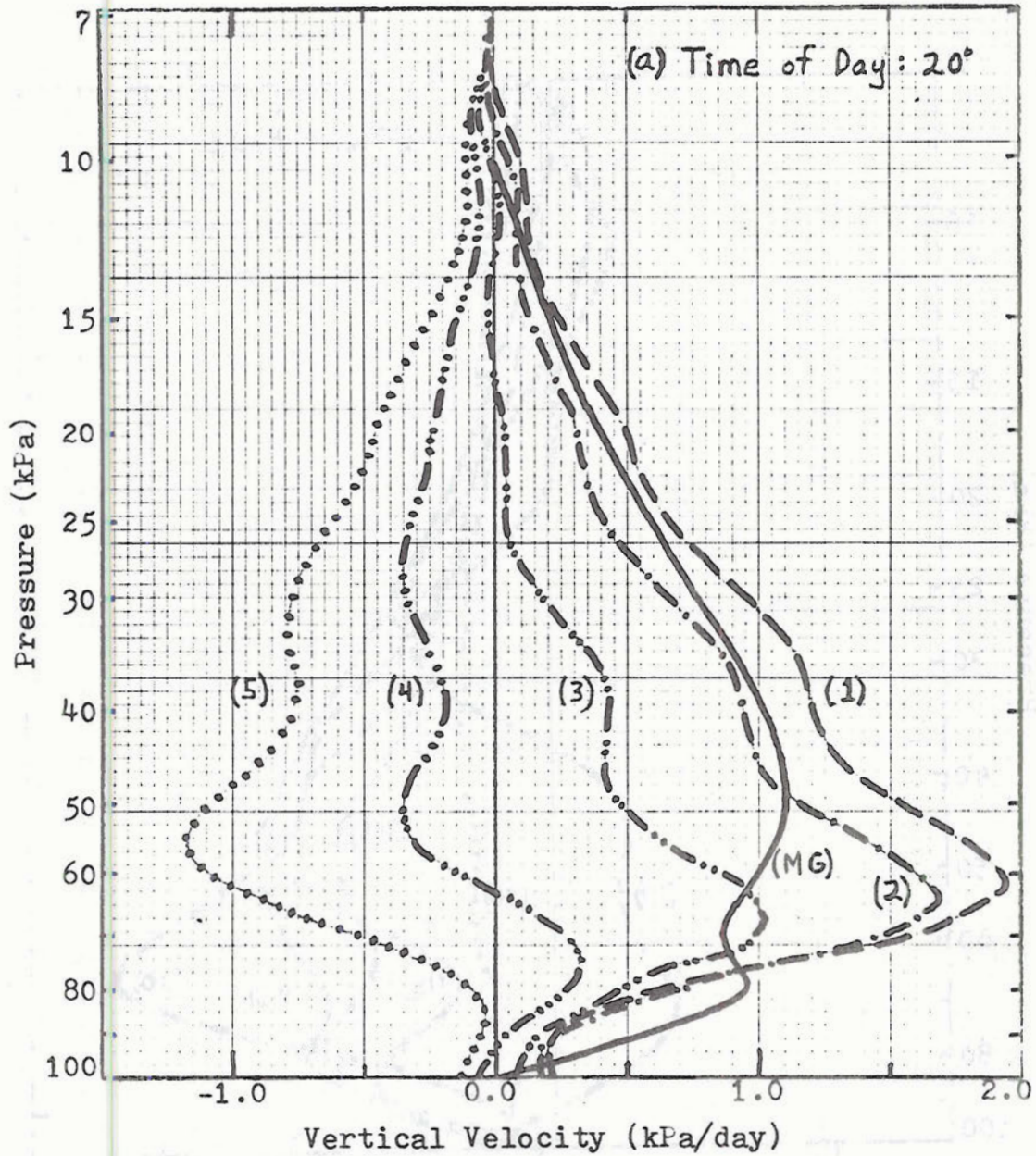


Fig. 4.19a Comparison of the ($w_{0700}^{-w_{1900}}$) background composite vertical profile of McBride and Gray (MG) to the theoretical (SW) twelve hour difference profiles at various times of day and at 20° from the equator: (1) ($w_{0100}^{-w_{1300}}$), (2) ($w_{0300}^{-w_{1500}}$), (3) ($w_{0500}^{-w_{1700}}$), (4) ($w_{0700}^{-w_{1900}}$), and (5) ($w_{0900}^{-w_{2100}}$).

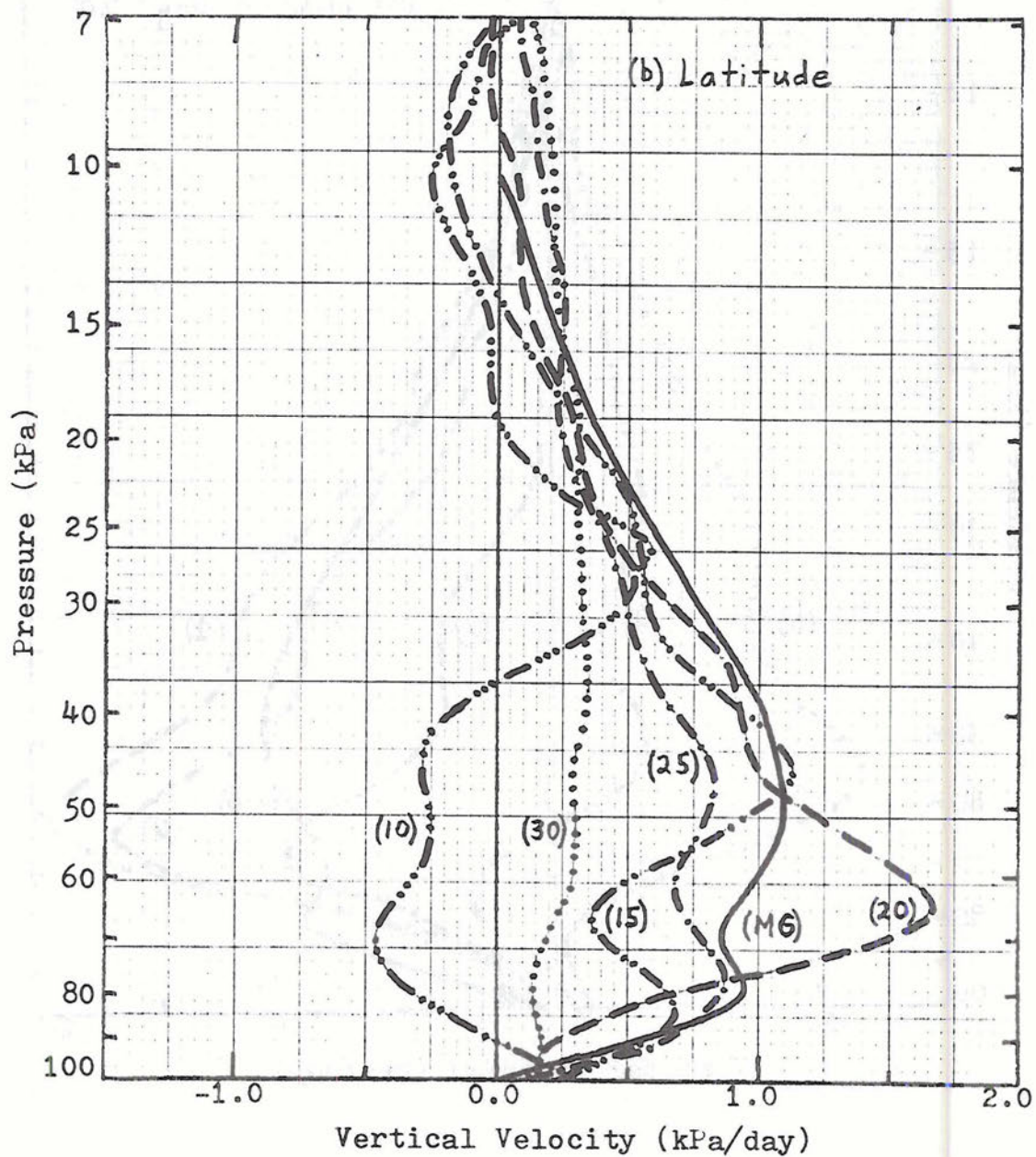


Fig. 4.19b Comparison of the ($w_{0700} - w_{1900}$) background composite vertical velocity profile of McBride and Gray (MG) to the theoretical (SW) ($w_{0300} - w_{1500}$) profiles at various latitudes: 10° , 15° , 20° , 25° , and 30° from the equator.

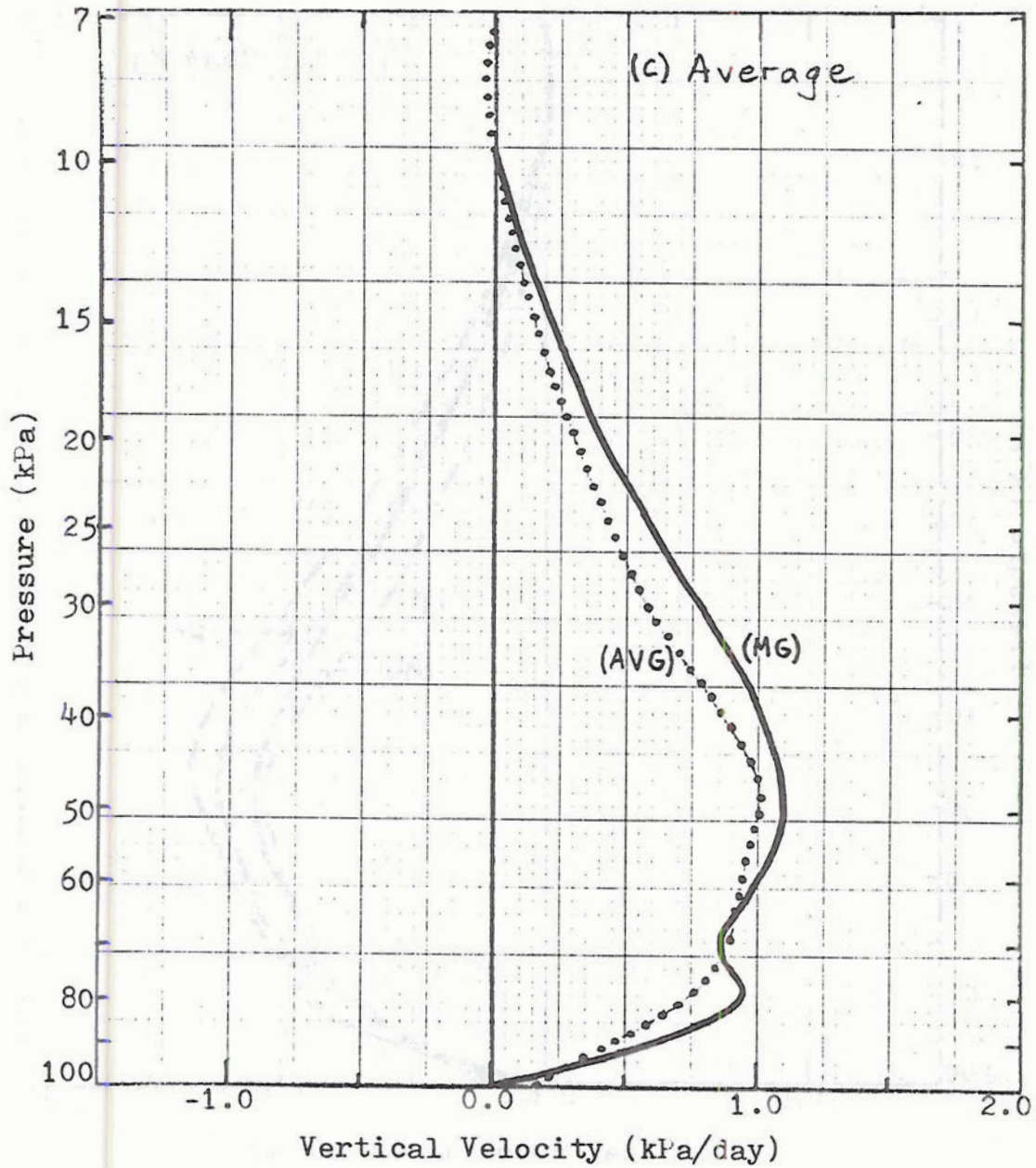


Fig. 4.19c Comparison of the ($w_{0700}^{-w_{1900}}$) background composite vertical velocity profile of McBride and Gray (MG) to the theoretical (SW) 15° to 25° average ($w_{0300}^{-w_{1500}}$) profile (AVG).

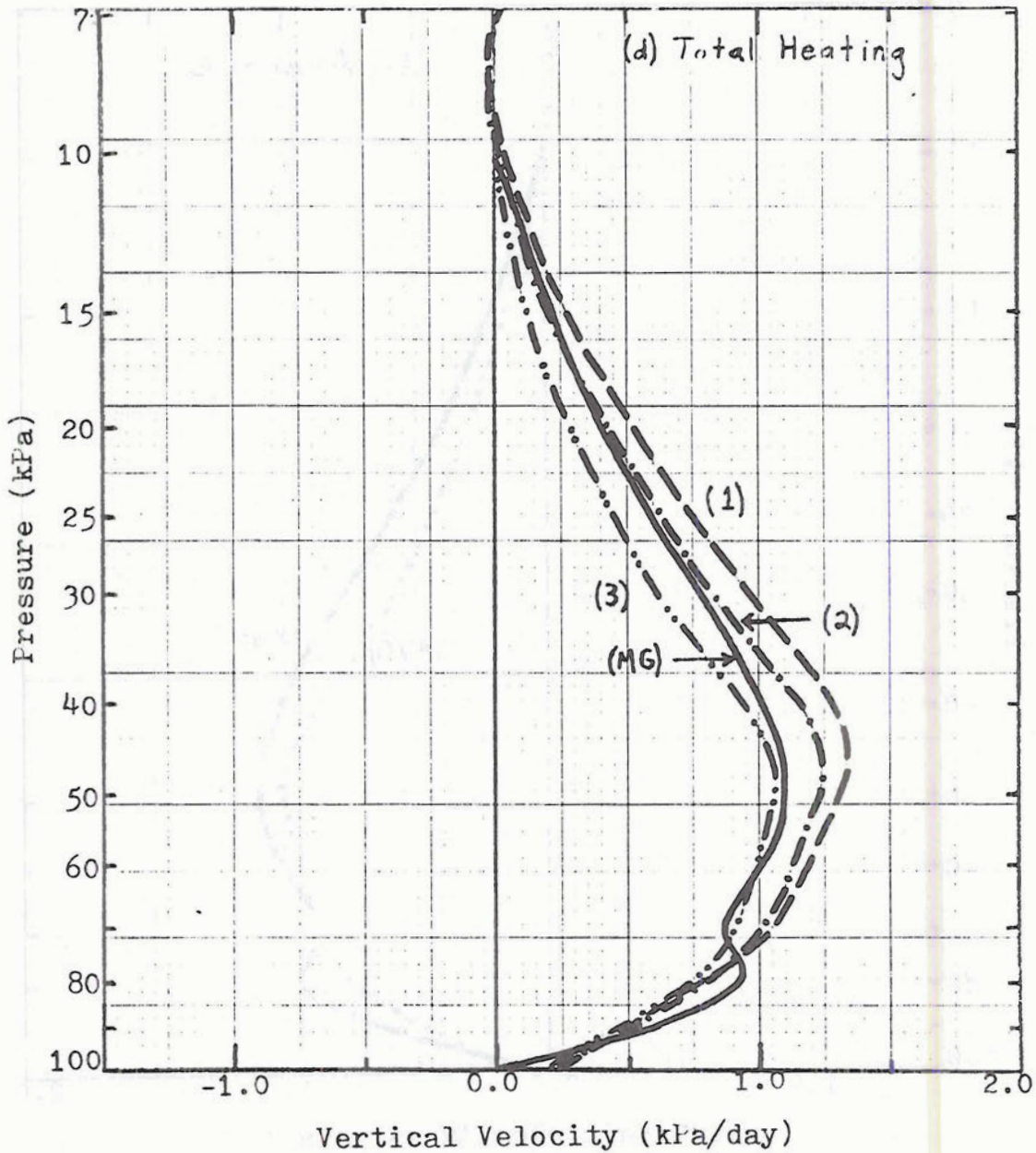


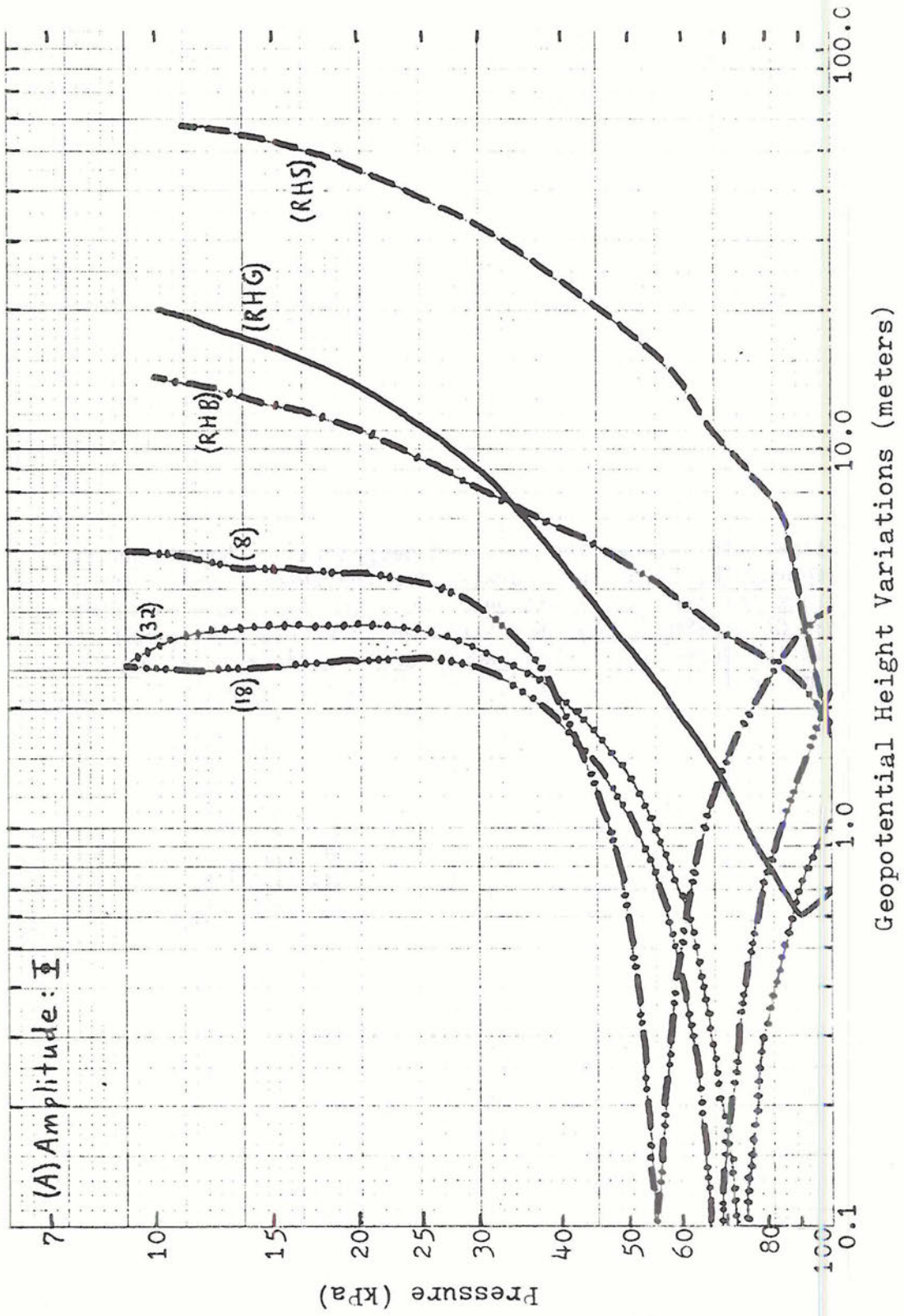
Fig. 4.19d Comparison of the ($w_{0700}^{-w_{1900}}$) background composite vertical velocity profile of McBride and Gray (MG) to the theoretical total (SW + Cumulus) heating 15° to 25° averaged vertical velocity profiles for several times of day: (1) ($w_{0000}^{-w_{1200}}$), (2) ($w_{0100}^{-w_{1300}}$), and (3) ($w_{0200}^{-w_{1400}}$).

between 0300 and 1500 LT -- again a four hour difference between the theory and the observations. But of course, little can be determined about the phase and amplitude of the vertical velocity profile from the two profiles, twelve hours apart, presented by McBride and Gray. So, this four hours may be merely coincidental. However, pursuing this line of thought yields other interesting results. Fig. 4.19b shows the latitudinal variation of the $(w_{0300} - w_{1500})$ vertical profile. In that between ten and thirty degrees from the equator there is quite a marked variation in the vertical profile, it is concluded that regional averages of the tidal vertical velocity field derived from observations must not span more than five or ten degrees of latitude. Averages should only be taken over stations within a fairly narrow latitude belt. Fig. 4.19c shows the average of the $(w_{0300} - w_{1500})$ vertical velocity profiles at 15° , 20° , and 25° from the equator in comparison to the profile shown by McBride and Gray. The similarity, is quite surprising. If nothing else, it at least shows that theoretical tidal oscillations are large enough in amplitude and (potentially) have appropriate structure to explain some observed diurnal variations. Fig. 4.19d shows the effect of adding cumulus heating and computing the same 15° to 25° average at three different times. The closest fitting curve here would be approximately $(w_{0130} - w_{1330})$. Because the time when the maximum 12 hour difference would occur cannot be determined from the results shown by McBride and Gray, the meaning of this time difference between when the two curves are most comparable is not clear; but in light of the comparison to the theoretical result without cumulus heating, it does not look like a step in the right direction.

The next comparison will be to results shown by Riehl and Haurwitz (1982) based upon an analysis of GATE data. They computed the diurnal variation of the heights of pressure surfaces at 10 kPa increments through the depth of the troposphere. Their new results from GATE and two older sets of results from Bermuda and San Juan, Puerto Rico are shown along with the theoretical results at corresponding latitudes in Fig. 4.20. The amplitude profiles are quite disappointing, because the observational results show amplitudes anywhere from two to twenty times the theoretical amplitudes. The phase profiles are more interesting though. Above about 700 mb, the observational profiles, which come from both sides of the Atlantic, very consistently show a time of maximum between 1230 and 1400 LT. The theoretical profiles for SW heating alone are likewise very consistent above 700 mb and show times of maximum at very nearly 1800 LT. Adding cumulus heating (not shown) reduces the phase differences between the two sets of profiles by about one to $1\frac{1}{2}$ hours. These phase results are very consistent with the phase results shown by Foltz and Gray for the temperature variations, but the amplitudes of the height changes appear excessive.

The next comparison is for data from the western Pacific. Observational results from two papers are shown in Fig. 4.21 and 4.22: Carlson and Hastenrath (1970) and Hastenrath (1972). In the latter paper, rawinsonde data from eight stations in the tropical western Pacific, seven of which are between 0° and 12°N , and all of which are between 155° and 175°E were averaged together. This may be the best region on the globe for trying to obtain tidal observations, because it is far from continents, consists of small islands and atolls, and does not span too broad a latitude band. Regional and local effects would be expected

Fig. 4.20a Comparison between the observed geopotential variations as reported by Riehl and Haurwitz and the theoretical variations for the same latitudes: observed amplitude profiles for GATE (8°N) (RHG); for San Juan, P.R. (18.5°N) (RHS); and for Bermuda (32.4°N) (RHB); and the theoretical amplitude profiles for 8° , 18° , and 32° from the equator.



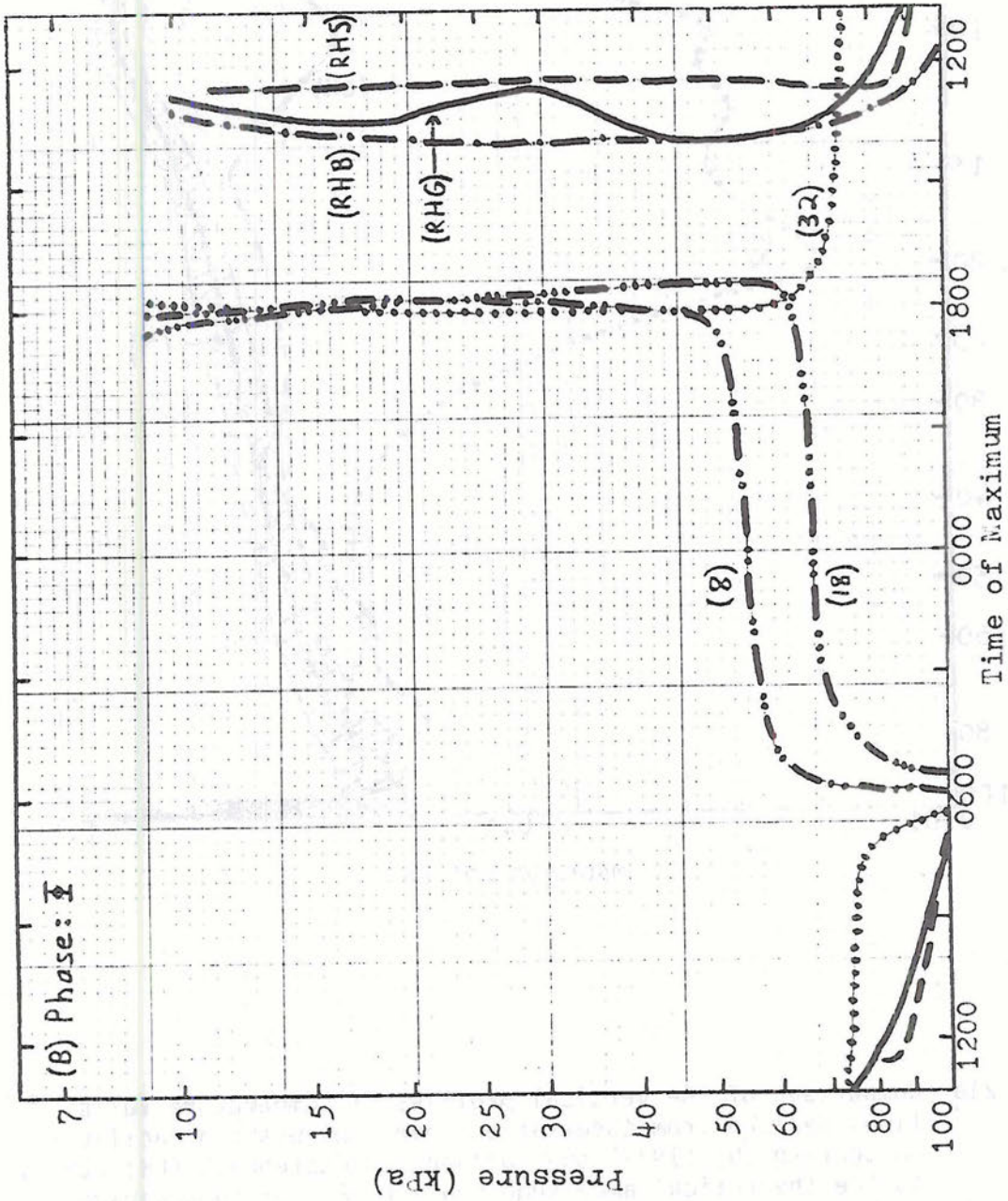


Fig. 4.20b Same as Fig. 4.20a, but for the observed and theoretical phase profiles of the geopotential variations.

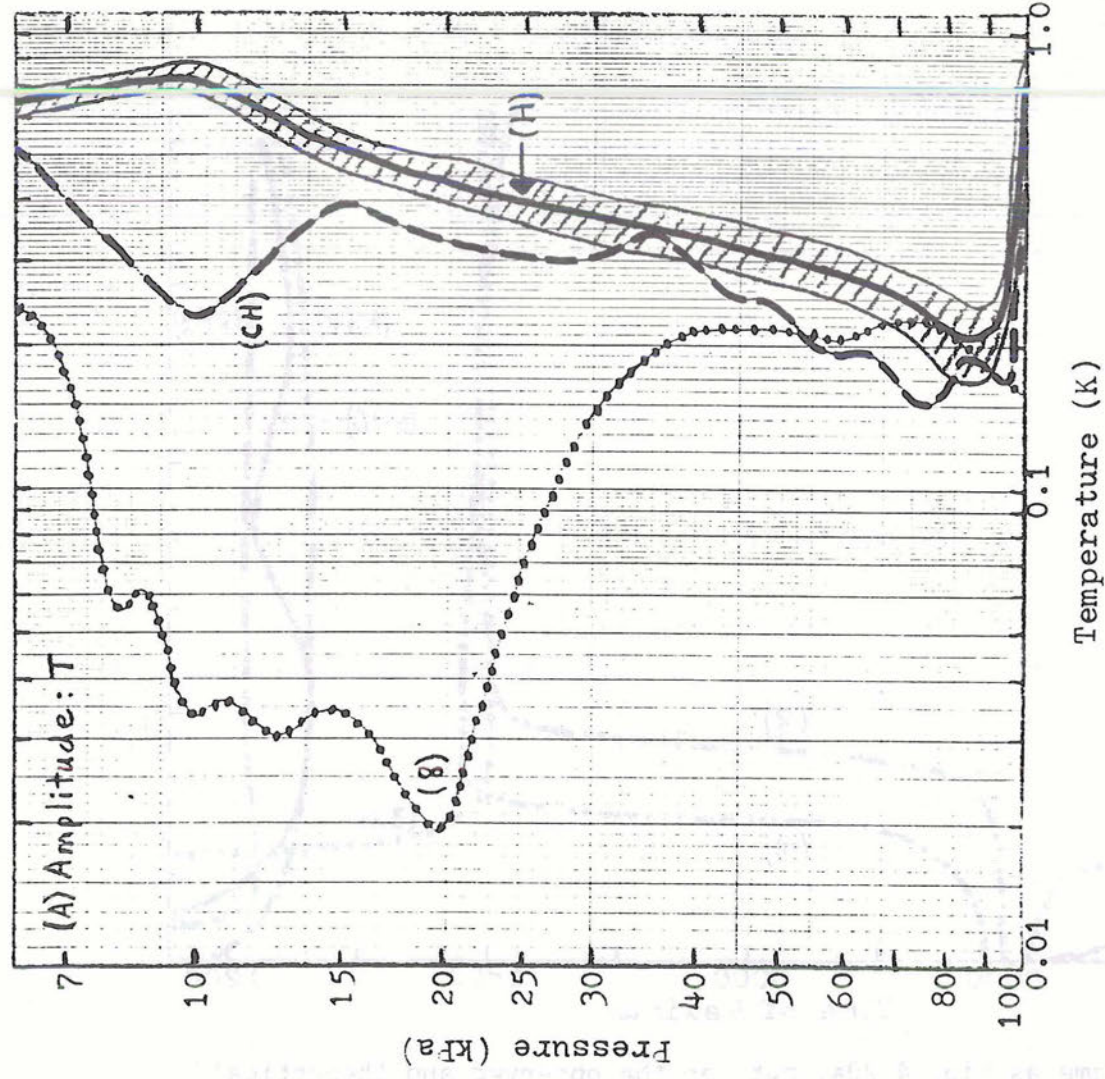


Fig. 4.21a Comparison of the vertical profiles of temperature variations derived from observations over the western Pacific by Hastenrath (H) (1972) and Carlson and Hastenrath (CH) (1970) to the theoretical amplitude profile (8) for the average station latitude: (H) eight station average for which the hatched area delineates the margins of error shown by Hastenrath, (CH) Eniwetok (12°N), and (8) theoretical amplitude profile for 8° from the equator.

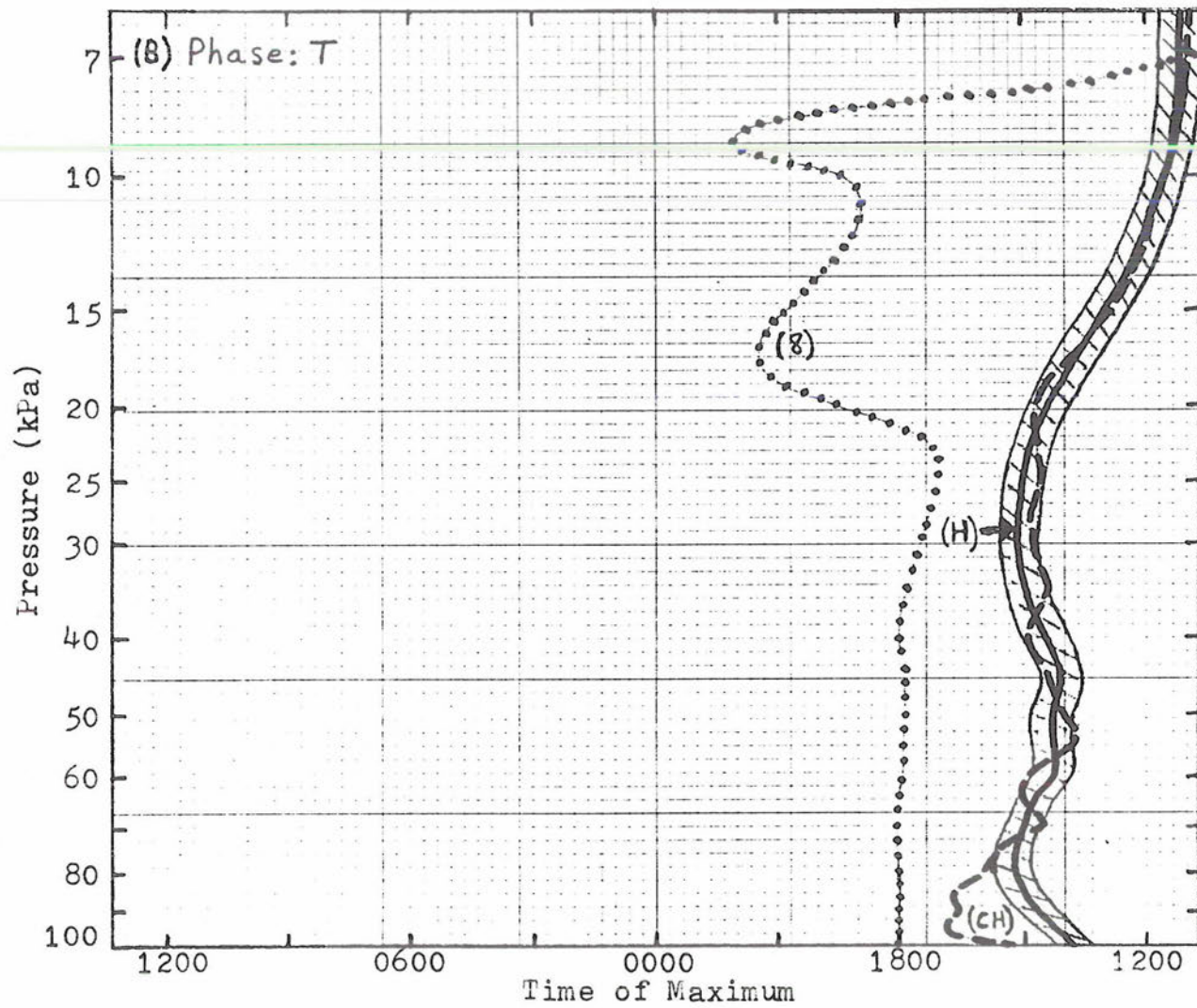


Fig. 4.21b Same as Fig. 4.21a, but for the observed and theoretical phase profiles of the temperature variations.

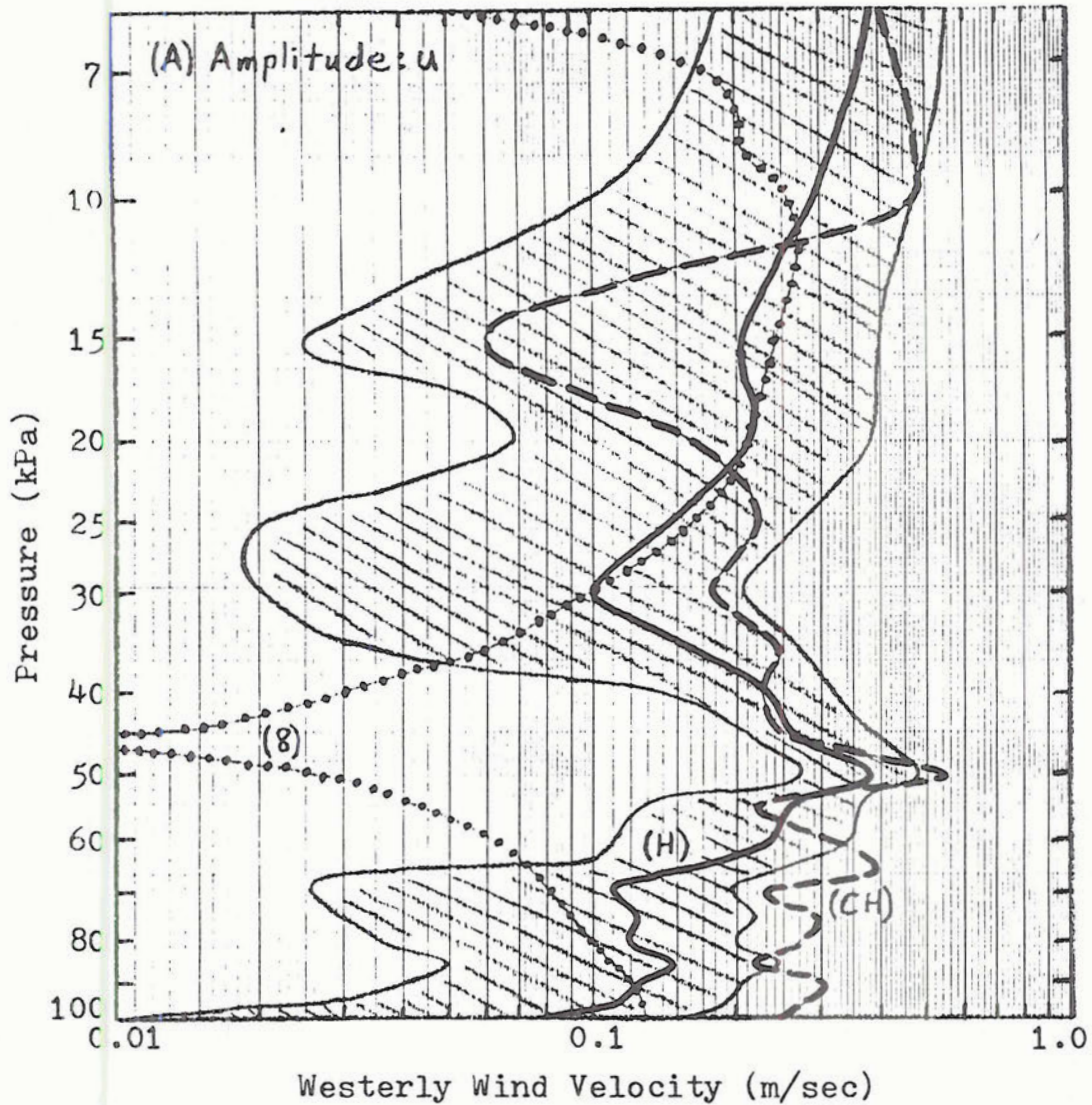


Fig. 4.2a Comparison of the vertical profiles of westerly wind variations derived from observations over the western Pacific by Hastenrath (H) (1972) and Carlson and Hastenrath (CH) (1970) to the theoretical amplitude profile (8) for the average station latitude: (H) eight station average for which the hatched area delineates the margins of error shown by Hastenrath, (CH) Eniwetok (12°N), and (8) theoretical amplitude profile for 8° from the equator.

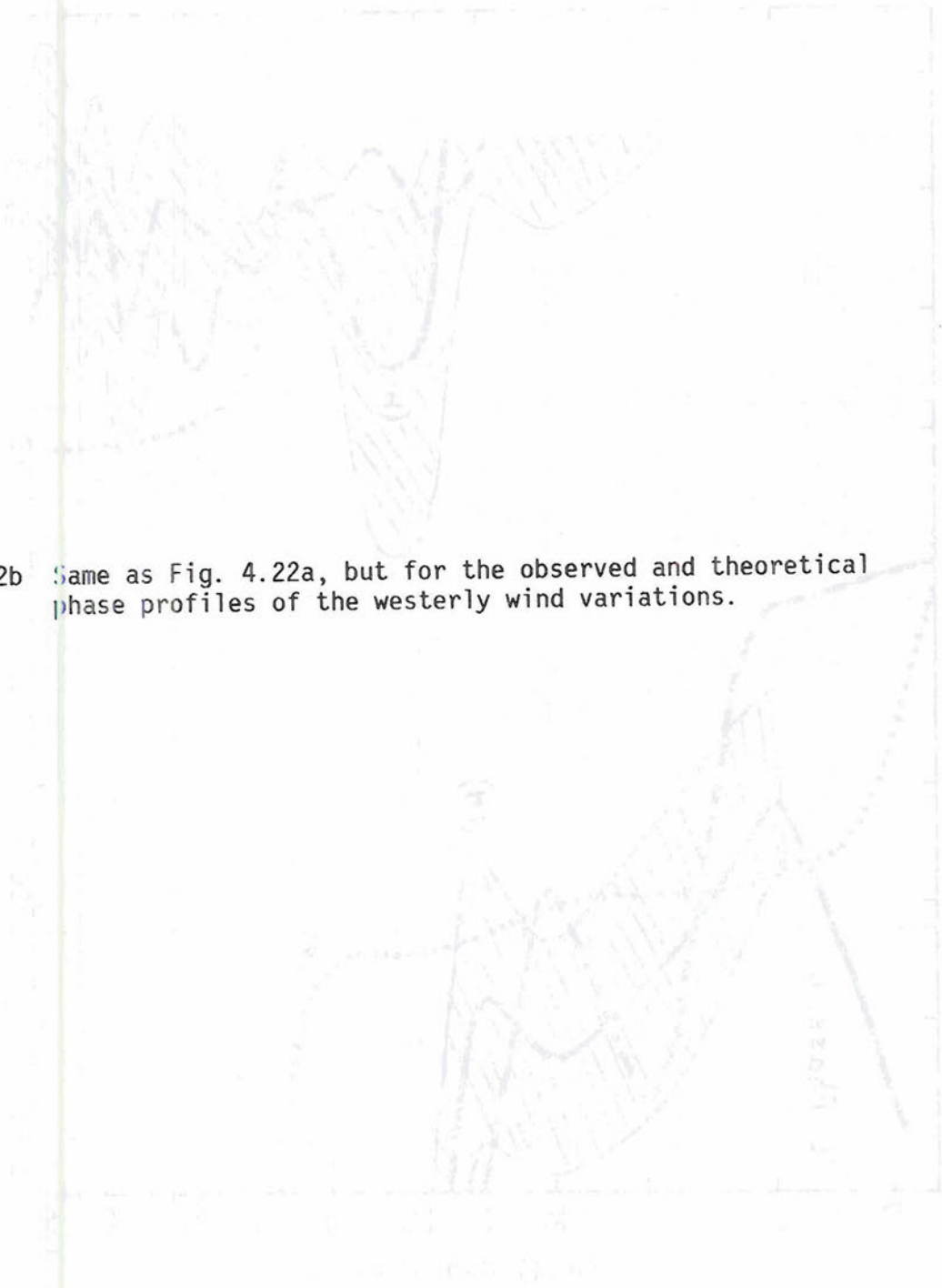
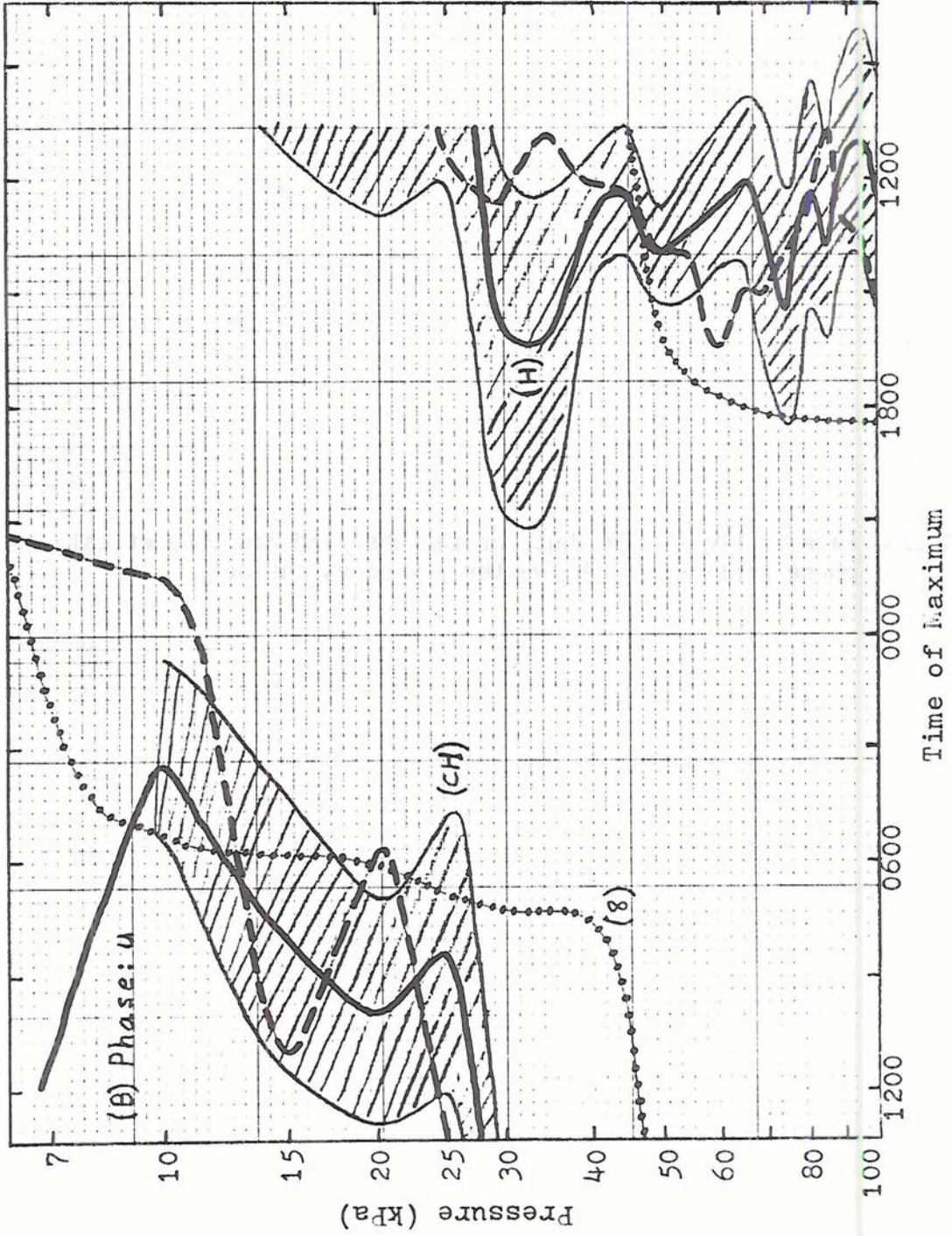


Fig. 4.22b Same as Fig. 4.22a, but for the observed and theoretical phase profiles of the westerly wind variations.



to be minimized here. The averaged temperature and westerly wind results are shown in Figs. 4.21 and 4.22. Hastenrath also showed error bounds on this data. For the temperature profiles these error bounds are quite restricted; whereas for the westerly wind profiles the errors may possibly be quite significant even for this eight station average. For comparison, the results for Eniwetok presented earlier by Carlson and Hastenrath are also shown. The large similarity between the single station profiles and the eight station average may be an indication that the tidal variations are fairly uniform over this whole region. The theoretical results for 8° from the equator are also given for comparison. For the temperature profiles, it can be seen that the amplitudes are fairly comparable in the lower half of the troposphere, though they are quite disparate in the upper troposphere. However, more notably, for the temperature phases, this three to four hour phase difference appears once again throughout most of the troposphere. This phenomenon seems to be quite pervasive in the temperature and the related geopotential fields. For the westerly wind profiles, the agreement between amplitude profiles is pretty good in the lower (below 70 kPa) and upper (above 30 kPa) troposphere. In fact, the theoretical amplitude profile lies within the error bound on the observational data throughout the troposphere except between 37.5 and 67.5 kPa. This is not so true for the phase profiles of the westerly wind, though they are still within four to five hours of each other throughout most of the troposphere.

Yoshida and Hirota (1979) showed results for the tidal variations in the horizontal wind at various stations in Japan. It would naturally be expected that topography would significantly affect the tropospheric

tidal variations over Japan, and thus it might be expected that averaging all the stations around Japan might minimize the discrepancy between the theoretical and observational results. So, the average annual profiles of the southerly wind component for eight stations were averaged together. The result of this procedure is shown in Fig. 4.23, where the theoretical results at the average station latitude of 36° from the equator are also shown. The agreement is not very good. The amplitudes are two to ten times greater than those predicted by theory, and the vertical structures of the phase profiles are quite different. With the proximity of the Asian land mass, the rugged topography of Japan, the Kuroshio current, and the very strong mean jet stream over Japan, it would be hypothesized that local and regional effects might be very important. Thus, it is not very surprising that the theory and observations are not in very good agreement for Japan. It should also be pointed out that even the single station annual averages of Yoshida and Hirota show very large error bounds (50-100%) and that their results are not therefore statistically very significant. However, it probably is significant that an eight station average of their results quite consistently shows larger variations at all levels than this treatment of classical tidal theory would predict, and this is almost certainly an indication that various influencing factors (such as those mentioned above) are playing a substantial role in producing the diurnal variations over Japan (as Yoshida and Hirota themselves concluded).

The results presented in several other papers will now be discussed without showing any figures. Nitta and Esbensen (1974) analyzed BOMEX data to the 50 kPa level to determine the characteristics of the diurnal

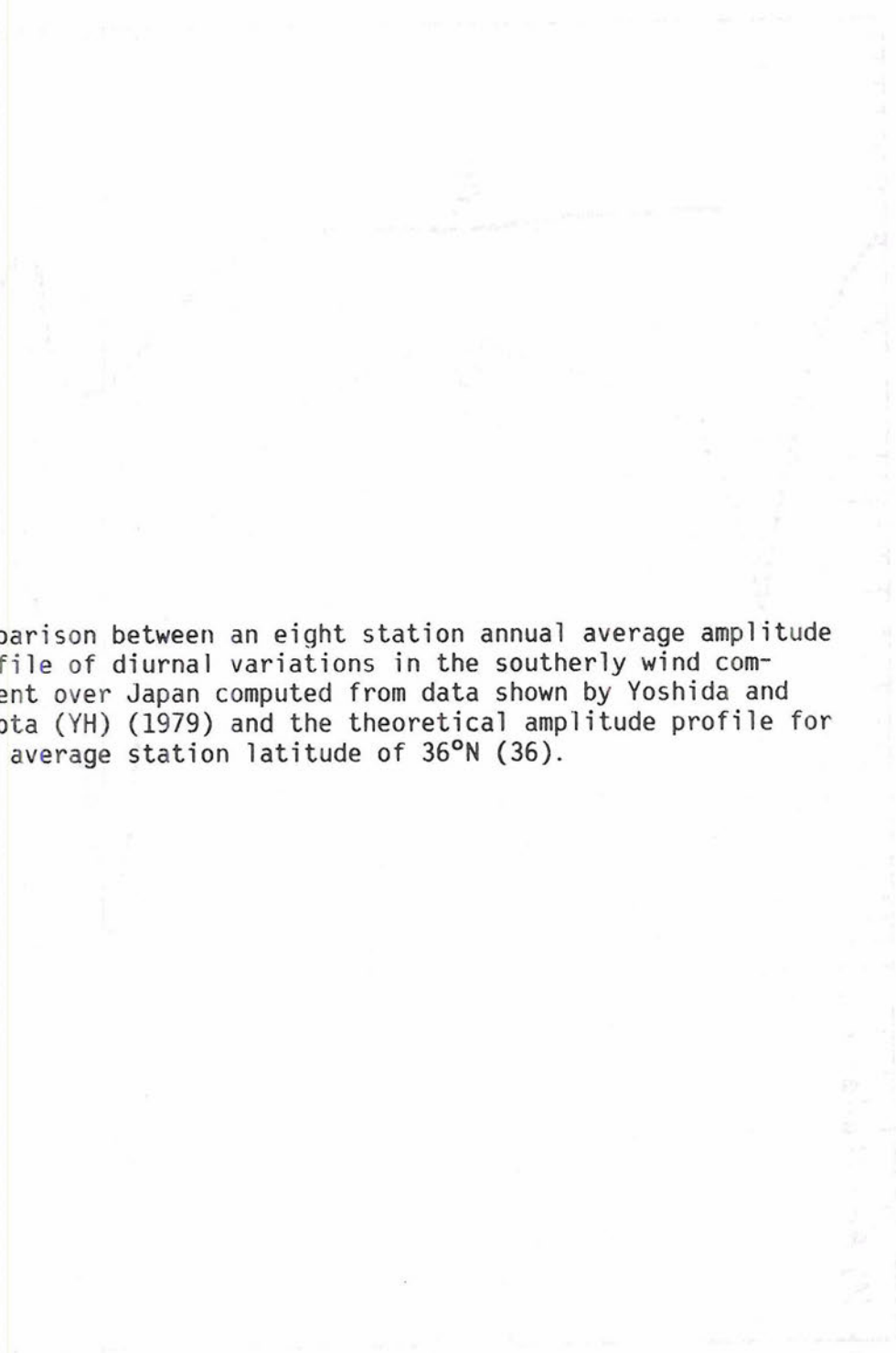
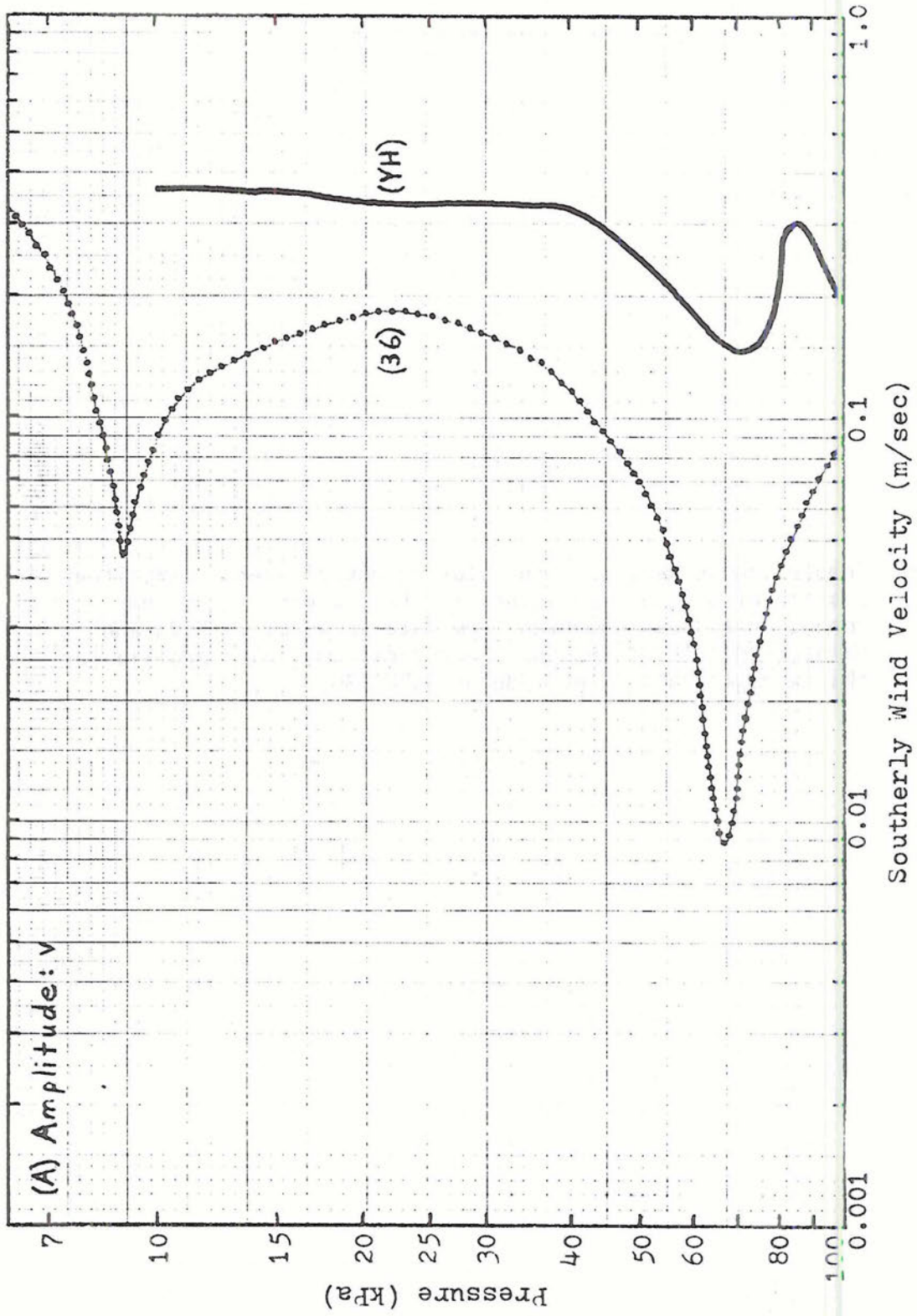


Fig. 4.23a Comparison between an eight station annual average amplitude profile of diurnal variations in the southerly wind component over Japan computed from data shown by Yoshida and Hirota (YH) (1979) and the theoretical amplitude profile for the average station latitude of 36°N (36).



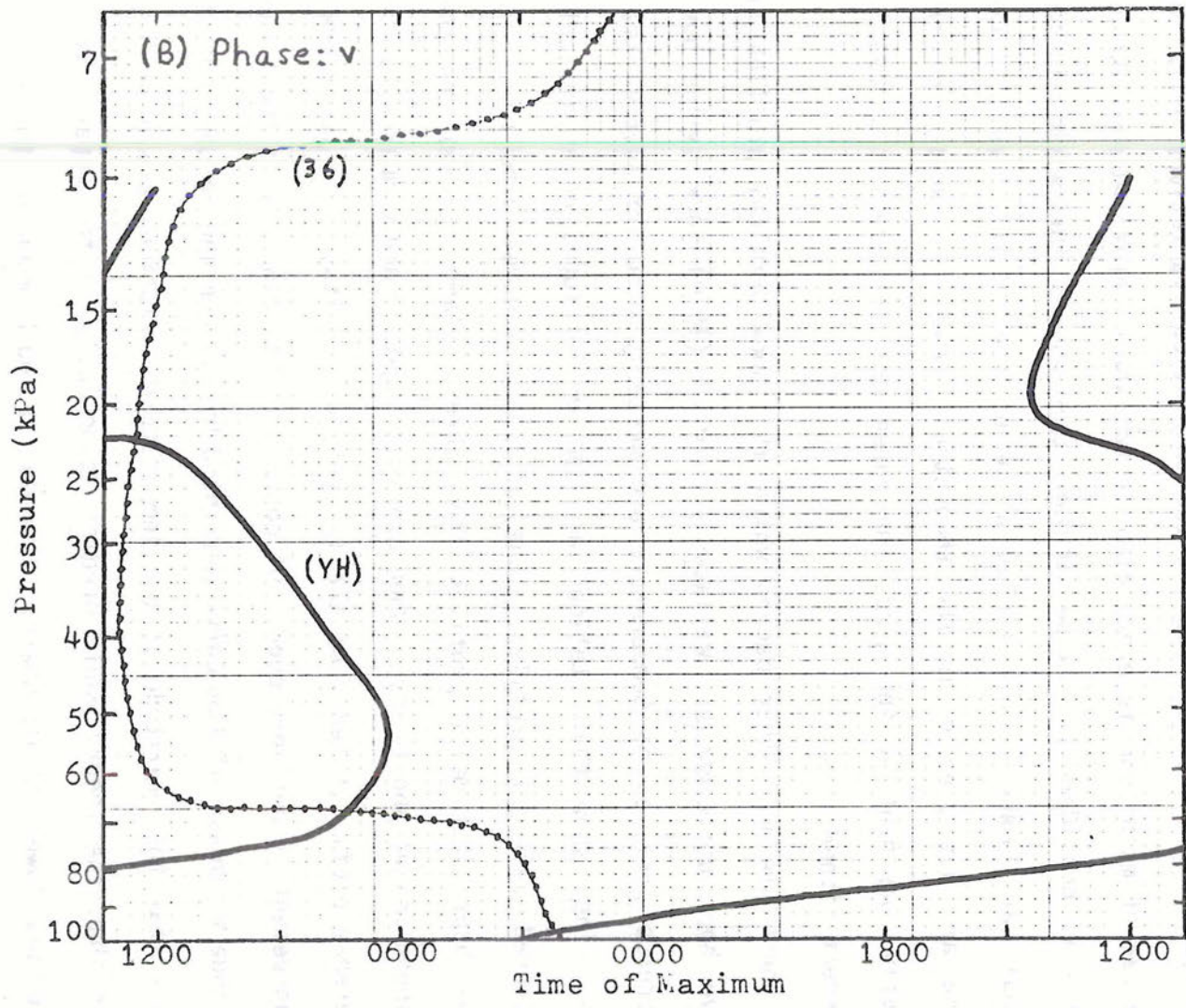


Fig. 4.23b Same as Fig. 4.23a, but for the phase profiles of the southerly wind component.

variations in this area. They analyzed the variations for the horizontal wind components, temperature, horizontal divergence, and the vertical velocity in pressure coordinates. They found much larger variations than were predicted in this treatment of classical tidal theory (though their claim that the observed and the theoretical variations differ by an order of magnitude is exaggerated if the whole layer between 100 and 50 kPa is considered). In particular, they show strong maxima in the diurnal variations of all fields at about the 70 kPa level. These maxima are not present in the theoretical results. Except for the westerly component of the wind, the phase profiles are not at all in agreement either.

There are two other papers which also show vertical profiles of twelve hour differences. Wallace and Patton (1970) show twelve hour difference profiles of temperature and westerly wind for several stations. They show that stations at similar latitudes have similarly structured vertical profiles. One of their figures displays three twelve hour difference profiles from three island stations in the Caribbean Sea at about 18°N. When averaged together and compared to the difference profile taken from the theoretical results, it is found that the agreement is not very good. Of course, little can be said about the amplitude or phase of the curve presented by Wallace and Patton, but it appears that the amplitude of the temperature variations are generally larger than the theory would predict, especially in the upper troposphere and lower stratosphere. However, through much of the troposphere, this factor is probably less than two. At this point, it must be remembered that this is once again a comparison to an observational result from a small region, and therefore that it is possible that

regional or local influences may have played a significant or perhaps even a dominant role in producing the observed diurnal variations.

Murakami (1979) presents vertical profiles of temperature and the vertical velocity in pressure coordinates at six hour intervals composited over the period of GATE. From these, two twelve hour difference profiles can be computed for each variable. These twelve hour difference profiles were then compared to corresponding profiles computed from the theoretical results. For the vertical velocity, it is quite apparent that the amplitude of the observed variations through much of the troposphere are two to three times greater than the theory would allow. For the temperature differences, the situation is quite different. Below about 45 kPa, the tidal theory predicts temperature variations with larger amplitudes than were observed. Above this level, the amplitude of the observed variations are several times larger than that for which the theory can account. It is well known that the GATE region is a somewhat atypical oceanic area. It has been proposed that squall lines propagating from West Africa and arriving in the GATE region most frequently in the late afternoon may provide (in a composite sense) a significant local diurnal forcing mechanism with a much different phase than the theoretical tidal forcing. Therefore, it is not surprising that the diurnal variations inferred from GATE observations differ significantly from the variations predicted in this treatment of classical tidal theory.

In answer to the question, "Does the diurnal tide have any impact on the day to day weather?", one other paper will be referenced. McBride and Gray (1979) discussed six different factors which contribute to the large-scale 85 kPa vertical motion forcing (see Table 1) in the

TABLE 1

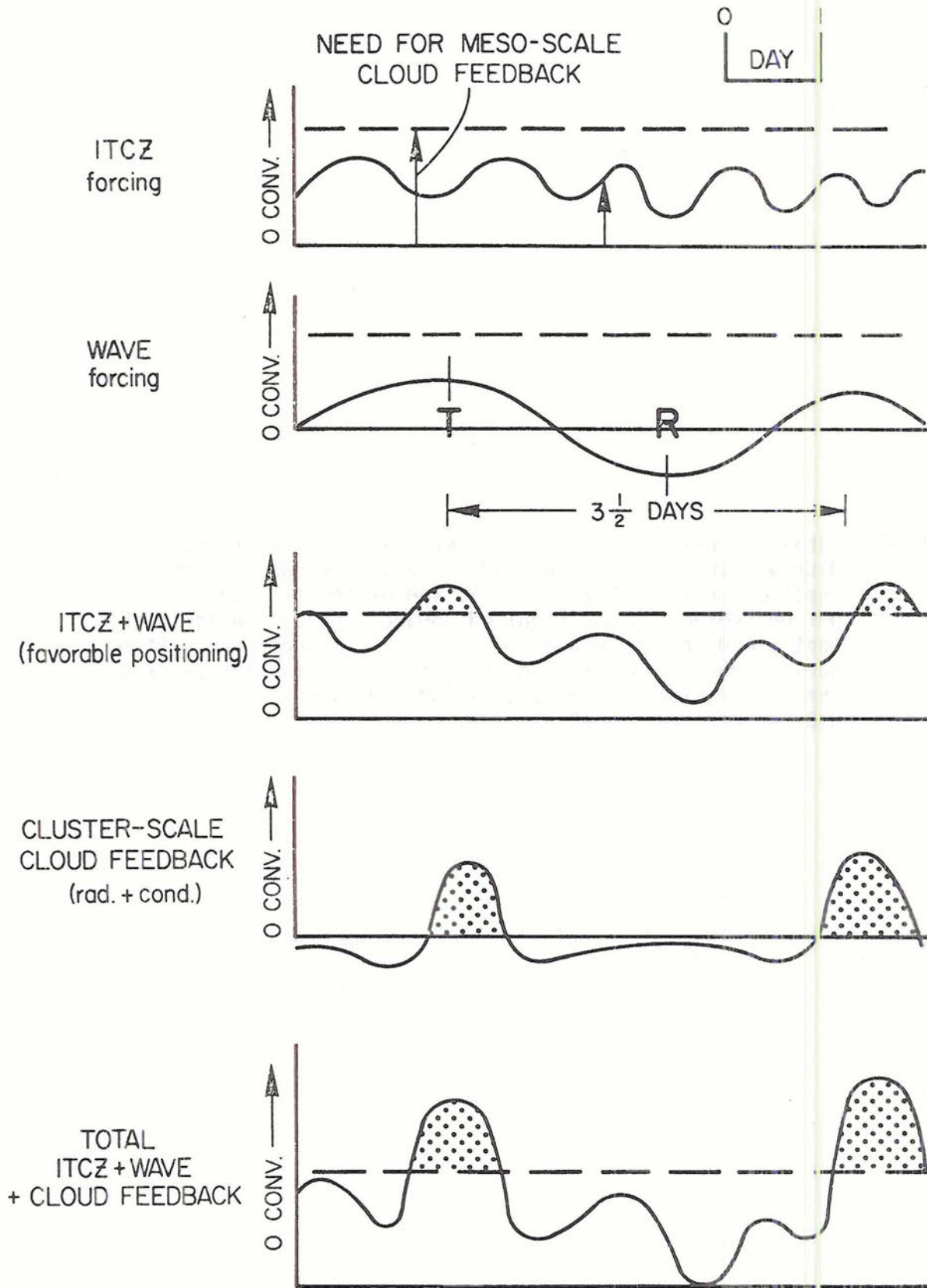
Estimated typical magnitude of various large-scale 850 mb vertical motion forcing components in mb/d.

		(A)	(B)	(C)	(D)	(E)	(F)
$\left(\begin{array}{c} \text{Magnitude of Lower} \\ \text{Tropospheric Vertical} \\ \text{(\sim 850 mb) Motion in} \\ \text{a Convective Weather} \\ \text{System} \end{array} \right) =$		$\left(\begin{array}{c} \text{ITCZ} \\ \text{Forcing} \end{array} \right) +$	$\left(\begin{array}{c} \text{Diurnal} \\ \text{Modulation} \\ \text{of ITCZ} \\ \text{Forcing} \end{array} \right) +$	$\left(\begin{array}{c} \text{Easterly} \\ \text{Wave} \\ \text{Forcing} \end{array} \right) +$	$\left(\begin{array}{c} \text{Frictional} \\ \text{Convergence} \end{array} \right) +$	$\left(\begin{array}{c} \text{Cluster} \\ \text{Scale} \\ \text{Diurnal} \\ \text{Modulation} \end{array} \right) +$	$\left(\begin{array}{c} \text{Convective} \\ \text{Feedback} \\ \text{in Cluster} \\ \text{Region} \end{array} \right)$
Region	Term	(1)	(2)	(3)	(4)	(5)	(6)
			AM/PM		Trough/Ridge	AM/PM	
Western Pacific		-30 mb/d	0 mb/d	$\bar{\pm}20$ mb/d	-7 mb/d	$\bar{\pm}60$ mb/d	-20 mb/d
Western Atlantic		+10 mb/d	± 5 mb/d	$\bar{\pm}15$ mb/d	-4 mb/d	$\bar{\pm}40$ mb/d	-25 mb/d
GATE		-80 mb/d	$\bar{\pm}45$ mb/d	$\bar{\pm}30$ mb/d	-3 mb/d	$\bar{\pm}30$ mb/d	-40 mb/d

(From McBride and Gray, 1978.)

tropics. They estimated the amplitude and phase for each of these terms for composited data over the western Pacific, the western Atlantic, and the GATE array. The term which is of particular interest here is the diurnal modulation of the ITCZ forcing. This is a very large-scale, global effect, just as the diurnal tide is also a global effect. McBride and Gray estimate the magnitude of this term to be small over the western Atlantic and Pacific, though it was found to be very large over the GATE array. The tidal theory predicts a vertical motion variation at 85 kPa which of course varies with latitude, but which can be as much as 3 to 4 mb/day. This is a very small variation relative to the other forcing terms in the forcing equation, but it is of the same order of magnitude as the diurnal modulation of the ITCZ forcing computed from observations over the western oceans. The role of this modulation in producing weather events is diagrammed by McBride and Gray (shown here in Fig. 4.24). As shown in the third diagram, there may be times when this small diurnal variation may be able to provide that little extra bit of forcing needed to reach the threshold required to obtain convective feedback. Or, it could sometimes provide just enough subsidence to prevent the forcing in an otherwise disturbed region from reaching this threshold. Admittedly, the times when this small diurnal variation would be sufficient for triggering or suppressing weather events should be infrequent. However, the tidal variation in the vertical motion field may also be able to slightly enhance or reduce disturbances which were triggered otherwise. Thus, in the tropics where the diurnal tidal variations are largest and where the large-scale forcing mechanisms are smaller (than in mid-latitudes), the diurnal tide may play some small

Fig. 4.24 Idealized association of ITCZ vertical motion forcing with diurnal cycle (top curve) and easterly wave modulation (second curve). Third curve is sum of top two curves. Dotted region denotes required upward vertical motion such that cloud region feedback will occur. Second from bottom curve denotes cloud region feedback. Bottom curve denotes the sum of ITCZ, diurnal, wave and feedback forcing. (From McBride and Gray, 1978.)



role in triggering and enhancing weather disturbances. Foltz and Gray (1979) also discuss the possible diurnal tidal enhancement of subsidence over continental size areas which, if concentrated in selective locations, could be locally significant. However, there are phase discrepancies between the tidal theory and the hypothesis proposed by Foltz and Gray. In particular, Foltz and Gray indicate that, for all latitudes, there should be maximum subsidence during the morning hours. The results of the current study do not show this, but show instead a cellular structure not observed or anticipated by Foltz and Gray. The present results show more downward motion at the equator during the daytime than at night, but they show more upward motion during the daytime than at night for all latitudes between at least 15° and 40° from the equator. Thus, if the observational analysis of Foltz and Gray is correct, then some other mechanism other than that provided by classical tidal theory must be sought to explain it; and it appears more appropriate at present to think of the tidal circulation in terms of its opposition to the Hadley circulation during the daytime and its enhancement of the Hadley circulation at night.

5. SUMMARY OF CONCLUSIONS

In this research, the classical tidal theory has been used to study the migrating diurnal thermal tide. Several refinements in the standard methodology outlined by Chapman and Lindzen (1970) were incorporated into the present calculations.

First, a greater number of Hough functions were used to represent the latitudinal structures of the tidal variables. It was discovered that even when using sixteen Hough functions, horizontal structures resembling Gaussian curves could not be well represented at higher latitudes. Since several of the tidal variables have this type of horizontal structure, it was concluded that even the results of this sixteen mode treatment are unreliable at more than about 45° from the equator.

Second, results were presented with a greater horizontal resolution than had been shown before. It was found that this was only necessary for the vertical velocity field. The earlier results presented by Lindzen (1967), which showed a 15° horizontal resolution, are adequate for resolving the horizontal structure of all but the vertical velocity fields. From an observational standpoint, this result also implies that regional or global observations of diurnal variations of, particularly, the vertical velocity must not be averaged over an area spanning more than 10° of latitude.

The third improvement was to use a radiative transfer scheme to obtain a better tropospheric heating function. As it turned out, the available radiative transfer model only allowed an improvement to the component of the heating due to the absorption of shortwave radiation by water vapor molecules. It was found that the simple functional form used by Lindzen (1967) differed quite significantly from that derived with the radiative transfer model.

A sensitivity study showed that the theoretical results are fairly sensitive to three factors. In order of decreasing importance, these are (1) the structure of the tropospheric heating, (2) the tropospheric static stability profile, and (3) the number of Hough functions used to represent the heating. The only other detailed presentations showing the theoretical tropospheric diurnal variations (computed by using classical tidal theory) are those of Lindzen (1967, 1968). His calculations utilized a significantly different tropospheric heating function, an isothermal atmosphere, and only five Hough functions for representing the horizontal structure. Thus, it was not surprising that the present results were quite different from Lindzen's in amplitude, phase, and structure. However, in general, the new results differed from the old results by much less than an order of magnitude. It was difficult to find any consistent differences between the two sets of results. For some variables and in some parts of the troposphere, Lindzen's results showed greater responses. In other cases the new results showed greater responses.

An analysis was done to determine the relative contributions to the tropospheric diurnal tidal response provided by each of the three heating mechanisms. Of the three (H_2O heating, ozone heating, and cumulus

heating), H_2O heating was clearly the component responsible for producing the largest fraction of the tropospheric response. For reasons discussed earlier, the stratospheric ozone heating, even with its much greater amplitude, produces only a very minor tropospheric response. Cumulus heating was put into the calculation in a very approximate and possibly underestimated form. Though the cumulus heating produced a greater tropospheric response than the ozone heating, it was still a relatively minor response compared to that produced by H_2O heating. In general, the effects of the cumulus heating were to increase the amplitude of the tropospheric response by 10% to 20% and to shift the phase so as to reach a maximum one to two hours earlier in the day. Another implication drawn from this analysis was the great importance of having an appropriate tropospheric forcing function for obtaining a representative tropospheric response.

An analysis of the way the energy is partitioned among the three terms of the thermodynamic energy equation proved to be quite enlightening. In the troposphere, the temperature change term and the heating term remain pretty nearly in balance, while the vertical velocity term behaves more like a residual quantity. In the troposphere, where the static stability is low, the vertical motion forced by the heating is insufficient for there to be much adiabatic heating or cooling by this means. Also, the near balance between the heating and temperature change terms implies that the temperature (and geopotential) variation lags behind the heating curve by very nearly 90° . This is true at all latitudes in the tropics and subtropics.

The new results showed an interesting circulation pattern in the tropics. During the daytime, a circulation is established which opposes

the Hadley cell in all three wind components. This means that there is downward vertical motion and adiabatic warming at the equator at the time of maximum heating -- a curious phenomenon for which no satisfying physical explanation was found. At night, the situation is reversed and the diurnal tidal circulation would serve to enhance the Hadley cell.

Comparisons between the new results and observations were not as favorable as had been anticipated. The most interesting discovery was that of a three to five hour phase difference between the observational and theoretical temperature (and geopotential) fields. This phase difference was found consistently in comparisons to three completely independent observational analyses.

Most of the empirically obtained measurements of tidal oscillations showed significantly greater amplitudes (two to three or more times greater) than the theoretical amplitudes computed in this study. The empirical results also showed very different phase profiles and vertical structures than predicted by the theory. Almost the sole exception to this was the result of the global temperature analysis carried out by Foltz and Gray (1979). However, even in this case, there was still a four hour phase discrepancy and a 30% amplitude difference.

It is important to try to account for this disparity between the theoretical and observational results. From the theoretical side, three factors could be contributing to the disparity. First, the diurnal variation of cumulus heating may be substantially underestimated (Hong and Wang, 1980). Second, it is possible that the diurnal variations of one or more of the heating mechanisms neglected in Chapter 2 may be of major significance. Third, because of longitudinal inhomogeneities in topography and heating, it is possible that a significant portion of the

observed diurnal tidal response resides in the components with zonal wavenumbers greater than one -- components which have not been treated in this study.

From the observational side, there are two factors which contribute to the discrepancy. First, the diurnal tide consists of variations with very small amplitudes -- much smaller than the ubiquitous tropospheric variations forced by other means. The diurnal variations isolated even from large quantities of data typically have error bounds of ± 30 to 50% or more. There is also still some uncertainty as to whether conventional rawinsondes provide sufficiently accurate data from which to compute tidal variations having such small amplitudes. Second, most observational analyses have been made for single stations or groups of stations contained within a fairly small region. Regional and local effects appear to dominate on these scales and to obscure the smaller global effect investigated theoretically in this research.

One other consideration which was discussed was whether or not the diurnal tide might have any impact on the weather in the tropics. Generally, the theoretical amplitudes of the tidal variations are much smaller (by as much as an order of magnitude) than tropical tropospheric variations forced by other means. However, as shown by McBride and Gray (1978), the diurnal tidal variation of the Hadley circulation may, at times, provide the extra kick required to surmount the threshold and initiate convective feedback in an otherwise inactive region, or to suppress convective activity in an otherwise disturbed region.

The conclusions of this study suggest two avenues for further research. First, it would be useful to re-evaluate the significance of

the neglected heating mechanisms and to further investigate the amplitude and phase of the diurnal variation of latent heat release. Second, it would be useful to have more global analyses of rawinsonde data stratified by latitude and longitude (as was done by Foltz and Gray (1979)). This would particularly facilitate a study to determine whether or not there is any evidence that a significant fraction of the diurnal thermal tide resides in the components with zonal wavenumbers greater than one.

LIST OF REFERENCES

- Butler, S.T. and Small, K.A., 1963: The excitation of atmospheric oscillations, Proc. Roy. Soc., A274, pp. 91-121.
- Carlson G.C., Jr. and Hastenrath, S., 1970: Diurnal variation of wind, pressure, and temperature in the troposphere and stratosphere over Eniwetok. Mon. Wea. Rev., 98, 408-416.
- Chapman S. and Lindzen, R.S., 1970: Atmospheric Tides: Thermal and Gravitational. Gordon and Breach, 200 pp.
- Cox, S.K.; Polifka, M.S.; Griffith, K.; Rockwood, A.; Starr, D; 1976: Radiative transfer computational routines for atmospheric science applications. Research Report, Atmospheric Science Department, Colorado State University, 75 pp.
- Flattery, T.W., 1976: Hough functions. Technical Report #21, Department of Geophysical Sciences, University of Chicago.
- Foltz, G.S. and Gray, W.M., 1979: Diurnal variation in the troposphere's energy balance. J. Atmos. Sci., 36, 1450-1466.
- Gray, W.M. and Jacobson, R.W., Jr., 1977: Diurnal variation of deep cumulus convection. Mon. Wea. Rev., 105, 1171-1188.
- Hamilton, K. 1981: Latent heat release as a possible forcing mechanism for atmospheric tides. Mon. Wea. Rev., 109, 3-17.
- Hastenrath, S., 1972: Daily wind, pressure, and temperature variation up to 30 km over the tropical western Pacific. Quar. J. Roy. Met. Soc., 98, 48-59.
- Holton, J.R., 1975: The dynamic meteorology of the stratosphere and mesosphere. Meteor. Monogr., No. 37, Amer. Meteor. Soc., 56-57.
- Hong, S.-S. and Wang, P.-H., 1980: On the thermal excitation of atmospheric tides. Bulletin of Geophysics No. 19. Institute of Geophysics, College of Science, National Central University, Chung-li, Taiwan, Republic of China. pp. 56-84.
- Jacobson, R.W., Jr., 1976: Diurnal variation of oceanic deep cumulus convection, I, observational evidence. Atmos. Sci. Paper No. 243, Colorado State University, 48 pp.
- Lindzen, R.S., 1967: Thermally driven diurnal tide in the troposphere. Quar. J. Roy. Met. Soc., 93, 18-43.

- Lindzen, R.S. 1968: The application of classical atmospheric tidal theory. Proc. Roy. Soc., A303, 299-316.
- Lindzen, R.S., 1978: Effect of daily variations of cumulonimbus activity on the atmospheric semi-diurnal tide. Mon. Wea. Rev., 106, 526-533.
- Lindzen, R.S. and Kuo, H.-L., 1969: A reliable method for the numerical integration of a large class of ordinary and partial differential equations. Mon. Wea. Rev., 97, 732-734.
- Manabe, S. and Strickler, R., 1964: Thermal equilibrium of the atmosphere with a convective adjustment. J. Atmos. Sci., 21, 361-385.
- Mastenbrook, H.J., 1968: Water vapor distribution in the stratosphere and high troposphere. J. Atmos. Sci., 25, 299-311.
- Matsuno, T., 1970: Vertical propagation of stationary planetary waves in the winter northern hemisphere. J. Atmos. Sci., 27, 871-883.
- McBride, J.L. and Gray, W.M., 1978: Mass divergence and vertical velocity in tropical weather systems, Part I: Diurnal variation, Part II: Large scale controls on convection. Atmos. Sci. Paper No. 299, Colorado State University, 109 pp.
- Murakami, M., 1979: Large-scale aspects of deep convective activity over the GATE area. Mon. Wea. Rev., 107, 994-1013.
- Nitta, T. and Esbensen, S., 1974: Diurnal variations in the western Atlantic trades during the BOMEX. J. Meteor. Soc. Japan, 52, 254-257.
- Panofsky, H.A. and Brier, G.W., 1958: Some Applications of Statistics to Meteorology. Mineral Industries Extension Services, College of Mineral Industries, Pennsylvania State University, University Park, Pennsylvania. 224 pp.
- Riehl, H., and Haurwitz, B., 1982: Diurnal variation of pressure-heights in the eastern Atlantic (GATE). Quart. J. Roy. Met. Soc., 108, 727-732.
- Thompson, R.M., Jr.; Payne, S.W.; Recker, E.E.; Reed, R.J.; 1979: Structure and properties of synoptic-scale wave disturbances in the intertropical convergence zone of the eastern Atlantic. J. Atmos. Sci., 36, 53-72.
- U.S. Standard Atmosphere Supplements, 1966: U.S. Govt. Printing Office. 289 pp.
- Wallace, J.M. and Hartranft, F.R., 1969: Diurnal wind variations, surface to 30 km. Mon. Wea. Rev., 97, 446-455.
- Wallace, J.M. and Patton, D.B., 1970: Diurnal temperature variations: surface to 25 km. Mon. Wea. Rev., 98, 548-552.

- Wallace, J.M. and Tadd, R.F., 1974: Some further results concerning the vertical structure of atmospheric tidal motions within the lowest 30 km. Mon. Wea. Rev., 102, 795-803.
- Wilkes, M.V., 1949: Oscillations of the Earth's Atmosphere. University Press: Cambridge, 76 pp.
- Yoshida, A. and Hirota, I., 1979: Diurnal wind variation in the troposphere and lower stratosphere over Japan. J. Met. Soc. Japan, 57, 29-38.

APPENDIX 1

THE FAILURE OF THE FINITE DIFFERENCE APPROACH

After linearizing the primitive equations, subtracting out the basic state, choosing a wave-like solution, and combining the five equations, the following single equation in the variable $\hat{w}^{\sigma,s}$ is derived (as was shown in chapter 2 of the main text of this report):

$$\left[\frac{\partial^2}{\partial z^{*2}} \right] - \frac{1}{4} - \frac{R\Gamma}{4a^2\Omega^2} F(\hat{w}^{\sigma,s}) = \frac{-ke^{-z^*/2}}{4a^2\Omega^2} F(J^{\sigma,s}), \quad (A1-1)$$

where $\mu = \sin\theta$ and F is the following θ -operator:

$$F: \frac{\partial}{\partial \mu} \left(\frac{\eta}{\delta} \frac{\partial}{\partial \mu} \right) - \frac{1}{\delta} \left(\frac{s}{f} \cdot \frac{f^2 + \mu^2}{\delta} + \frac{s^2}{\eta} \right).$$

Here, $\eta = 1 - \mu^2$ and $\delta = f^2 - \mu^2$. This is the equation that must be solved to obtain the tidal field of the perturbation variable $\hat{w}^{\sigma,s}$. It is a second order partial differential equation in both μ and z^* . The most obvious approach to take to solve this problem is to make a straight forward application of finite difference techniques in both dimensions, and so this is the approach that was first pursued. It was unclear at first why all previous tidal calculations had been carried out using the conceptually more difficult Galerkin methods and why no one previously had ever reported trying to solve the problem using finite-difference methods. However, it was not long before the shortcomings of the finite difference approach became clearly evident.

The major problem arises when trying to use the radiation/boundedness condition at the upper boundary. Following the method of Matsuno (1970), it turns out that, in order to apply the radiation condition at the upper boundary, the method of separation of variables must be used at the top of the model domain. The resulting two equations in their finite difference forms can then be solved simultaneously with the appropriate boundary condition equations. One of these two equations is Laplace's tidal equation, which can be written in this form:

$$\frac{d}{d\mu} \left(\frac{\eta}{\delta} \cdot \frac{d}{d\mu} \right) \theta_n - \frac{1}{\delta} \left[\frac{s}{f} \cdot \frac{f^2 + \mu^2}{\delta} + \frac{s^2}{\eta} \right] \theta_n = \frac{-4a^2 \Omega^2}{gh_n} \theta_n. \quad (A1-2)$$

Except for the apparent singularities at $f^2 = \mu^2 = 0.25$ and at $\mu = \pm 1$, this equation otherwise satisfies all the criteria for being in a Sturm-Liouville form. When put into a finite difference form (using centered difference schemes for the derivatives and assuming that $\theta_n = 0$ at the poles), this equation can be solved as a matrix eigenvalue problem. It was discovered, however, that even though the IMSL routines EIGRF and EIGZF would solve the eigenvalue problem and would indicate an excellent performance index, the eigenvalues would not converge to the right values as the number of grid points was increased, and the eigenvectors had peculiar features not characteristic of the Hough functions (which are the real solutions, or eigenfunctions, of Laplace's tidal equation). The apparent singularity at $f^2 = \mu^2$ seems to render the solutions inaccessible by finite-difference methods, and no simple way was found to get around this problem.

For the record, the three methods used in trying to solve this problem will be shown. The results obtained using each method will be briefly discussed.

In the first method, the following equation was obtained by carrying out the two differentiations in the left-hand term of equation (A1-2):

$$\frac{\eta}{\delta} \frac{d^2 \theta_n}{d\mu^2} + 2\mu \left(\frac{\eta}{\delta^2} - \frac{1}{\delta} \right) \frac{d\theta_n}{d\mu} + \left[\frac{4a^2 \Omega^2}{gh_n} - \frac{1}{\delta} \left(\frac{s}{f} \cdot \frac{f^2 + \mu^2}{\delta} + \frac{s^2}{\eta} \right) \right] \theta_n = 0. \quad (A1-3)$$

This equation is now no longer in Sturm-Liouville form. In finite difference form, this equation looks like the following:

$$\frac{1}{\delta(\Delta\mu)} \left[-\mu + \frac{\mu\eta}{\delta} + \frac{\eta}{(\Delta\mu)} \right] \theta_{n,j+1} + \left[\frac{2\eta}{\delta(\Delta\mu)^2} - \frac{1}{\delta} \left(\frac{s}{f} \cdot \frac{f^2 + \mu^2}{\delta} + \frac{s^2}{\eta} \right) \right] \theta_{n,j} + \frac{1}{\delta(\Delta\mu)} \left[\mu - \frac{\mu\eta}{\delta} + \frac{\eta}{(\Delta\mu)} \right] \theta_{n,j-1} = -\frac{4a^2 \Omega^2}{gh_n} \theta_{n,j}. \quad (A1-4)$$

Evaluating the terms of this equation at each of the interior points results in a tri-diagonal matrix. The first and last rows of the matrix, determined by the boundary conditions, had only one non-zero element on the diagonal. Solving this matrix eigenvalue problem, it was found that the resulting eigenvalues and eigenvectors were very unsatisfactory. The eigenvalues (a constant factor divided by the equivalent depths) were not only not anywhere near what they should be, but some of them were complex -- the imaginary part being very sensitive to the exact value chosen for f , which, as mentioned in section 4.1 of the main text, can be set equal or nearly equal to 0.5. Most of the equivalent depths with smaller absolute values had associated eigenvectors which appeared to indicate that the eigenfunctions would pass through $\pm\infty$ at the critical latitudes.

The second method used to solve this problem was designed to retain the quasi-Sturm-Liouville form of equation (A1-2) in the finite-difference scheme. This required that μ be evaluated at the midpoint of each

increment in addition to evaluating it at each gridpoint. The finite-difference equation then takes this form:

$$\begin{aligned} & \frac{1}{(\Delta\mu)^2} \left[\frac{\eta_{j+\frac{1}{2}}}{\delta_{j+\frac{1}{2}}} \right] \theta_{n,j+1} - \left[\frac{1}{(\Delta\mu)^2} \left(\frac{\eta_{j+\frac{1}{2}}}{\delta_{j+\frac{1}{2}}} + \frac{\eta_{j-\frac{1}{2}}}{\delta_{j-\frac{1}{2}}} \right) + \frac{1}{\delta_j} \left(\frac{s}{f} \cdot \frac{f^2 + \mu^2}{\delta_j} + \frac{s^2}{\eta_j} \right) \right] \theta_{n,j} + \\ & + \frac{1}{(\Delta\mu)^2} \left[\frac{\eta_{j-\frac{1}{2}}}{\delta_{j-\frac{1}{2}}} \right] \theta_{n,j-1} = -\frac{4a^2\Omega^2}{gh_n} \theta_{n,j}, \end{aligned} \quad (A1-5)$$

where $\delta_{j\pm\frac{1}{2}} = (f^2 - \mu^2)_{j\pm\frac{1}{2}}$ and $\eta_{j\pm\frac{1}{2}} = (1 - \mu^2)_{j\pm\frac{1}{2}}$. This method produced somewhat better results, but they were still unsatisfactory. It was found that, as the gridpoint density was increased from 12 to 48 points between the poles, the eigenvalues did converge to limiting values. However, the values were not anywhere near the values shown by Flattery (1967) or others. The eigenvalues were found in this case to be fairly insensitive to variations of f in the range between 0.49 and 0.50, but the behavior of the eigenvectors around the critical point did vary noticeably as f was varied. In particular, setting f equal to 0.49 and using a 48 point grid placed the critical point equatorward of the μ grid point nearest to, but less than 0.5. This made all the eigenvectors go to zero poleward (for positive equivalent depth modes) or equatorward (for negative equivalent depth modes) of this point. Also, for $f \approx 0.500$, it seemed that the numerical method was causing the derivative of θ_n to go to zero near the critical point. This behavior, which was undesirable, motivated the third method.

Since the difficulty appeared to be related to evaluating the finite-difference equation very near the critical point, an alternate equation was sought for evaluation at this point. Equation (A1-3) was multiplied by δ^2 and evaluated at $\mu = \pm f = \pm 0.5$. Assuming that θ_n is non-

singular, this reduces equation (A1-3) to the following:

$$2\mu(1-f^2) \frac{d\theta_n}{d\mu} - \frac{5}{f} (f^2 + \mu^2)\theta_n = 0. \quad (\text{A1-6})$$

In finite-difference form at $\mu = \pm 0.5$ and for $f = 0.5$, this equation looks like the following:

$$\pm \frac{0.375}{(\Delta\mu)} \theta_{n,j+1} + \theta_{n,j} \mp \frac{0.375}{(\Delta\mu)} \theta_{n,j-1} = 0. \quad (\text{A1-7})$$

Equation (A1-5) was used at all points except at the critical points, where equation (A1-7) was used instead. This still did not solve the dilemma. It was found that multiplying (A1-7) by 1, 100, and 1000 made quite a difference in the results, whereas no difference should have arisen if there were no numerical problems involved. Multiplying (A1-7) by 1000 produced some eigenvalues very close to the correct values, but it also produced a number of complex equivalent depths. Using (A1-7) as shown above (multiplied by 1) produced equivalent depths which were all real and which, with the exception of two very large equivalent depths, were closer to those produced by the second method. This appeared to be proof that there was some kind of numerical instability at the heart of the problem. Both of the IMSL routines mentioned before were used to do this third method. Though the two routines use different methods to do the matrix eigenvalue problem, both yielded very similar, but not identical results.

This was a baffling obstacle which appeared insurmountable. For the diurnal tide, where f is smaller than one, the θ -operator, F , appears to be unmanageable with finite-difference methods, and no way could be found to avoid having to handle this operator. Although using

a different upper boundary condition (e.g. Newtonian cooling) obviates the need to solve Laplace's tidal equation, this operator must still be handled when solving the differential equation in the interior part of the model domain. It was decided that the results of such a calculation would be, at best, suspect. So, it was understood why no one uses finite difference methods in two dimensions (θ and z^*) to compute diurnal tidal variations, and it was concluded that the finite-difference approach would have to be abandoned.

APPENDIX 2
NOTES ON THE COMPUTER MODEL

In this appendix, a brief sketch is given of the routines, equations, and methods used to perform the tidal calculation. The six programs used in the calculation are discussed individually. The course of the calculation is summarized in the schematic diagram shown in Fig. A2.1. At the outset of this discussion, one point should be made. For convenience, various parameters will be said to be "functions" of particular variables. In fact, only a couple of the parameters handled were actually in a functional form. Here, "function" will mean a set of discrete values for a one, two, or three dimensional grid of points.

The first program in the sequence was the radiative transfer routine, IRADSOL. This program was developed at Colorado State University and was more fully documented by Cox, et al. (1976). It was modified somewhat so as to omit unnecessary routines and to obtain results in a format suitable for the next program. As stated in Chapter 3, this routine was used only to obtain a representation of the H₂O heating function. For this purpose, the only data which were required were the vertical profiles of temperature and water vapor mixing ratio at a number of latitudes. The routine must be executed once for each latitude and each time of day at which a vertical profile of the heating rate is desired. For this equinoctial study, the temperature and mixing ratio data were interpolated to 10° increments of latitude. IRADSOL was

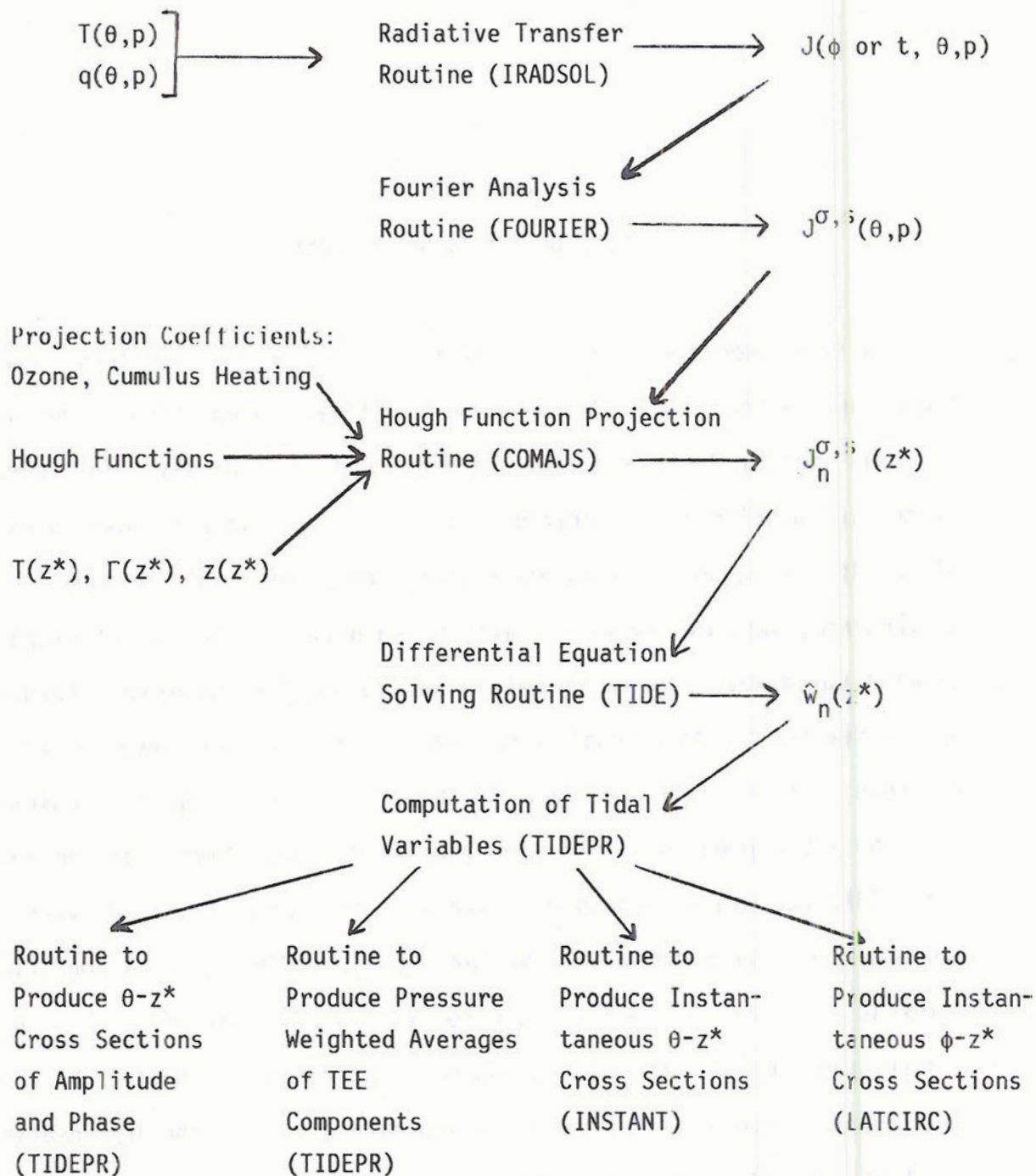


Fig. A2.1. Schematic diagram of the system of routines used to do the tidal calculation.

then run for each 10° latitude increment and for each half hour from 0630 to 1200 hrs. It was assumed that the daily heating curve was symmetric about local noon, and that the shortwave heating is zero between 1800 and 0600 hrs. From this routine, the H_2O heating rate was obtained as a function of time (or longitude), latitude, and pressure-height.

In order to extract the diurnal component of the heating, the H_2O heating function was subjected to Fourier analysis (in time or, equivalently, in longitude) at each latitude increment and pressure-height. This was accomplished in the routine FOURIER. The equations used for the analysis were obtained from Panofsky and Brier (1958). It was found to be most convenient to obtain the amplitude and phase of the diurnal component in this form:

$$J^{\sigma, S}(\theta, p) \cos(\sigma t + \rho),$$

where J is the amplitude of the heating rate as a function of latitude and pressure, ρ is the phase, and σ equals $2\pi/\text{day}$. For the equinoctial case with $t = 0$ at midnight, the phase of the diurnal component of the H_2O heating is $\pm 180^\circ$.

The task of the next program, COMAJS, was to compute as a function of z^* the sixteen Hough function projection coefficients of the total (H_2O , ozone, and cumulus) heating or any component thereof. For the amplitude of the diurnal component of the H_2O heating function, $J^{\sigma, S}(\theta, p)$, a Hough analysis was carried out by doing the following integration for $n = 1$ to 16:

$$\int_{-1}^{+1} J^{\sigma, s}(\theta, z^*) \cdot \theta_n(\theta) \cdot \cos\theta d\theta = J_n^{\sigma, s}(z^*).$$

Because the H₂O heating was not separable in θ and z^* , this had to be done at all of the thirty to forty levels where heating rates were obtained. The integration was done using Simpson's method, where $J^{\sigma, s}(\theta, z^*)$ was first interpolated to 1° increments. The Hough functions were also required for this integration. The values of the sixteen Hough functions at 1° increments were taken from a data file developed in earlier work on the diurnal tide. After computing the projection coefficients at thirty to forty levels, the results were interpolated to obtain values at z^* increments of 0.02.

The ozone and cumulus heating, for which the θ and z^* dependences were separable, were handled somewhat differently. For these two heating components, the amplitude of the diurnal component of the heating can be written in this way:

$$J^{\sigma, s}(\theta, z^*) = A \cdot f(z^*) \cdot g(\theta),$$

where f and g are normalized functions, and A is an amplitude factor. Here, f and g were originally continuous functions for both the ozone and cumulus heating. However, even though they were continuous functions, they had to be evaluated at discrete points. The sixteen Hough mode projection coefficients for the function g were computed using a separate program and were just entered into COMAJS on a data file. At each increment of z^* (for $\Delta z^* = 0.02$), the projection coefficients were multiplied by the constant A and the appropriate value of $f(z^*)$ in order to obtain the same type of vertical profiles of the projection coefficients as were obtained for the H₂O heating. This process was done

twice -- once for the ozone heating and once for the cumulus heating -- and then all three sets of vertical profiles were summed together mode by mode. It should be remembered at this point that if the three heating functions do not all have phases of 0° or $\pm 180^\circ$, then these projection coefficients will be complex quantities.

The vertical profiles of temperature, static stability, and geopotential height (as functions of z^*) were stored on a separate data file. This data was entered into the calculation in COMAJS. Here again, the increment of z^* was 0.02. The profiles were for a specific latitude (15°N or 30°N). The temperature (as a function of pressure) was obtained from the U.S. Standard Atmosphere Supplements, 1966. A coordinate transformation was made, and the temperature profile was interpolated to z^* increments of 0.02. The IMSL cubic spline interpolation schemes ICVICU and ICSEVU were used to do this interpolation, and second order one-sided second derivative schemes were used to provide the boundary conditions for the interpolation routines. The static stability profile was obtained by differentiating the interpolated temperature profile using a simple centered difference scheme. This yielded the poor profiles shown in Fig. 4.3b, indicating that this was not an advisable sequence to follow. The geopotential height was obtained by integrating the hydrostatic equation using the interpolated temperature profile:

$$z = z_0 + \frac{R}{g} \int_0^{z^*} T(x) dx,$$

where z_0 is the geopotential height of the 100 kPa surface.

The fourth program, TIDE, was the differential equation solver. For each of the sixteen vertical profiles of projection coefficients, this routine solved the vertical structure equation (equation 22 in Chapter 2) to obtain the sixteen component profiles of the vertical velocity that is, to obtain $\hat{w}_n(z^*)$. The program was based upon a method shown in a note by Lindzen and Kuo (1969). It is basically just a version of Gaussian elimination which is particularly useful for solving a tridiagonal matrix problem. The method was designed to solve the more general equation,

$$c(x) \frac{d^2f}{dx^2} + g(x) \frac{df}{dx} + h(x)f = r(x),$$

with the following two boundary conditions:

$$d_1 \frac{df}{dx} + a_1 f = b_1 \text{ at } x = 0,$$

and

$$d_2 \frac{df}{dx} + a_2 f = b_2 \text{ at } x = x_{\text{top}}.$$

The program was structured so as to be flexible enough to solve the general problem; however, with the coefficients required for this specific application of the routine, the problem was effectively reduced to solving the following set of equations:

$$\frac{d^2\hat{w}_n}{dz^{*2}} + \left(\frac{RT}{gh_n} - \frac{1}{4}\right)\hat{w}_n = \frac{\kappa}{gh_n} e^{-z^*/2} J_n,$$

$$\frac{d\hat{w}_n}{dz^*} + \left(\frac{RT_0}{gh_n} - \frac{1}{2}\right)\hat{w}_n = 0 \text{ at } z^* = 0,$$

and

$$\frac{d\hat{w}_n}{dz^*} + \left(\frac{R\Gamma_T}{gh_n} - \frac{1}{4} \right)^{\frac{1}{2}} = 0 \quad \text{at } z^* = z_T^*,$$

where x and $f(x)$ are now replaced by z^* and \hat{w}_n , Γ is a function of z^* , T_0 is the temperature at the lower boundary, and Γ_T is the static stability at the upper boundary. Lindzen and Kuo reported their method to be very reliable for all of the inhomogeneous, well-posed problems to which they had applied it. Lindzen applied this method to the classical tidal calculation (using the radiation condition) in 1968. The output from the program consisted of the sixteen vertical profiles of \hat{w}_n ; where again, \hat{w}_n is generally a complex quantity.

The next program, TIDEPR, performed three functions. First, it reconstituted the heating function (equation A2-6), computed the total vertical motion variable \hat{w}_n (equation A2-1), and from these computed all of the other tidal fields. The sequence observed in the computation of the tidal fields is diagrammed in Fig. A2.2. For reference, the finite difference equations which were used are shown below. The subscripts j and k are the latitudinal and vertical indices, respectively, where generally $j = 1$ at the equator and $k = 1$ at $z^* = 0$. The latitudinal increment was again 1° and the vertical increment was again 0.02. The index n refers to the number of the Hough function. Sixteen Hough modes were used in the representation of all of the tidal variables. The constants p_0 and T_0 are the pressure and environmental temperature at $z^* = 0$. The variable \bar{T}_k is the environmental temperature. All other notation is the same as in Chapter 2.

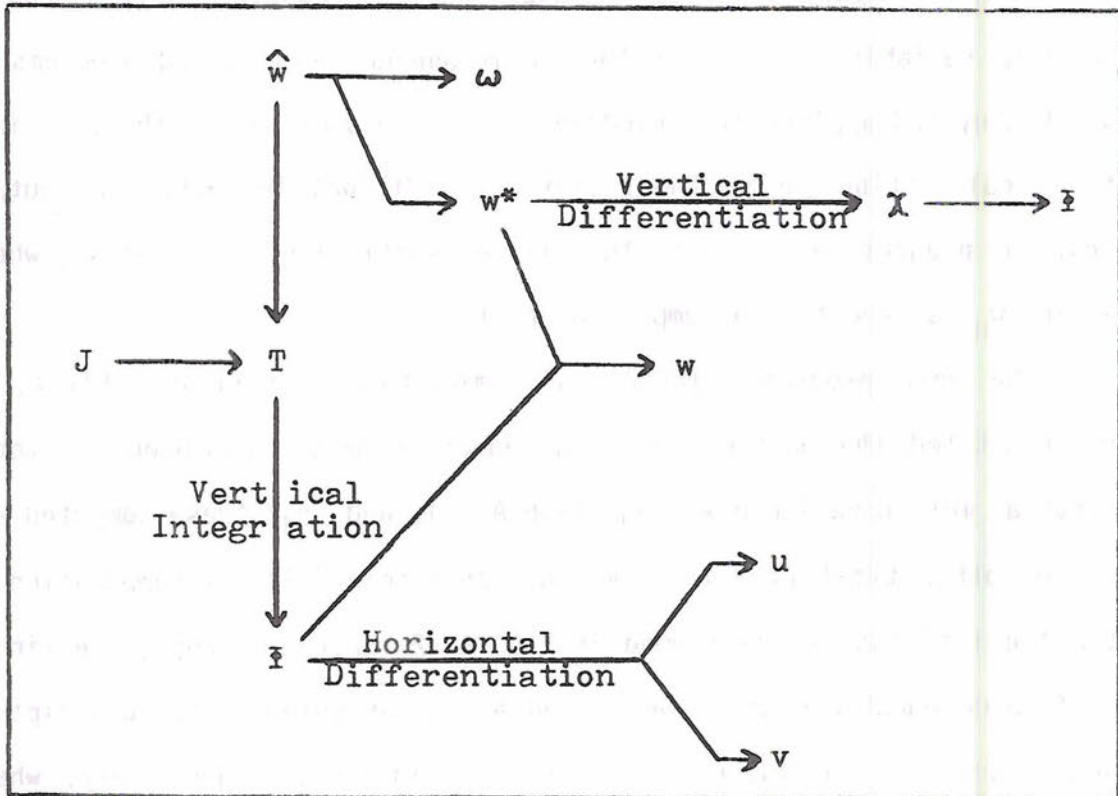


Fig. A2.2 Sequence used in computing the different tidal variables.

$$\hat{w}_{jk} = \sum_n (\hat{w}_{nk} \theta_{nj}) \quad (\text{A2-1})$$

$$w_{jk}^{*\sigma,s} = e^{\frac{(k-1)\Delta z^*}{2}} \hat{w}_{jk} \quad (\text{A2-2})$$

$$w_{jk}^{\sigma,s} = -p_0 e^{-\frac{(k-1)\Delta z^*}{2}} \hat{w}_{jk} \quad (\text{A2-3})$$

$$\chi_{jk}^{\sigma,s} = e^{\frac{(k-1)\Delta z^*}{2}} \sum_n (\hat{\chi}_{nk} \theta_{nj}) \quad (\text{A2-4})$$

$$\hat{\chi}_{nk} = \frac{1}{2} \left[\hat{w}_{nk} - \frac{\hat{w}_{n,k+1} - \hat{w}_{n,k-1}}{\Delta z^*} \right] \quad (\text{A2-4a})$$

$$\hat{\chi}_{n,1} = \left(\frac{\hat{w}_{n,1}}{2} - \frac{\hat{w}_{n,2} - \hat{w}_{n,1}}{\Delta z^*} \right) \quad (\text{A2-4b})$$

$$\hat{\chi}_{n,T} = \left(\frac{\hat{w}_{n,T}}{2} - \frac{\hat{w}_{n,T} - \hat{w}_{n,T-1}}{\Delta z^*} \right) \quad (\text{A2-4c})$$

$$\phi_{jk}^{\sigma,s} = \frac{-i g h_n e^{\frac{(k-1)\Delta z^*}{2}}}{2\sigma} \chi_{jk}^{\sigma,s} \quad (\text{A2-5})$$

$$J_{jk}^{\sigma,s} = \sum_n (J_{nk} \theta_{nj}) \quad (\text{A2-6})$$

$$T_{jk}^{\sigma,s} = \sum_n (T_{nk} \theta_{nj}) \quad (\text{A2-7})$$

$$\Gamma_{nk} = \frac{-i}{\sigma} \left[\frac{J_{nk}}{C_p} - e^{\frac{(k-1)\Delta z^*}{2}} \Gamma_k \hat{w}_{nk} \right] \quad (\text{A2-7a})$$

$$\phi_{jk}^{\Sigma,s} = \sum_n (\phi_{nk} \theta_{nj}) \quad (\text{A2-8})$$

$$\phi_{n,1} = - \frac{RT_0}{i\sigma} w_{n,1}^{*\sigma,s} \quad (\text{A2-8a})$$

$$\phi_{nk} = \sum_{m=2}^k \left[\frac{R \cdot \Delta z^*}{2} (T_{n,m} + T_{n,m-1}) \right] \quad (\text{A2-8b})$$

$$w_{jk}^{\sigma,s} = \frac{i\sigma}{g} \phi_{jk}^{\sigma,s} + \frac{R\bar{T}_k}{g} w_{jk}^{*\sigma,s} \quad (\text{A2-9})$$

$$u_{jk}^{\sigma,s} = \frac{1}{4\Omega^2 a (\sin^2 \theta_j - f^2)} \sum_n (\phi_{nk} E_{nj}) \quad (\text{A2-10})$$

$$E_{nj} = \left[\frac{\sigma \theta_{nj}}{\cos \theta_j} - 2\Omega \sin \theta_j \left(\frac{\theta_{n,j+1} - \theta_{n,j-1}}{2\Delta\theta} \right) \right] \quad (\text{A2-10a})$$

$$E_{n,1} = \left[\frac{\sigma \theta_{n,1}}{\cos \theta_1} - 2\Omega \sin \theta_1 \left(\frac{-1.5\theta_{n,1} + 2\theta_{n,2} - 0.5\theta_{n,3}}{\Delta\theta} \right) \right] \quad (\text{A2-10b})$$

$$v_{jk}^{\sigma,s} = \frac{i}{4\Omega^2 a (\sin^2 \theta_j - f^2)} \sum_n (\phi_{nk} N_{nj}) \quad (\text{A2-11})$$

$$N_{nj} = \frac{2s\Omega \sin \theta_j}{\cos \theta_j} \theta_{nj} - \sigma \left[\frac{\theta_{n,j+1} - \theta_{n,j-1}}{2\Delta\theta} \right] \quad (\text{A2-11a})$$

$$N_{n,1} = \frac{2s\Omega \sin \theta_1}{\cos \theta_1} \theta_{nj} - \sigma \left[\frac{-1.5\theta_{n,1} + 2\theta_{n,2} - 0.5\theta_{n,3}}{\Delta\theta} \right] \quad (\text{A2-11b})$$

There are several things to note about these equations. First, these quantities are again generally complex. Second, there are two ways to compute the geopotential field. One involves a simple vertical integration of the hydrostatic equation (equation A2-8). The other method is not as obvious. Eliminating $T^{\sigma,s}$ between the thermodynamic energy equation and the hydrostatic equation (equations 13 and 15 of Chapter 2), it can be inferred that $\phi^{\sigma,s}$ and $w^{*\sigma,s}$ (and hence $\chi^{\sigma,s}$) have the same horizontal structure. After a fair amount of manipulation, the

horizontal momentum equations and the continuity equation (equations 11, 12, and 14 of Chapter 2) can be combined into one equation in the two unknowns $\phi^{\sigma,s}$ and $\chi^{\sigma,s}$. With some use of Laplace's tidal equation, it can finally be shown that $\phi^{\sigma,s}$ is equal to a (pure imaginary) constant times $\chi^{\sigma,s}$ (equation A2-5). As a cross check, both methods were used, and it was found that they yielded results which differed by less than 1%. A third thing to notice is that the computation of the horizontal wind components involves a horizontal differentiation, and that the basis functions which represent the horizontal structure of the wind components are different than the basis functions (the Hough functions) for all of the other variables. The structures of these new basis functions were compared to the corresponding structures shown by Chapman and Lindzen (1970). The agreement was good. The horizontal wind components can only be computed at the poles if l'Hospital's rule is applied. The same is true at 30° from the equator if $f=\sigma/2\Omega=0.5$. Finally, the methods used for integration and differentiation should be noted. For computing $\chi^{\sigma,s}$, the vertical derivative of \hat{w}_n was computed using a simple centered difference scheme in the interior and first order one-sided difference schemes at the boundaries. The integration of the hydrostatic equation was carried out using the trapezoidal method. For the computation of the horizontal wind components, a simple centered difference scheme was used for the interior differentiation, while a second order forward difference scheme was applied at the equator.

The second function of program TIDEPR was to print out amplitude and phase cross sections (in the θ - z^* plane) for each of the tidal variables. The following equations were used for computing the amplitude and phase of the (complex) tidal variables:

$$w = w_r + iw_i$$

$$|w| = (w_r^2 + w_i^2)^{1/2}$$

$$\rho = \pm \cos^{-1} \left(\frac{w_r}{w} \right) \quad \left\{ \begin{array}{l} + \text{ for } w_i > 0 \\ - \text{ for } w_i < 0 \end{array} \right.$$

Here, w_r and w_i are the real and imaginary parts of w respectively, $|w|$ is the amplitude of w , and ρ is the phase. The phase was defined such that 0° corresponded to a time of maximum at local midnight, and so that increasing the phase to $+180^\circ$ corresponded to a backwards shift in the time of maximum to local noon. The amplitudes for each variable were divided by a power of ten chosen such that all of the amplitudes printed out in the cross section would be between zero and ten. The phases were divided by one hundred so as to yield a phase cross section with values between -1.80 and $+1.80$. The results were printed to three decimal places relative to the largest amplitude of the cross section. The cross sections were printed in a two dimensional array with data at 5° increments of latitude and with a vertical increment of 0.04 .

The third function of TIDEPR was to compute pressure-weighted averages of the three terms of the thermodynamic energy equation and of the temperature variation for the layer between 81.8 and 28.9 kPa (or, in one case, between 81.8 and 44.9 kPa). These averages were computed at 5° increments of latitude for each of the four quantities $J^{\sigma,s}/c_p$, $\Gamma_w^{\sigma,s}$, $i\sigma T^{\sigma,s}$ and $T^{\sigma,s}$, and the results were printed out in terms of amplitude and phase. The equation used to compute the pressure weighted average was of the following form:

$$J_j^{\sigma,s} = \frac{\int_{z_B^*}^{z_T^*} J_{jk}^{\sigma,s} e^{-z^*} dz^*}{(e^{-z_B^*} - e^{-z_I^*})},$$

for which the integration was executed using Simpson's rule.

The tidal fields computed in TIDEPR were also saved (as complex numbers) on permanent files and used later as input for the routines INSTANT and LATCIRC. Both of these routines utilized the following equation:

$$w = |w| \cos(\sigma t + s\phi + \rho), \quad (A2-12)$$

where ϕ was chosen to be zero for use in these two routines. The program INSTANT produced θ - z^* cross sections with the same specifications as the amplitude cross sections produced by TIDEPR. However, in this case, a particular time, t , was chosen, and the equation was evaluated at each grid point in the cross section. The cross sections so derived therefore provided an instantaneous portrayal of the tidal fields along the particular meridian $\phi=0$. The time was varied so as to obtain cross sections at two hour increments from 0000 to 1200 hrs.

Finally, the program LATCIRC utilized the same data produced in program TIDEPR to produce 24 hour time sections of the various tidal fields for a chosen point ($\phi=0$) on a specified latitude circle (or, viewed another way, if a fixed time were chosen instead, to produce instantaneous cross sections around the specified latitude circle). Equation A2-12 was used again; however, in this case, the time was varied by one hour increments, and the vertical profiles of the tidal variables were computed at the specified latitude for each hour. Such

$t-z^*$ (or $\phi-z^*$) cross sections were computed for 0° , 10° , 20° , and 30° from the equator with a horizontal resolution of one hour (or 15° longitude).

The instantaneous $\theta-z^*$ cross sections and the 24 hour time sections were quite easy to produce and proved to be very helpful in the interpretation of the amplitude and phase profiles produced by program TIDEPR. Trends, relationships, and the three dimensional structure of the diurnal tide all became much more recognizable.

APPENDIX 3

STUDY OF ANALYTIC AND QUASI-ANALYTIC SOLUTIONS

When the method of separation of variables is applied to the single tidal equation in $\hat{w}^{\sigma,5}$, (Eq. 17 of chapter 2), the following vertical structure equation is obtained:

$$\frac{d^2 w_n}{dz^2} + \lambda_n^2 w_n = \frac{ke^{-z^*/2}}{gh_n} J_n, \quad (\text{A3-1})$$

where

$$\lambda_n = \left(\frac{R\Gamma}{gh_n} - \frac{1}{4} \right)^{\frac{1}{2}}.$$

This is the equation which is solved (using appropriate boundary conditions) in order to determine the vertical velocity field, and from that to determine all the other tidal fields.

Solutions to this equation were obtained in three ways. First, solutions were obtained analytically by applying the straight forward method of undetermined coefficients to solve this non-homogeneous ordinary differential equation. Second, another solution was obtained analytically using Green's functions. Third, numerical solutions were evaluated using the same numerical model (with slight modifications) that produced all of the results shown in the main text of this report.

There were three reasons why it was deemed desirable to obtain, evaluate, and compare the solutions obtained by these three methods.

First of all, it was essential to be sure that the numerical model was yielding the same results as the analytical solutions. It was verified that the results were the same to at least three decimal places. It was also found that the numerical results in the troposphere are not very sensitive to where the top of the model is placed.

The second reason was to test the sensitivity of the results to changes in the heating and static stability profiles. Very simple static stability profiles and functional heating profiles were put into the model to see if they would give realistic results. These profiles were varied in simple ways to see how the character of the results would be altered.

However, it was really a third reason that motivated this exercise. Simple analytical solutions were obtained and evaluated in order to try to find a mathematical explanation for the results obtained from the full numerical calculation using real data. It was hoped that once a mathematical explanation was found it would be possible to find a physical explanation as well. In particular, an explanation was sought for why there should be downward vertical motion at the equator at the time of maximum heating. In this respect, this exercise failed. It was found that this phenomenon occurs for even very simple approximations to the real atmosphere and that the phenomenon is not very sensitive to changes in any particular parameter. It was encouraging to find this insensitivity in the results, but no new physical insight was gained. In fact, even the mathematical insight was not very satisfying. This was disappointing.

Various heating profiles were plugged into equation (A3-1):

$$(1) \quad J_n = A p_n e^{z^*/2} \cos \mu z^* \quad \text{for } \mu = 6/7$$

$$z_T^* = 2.25$$

$$(2) \quad J_n = A p_n e^{z^*/2} \cos(\mu z^* + \phi) \quad \text{for } \mu = 6/7, \phi = -0.358$$

$$z_T^* = 2.25$$

(This will be called the "phase shifted profile".)

$$(3) \quad J_n = A p_n \cos \mu z^* \quad \text{for } \mu = 0.75, 1.00, 1.50$$

$$z_T^* = \frac{2\pi}{3}, \frac{\pi}{2}, \frac{\pi}{3}$$

$$(4) \quad J_n = A p_n \cos(\mu z^* + \phi) \quad \text{for } \mu = 6/7, \phi = -0.358$$

$$z_T^* = 2.25$$

$$(5) \quad J_n = A p_n e^{z^*/6}$$

$$z_T^* = 3\pi, \frac{2\pi}{3}$$

$$(6) \quad J_n = A p_n e^{-z^*/3}$$

$$z_T^* = 3\pi$$

The top of the heating layer was z_T^* , the constant A was the amplitude of the total heating, and p_n was the projection coefficient for the corresponding Bough function projection of the heating. The straight forward ordinary differential equation solutions were obtained using only the third and fifth heating functions. Only one solution was obtained by using the Green's function method, and the fifth heating profile was used in that case. Once it was verified that the numerical model was giving the same results as the analytic solutions, all subsequent tests were run using the numerical model. These tests will be called here "quasi-analytic" because they could have been done analytically without too much difficulty, but it was more convenient to use the model.

In running these tests, several parameters were varied to see what effects would be produced:

1. Effect of changing the boundary conditions.
 - a. Perfect energy reflecting boundaries ($\hat{w} = 0$ at top and bottom).
 - b. Perfect energy reflecting bottom ($\hat{w} = 0$) and radiation/boundedness condition at the top.
 - c. Rigid bottom ($w' = 0$) and radiation/boundedness condition at the top.
2. Effect of putting in the $e^{-z^*/2}$ factor.
3. Effect of varying the static stability profile.
 - a. Constant everywhere ($\Gamma = 25$).
 - b. Two Γ 's: $\Gamma = 25$ K in the region of heating, 80 K above.
 - c. Three Γ 's: same, but with Γ reduced to 45 in the mesosphere.
4. Effect of a vertical discontinuity in the heating at a given height.

Cross sections in the θ - z^* plane were made by assuming the θ -structure of the heating to be a cosine function. Individual θ - z^* cross sections were produced for the responses in each of the first six modes (the modes with the three largest positive equivalent depths and the three largest negative equivalent depths). Also, θ - z^* cross sections were produced for the sum of the responses in the first five modes (three positive and two negative equivalent depth modes) and for the sum of sixteen modes (eight positive and eight negative).

It should be noted that each of these heating profiles involves different amounts of energy. No effort has been made to make them

involve the same integrated amount of energy or any other quantity. The only constraint is that they all have the same maximum heating value at the surface (or near the surface in the case of the phase shifted profiles).

Quite a number of things were observed in the results.

(1) The rigid lid case produced a much greater (16 mode summed) response than did the cases using a radiation condition at the upper boundary. (The rigid lid was set very low -- just above the top of the heating.) Presumably, this is because energy is trapped between the boundaries. However, the phase of the response at the equator was still such that there was downward vertical motion at the time of maximum heating.

(2) Changing the lower boundary condition from $w^* = 0$ to $w = 0$ only produced a small, consistent decrease in the amplitude of the response and a small shift in the phase of the response throughout the troposphere.

(3) In changing the wavenumber of the heating, μ , two effects were sought. In the coefficient in front of all the terms of the analytic solution, the factor $(\lambda_n^2 - \mu^2)$ appears in the denominator. It was thought that, as μ switched from being smaller than λ_1 ($= 0.899$) to being larger than λ_1 , the sign of the response in the mode with the largest positive equivalent depth would switch sign. Such was not the case. When averaged throughout the troposphere, all three cases ($\mu = 0.75, 1.00, \text{ and } 1.50$) produced downward motion at the equator very near the time of maximum heating. The reason for this was never really discovered.

The second effect sought was evidence of resonance. The quantity $(\lambda_1^2 - \mu^2)^{-1}$ should grow without bound as μ approaches λ_1 . It was verified that the amplitude of the response at the equator was everywhere greater as μ grew closer to λ_1 . At 20° from the equator, where the Hough function corresponding to λ_1 , has a node, it was verified that little change occurred as μ was varied.

(4) It was found that it is possible for an exponential heating profile (like Lindzen's) and a cosine heating profile (more like the H_2O heating derived from the radiative transfer routine) can give nearly identical equatorial responses in both phase and amplitude.

(5) Changing the static stability from a constant value of 25 K everywhere, to 25 K in the heating region and 80 K everywhere above that, had no significant effect on the equatorial amplitude profile. However, there was a large decrease in the amplitude of the stratospheric vertical velocity.

(6) Adding a reduced mesospheric static stability of 45 K to the preceding case (to make a system with three Γ 's) had a surprising effect. For the equatorial amplitude profiles, a greater change was incurred by going from a two Γ system to a three Γ system than by going from the constant Γ system to the two Γ system; though the largest change in amplitude was still only about 20%. Thus, the structure of the upper atmosphere does affect the tropospheric response. However, it is not the predominant influencing factor by any means.

For the phase profiles, going from a two Γ system to a three Γ system produced almost no distinguishable change, whereas going from a constant Γ system to the two Γ system pushed the time of maximum to between one and two hours later in the troposphere.

(7) One purpose of these quasi-analytic tests was to try to duplicate the tidal response to the H_2O heating by using a simple static stability profile and heating function to represent the real atmospheric system. The two Γ system with the phase shifted heating does this quite well for both phase and amplitude. However, there are some structural differences in the amplitude profiles. In general, the quasi-analytic case yielded greater amplitudes in the lower (85 to 60 kPa) and upper (22.5 to 9 kPa) troposphere. The differences were as much as a factor of two, but they were smaller than the differences caused by many of the other changes made in this series of tests. Presumably these differences were caused more by the different tropospheric static stability profiles than by the different heating profiles.

The next step was to examine the contributions of the responses within individual modes to the total response. The case which had a response most closely resembling that due to H_2O heating was chosen for analysis -- i.e. the case using the phase shifted cosine heating function and a two Γ structure. Two latitudes were chosen for examination: the equator and 20° away from the equator.

First consider the situation at the equator. Three things should be noted. First of all, no single mode is clearly and dominantly responsible for the character of the response at the equator. Through all of the troposphere, except the lowest 20 kPa, the gravest positive equivalent depth mode (the mode with the greatest positive equivalent depth) produces the largest response; however, it is clearly evident that the second and even the third positive equivalent depth modes are not negligible in their contributions to the amplitude profile. From the phase profiles, it appears that the total response (5 or 16 modes)

tends to be a compromise between the responses in the first and second modes. The negative equivalent depth modes, on the other hand, provide no significant response at the equator.

Second, it should be noted that when averaged through the troposphere, it is the first and second positive equivalent depth modes which are primarily responsible for the downward motion at the equator at the time of maximum heating. The response in the gravest mode changes phase quite slowly through the troposphere. The response in the second mode, when averaged through the troposphere, still yields downward motion at the equator, but there is greater than a 180° phase variation through the troposphere for this mode. The higher the order of the positive equivalent depth mode, the more rapidly the phase of the mode varies with height. This is because of the decreasing vertical wavelength with higher order modes. As a general conclusion, it can be hypothesized and verified that it is the higher order modes, with their more rapid variation of phase with height and their more frequent sign changes between the equator and the pole, which are primarily responsible for the tilted cell in the total (16 mode) vertical motion field. The response in the gravest mode cannot do it alone.

There is also a third trend which is quite interesting. The total forcing on the right side of equation (A3-1) can be written in its complete form as follows:

$$F = \left(\sum_n \frac{\kappa A}{gh_n} p_n e^{-z^*/2} J_n(z^*) \theta_n(\theta) \right) e^{i(\sigma t + s\phi)},$$

where p_n is the n th Hough mode projection coefficient of the horizontal structure of the heating (a cosine function). In the case that the

forcing is separable in θ and z^* (as it is for the analytic solutions), a single component of the forcing can be written in this form:

$$F_n = \frac{kA}{j} \left(\frac{p_n}{h_n} \right) e^{-z^*/2} J(z^*) \theta_n(\theta) \quad (\text{A3-2})$$

At the equator, and considering only positive equivalent depth modes, the only parameter which varies from mode to mode is (p_n/h_n) . This parameter increases by a factor of three in going from the gravest mode to the eighth positive equivalent depth mode, thereby implying that forcing increases as one goes to higher order modes, whereas the fraction of the heating projected onto an individual mode decreases as one goes to higher order modes. However, the response decreases with the higher order modes, despite the fact that the forcing increases. Considering the particular form of the solution (which is roughly proportional to $1/\lambda_n^2$), it is not difficult to see how this decrease comes about. However, physically it is a little hard to understand what this means. It should probably be visualized in terms of trying to force oscillations with differing vertical and horizontal scales in a stable atmosphere. It is apparently easiest to get the atmosphere to respond to the forcing with long wavelengths. This seems intuitively plausible.

Now consider the situation at 20° from the equator. At this latitude, the gravest mode is near a node, and the forcing in this mode produces only a very small response. The responses in the second and third modes are of very similar amplitude, with the third mode dominating below 30 kPa, and the second mode dominating above this point. The individual responses in the first three negative equivalent depth modes are small; but when summed together, because they all have the same phase, they do make a significant contribution to the total response.

What is to be concluded from these observations? At the equator, the first and second positive equivalent depth modes are primarily responsible for producing the downward motion at the equator at the time of maximum heating. That is, the equatorial response is primarily forced by the heating in these two modes. These two modes also force upward motion away from the equator at the same time, but not in the same place. In examining the θ - z^* cross section of the total (16 mode) vertical motion field, it is quite evident that the higher order positive equivalent depth modes cannot be neglected in an explanation of the total response. Nor can the negative equivalent depth modes be neglected completely beyond about 10° or 15° from the equator. Whereas two modes are primarily responsible for the equatorial response, it cannot be said of even all the tropics that these are the only important or even the largest contributors to the total response. One other evidence to support this statement comes from a comparison of the five and sixteen mode summed responses at 20° from the equator. The difference between the amplitude profiles of these responses is much greater at this latitude than at the equator. In fact, the sixteen mode response is more than 30% greater than the five mode response through most of the troposphere.

Does the solution obtained by using a Green's function approach provide any further insight? No, it really does not. A solution was obtained for the case with a simple cosine heating having a maximum at the ground, with a single constant static stability, and with the boundary condition $w^* = 0$ at $z^* = 0$ and the radiation/boundedness condition at the top. The solution (in the region for which $0 \leq z^* \leq z_T^*$) takes the following form:

$$\hat{w}_n(z^*) = -\frac{1}{\lambda_n} e^{i\lambda_n z^*} \int_0^{z^*} \sin\lambda_n z^* F(x) dx - \sin\lambda_n z^* \int_{z^*}^{z_T^*} e^{i\lambda_n x} F(x) dx ,$$

where z_T^* is the top of the heating, and $F(x)$ is the same forcing as in equation (A3-2). This quantity, \hat{w}_n , must of course then be multiplied by the appropriate Hough function to obtain the vertical motion field in a given mode.

It can be argued that, if the forcing is a monotonically decreasing function of height, the first integral will always be positive, and hence that the coefficient in front of the exponential phase factor of the first term will always be negative. It should also be noted that, at the top of the heating layer, the second term will vanish. This permits the determination of the sign of the vertical velocity at or near the top of the heating. However, even in the case for which this solution was derived and evaluated, there was weak upward vertical motion at the equator at the time of maximum heating for the first two positive equivalent depth modes. So, this is not a very helpful piece of information.

Neither term of the solution is clearly dominant throughout the troposphere for either of the first two positive equivalent depth modes. In the lower half of the troposphere, the second term is responsible for the majority of the response in these two modes; while in the upper troposphere, the situation is reversed. Since the character of the vertical motion field produced by the second term is rather obscure, it is hard to say whether or not this term will produce downward vertical motion. Likewise, it is not obvious from looking at the terms what the vertical motion field will look like when the two contributions are added together.

So, from the Green's function approach, it has been concluded that the sign of the vertical velocity at the top of the heating can be determined, but that it can be of either sign, depending on how high the heating extends. The vertical velocity will have the same sign down into the heating layer for some distance, but not too far. In general, the first term is more important (especially for higher order positive equivalent depth modes), but the character of the solution cannot be determined without considering the contribution of the second term. It appears that no new mathematical or physical insight is gained from this approach.

The three terms of the solution obtained by applying a straight forward method of undetermined coefficients to solve the differential equation were also evaluated. No insight was gained. The final result takes the form of a small difference between much larger numbers. Thus, it could not be said which term was most important.

This study of analytic and quasi-analytic solutions to the vertical structure equation was fruitful, but not totally successful. Much confidence was gained from the knowledge that the numerical model could produce the same results as a completely independent analytic solution. Also, a much better understanding of the sensitivity of the model and of the relative contributions of the responses in each mode was obtained. However, the physical interpretation sought after remained undiscovered.

APPENDIX 4

REQUIREMENTS FOR A SOLSTICE CALCULATION

According to the original design for this project, the tidal variations were to be computed for the time of solstice as well as for equinox. This part of the project was deleted for two reasons. First, in the light of the results presented in this report, it appeared that doing a calculation at solstice would probably not provide much better agreement between theory and observations than was obtained for the calculation at equinox. As discussed in section 4.3 of this report, it does not seem likely that in the tropics the seasonal changes of the tidal variations should be very great, and therefore it did not appear probable that any significant new understanding would be gained from doing a calculation for the time of solstice. The results of such a calculation might be quite different in middle and upper latitudes, but the results are of somewhat questionable reliability there anyway.

Second, considering the limited gain in understanding expected to result from doing a solstice calculation, the amount of work required to do it did not seem justifiable. As will be shown here, the changes required are significant.

Because of the differences in the solstice calculation, the following steps would have to be taken.

(1) Vertical profiles of temperature, water vapor mixing ratio, and ozone mixing ratio would have to be obtained at a number of latitudes for both the summer and winter hemispheres. These should be obtained as functions of pressure -- not of geometric height.

(2) It would be wise to use a radiative transfer model which is valid at least to the mesopause. Perhaps some functional form of the ozone heating could be deduced from physical reasoning, but it would be much better to use a reliable radiative transfer routine. Perhaps the routine developed by Hong and Wang (1980) could be used. It would also probably be good to include SW absorption by CO_2 .

(3) The Fourier analysis of the daily heating curves derived from the radiative transfer routine would be somewhat more complex for a solstice calculation, because the length of the day would vary with latitude. If radiative transfer data are used, one cannot assume θ - and z^* -dependences for the diurnal component of the H_2O and ozone heating as Lindzen did. This implies that Fourier analysis would have to be done at every pressure level where heating rates were obtained and for all three heating components.

(4) If radiative transfer data are used, the heating function is no longer separable in θ and z^* . Consequently, Hough analysis (projecting the diurnal component of the heating onto Hough functions) would have to be done at every pressure level where heating rates were obtained.

(5) The antisymmetric Hough functions would have to be computed.

(6) The methods incorporated into the programs used in this research (especially the program which prints out all of the tidal fields) would have to be significantly altered to handle 32 modes.

(7) Results would have to be printed out from pole to pole rather than from equator to pole. This would also imply a significant alteration to the routine used to print out the data for equinox.

(8) If cumulus heating were used in a solstice calculation, it should probably be shifted so as to have its maximum about 10° into the summer hemisphere in order to simulate the shift of the ITCZ.

(9) A more satisfactory interpolation scheme should be found. Or at least a better way should be found to handle the boundary conditions for the IMSL cubic spline interpolation scheme. Two important interpolations need to be done. The amplitudes of the diurnal component of the heating must be interpolated to obtain data at 1° increments of latitude. This must be done at each pressure level and is requisite for the Hough analysis. Then, the projection coefficients resulting from the Hough analysis must be interpolated to a very fine grid spacing in the z^* -direction. This is for the differential equation solving routine. The limited amount of real data makes the interpolation quite a severe test for any interpolation routine. It might be sufficient to use second-order forward and backward differenced second derivative expressions at the boundaries for a cubic spline interpolation routine.

(10) One other problem arises. What static stability profile should be used? It was assumed in developing this model that Γ is not a function of θ . Therefore, the logical latitude at which to take the static stability profile would be at the equator. But this profile is pretty nearly constant throughout the year; and thus, little change from the equinox calculation would be expected. In a study of the mid-latitude tidal response, perhaps the summer and winter profiles of Γ at 45°N could be put into the model in separate runs, keeping in mind that the results in the opposite hemisphere should be disregarded. It would,

however, be interesting to see how different the tidal response would be for, say, the winter hemispheres, using the two different profiles for 45°N .

All of this would require a great deal of work beyond what has already been done, and the insight gained from such a calculation would probably be limited, or perhaps even misleading.